Study on Liquid-Liquid Phase Separation Mechanism of DNA and Cationic Polypeptide

MASAHIRO MIMURA

February 2022

Study on Liquid-Liquid Phase Separation Mechanism of DNA and Cationic Polypeptide

MASAHIRO MIMURA

Doctoral Program in Materials Science

Submitted to the Graduate School of

Pure and Applied Sciences

in Partial Fulfillment of the Requirements

for the Degree of Doctor of Philosophy in

Engineering

at the

University of Tsukuba

Contents

Chapter 1.

General Introduction

1.1. Liquid-liquid phase separation (LLPS) in the control of biological processes

Proteins and nucleic acids are essential substances that play a fundamental role in living systems due to their diverse functions and physicochemical properties. The intracellular environment contains a myriad of these biomolecules, with total concentrations reaching about 300 mg/ml.[1] Molecular compartmentalization allows biomolecules to interact properly even in such a highly crowded environment, which is one of the key mechanisms to control biological reactions. Well-known intracellular compartments are membrane-bound organelles such as the nucleus, mitochondria, and endoplasmic reticulum. They selectively uptake molecules through membrane proteins such as the nuclear pore complexes,[2] which enable them to perform different cellular functions.

Membrane-less organelles are another type of compartments formed through liquid-liquid phase separation (LLPS) of proteins and/or nucleic acids.[3] These compartments are fluid in nature and lack physical boundaries as lipid membranes, resulting in dynamic spatiotemporal organization of complex cellular milieu. Based on their fluid properties as liquids, membrane-less organelles are called by various names such as droplets,[4] liquid droplets,[5] biomolecular condensates,[6] and liquid condensates,[7] and in this chapter, they are referred to as droplet(s). The first report on intracellular droplets is by Brangwynne *et al*. in 2009, who found that the germline P-granules of *Caenorhabditis elegans*, are formed through the LLPS mechanism.[5] Since then, about 10 years to the present, it has been suggested that diverse intracellular droplets including stress granules,[8] cajal bodies,[9] nucleolus,[10] heterochromatin,[11,12] and paraspeckles[13] are formed through LLPS.

Droplets have several properties that are expected to be advantageous for the control of biological processes, as follows. (1) Reversibility. Droplets are formed reversibly in response to physicochemical stresses such as pH,[14] temperature,[15] osmotic pressure,[16] and oxidation.[17] This property leads it to act as a 'stress sensor' involved in various biological reactions. In addition, biomolecules that diffuse into the cell form droplets when they exceed a critical concentration.[18] Therefore, the droplet acts as a 'storage compartment' of molecules, which may have a buffering effect on intracellular protein concentrations, and these are dissolved as the

expression level decreases.[19] (2) Molecular selectivity. Droplets are expected to act as 'reaction compartments' that control chemical reactions by selectively uptake and exclusion of biomolecules.[20] For instance, when all components necessary for the enzymatic reactions are concentrated in the droplets, the reaction efficiency is improved.[21] In contrast, the reaction is inhibited when only key molecules for the reaction are sequestered/excluded in the droplets.[22]

The dynamic properties of the droplets described above have been proposed to play an important role in the control of a wide range of biological processes, including gene expression,[23–25] metabolism,[26,27] signal transduction,[28,29] autophagy,[30] and skin barrier.[31] In addition to these positive effects, it has been proposed that dysregulation of LLPS may lead to the toxic aggregation of disease-related protein.[32,33] For instance, amyotrophic lateral sclerosis (ALS)-related proteins such as FUS and TDP-43, as well as Parkinson's disease-related α-synuclein, can form droplets and then mature to become cross β-sheet amyloid fibrils.[34–36] Therefore, LLPS of biomolecules has emerged as an attractive research target for a better understanding of the mechanisms of complex intracellular processes and for drug discovery.

1.2. LLPS mechanisms of biomolecules and their challenges

LLPS is a physicochemical process in which a solution separates into two or more phases of different composition that are thermodynamically stable. In the field of polymer physics, the phase behavior of chemically synthesized homopolymers and heteropolymers has been extensively studied through both theoretical and experimental approaches.[37,38] However, the intracellular phase behavior of proteins and nucleic acids is more complicated given that they are biopolymers composed of various monomeric elements (20 amino acids for proteins and 4 deoxyribonucleotides and ribonucleotides for DNA and RNA, respectively.) and form various higher-order structures, as well as the complex intracellular environment.

The components of intracellular droplets can be classified into scaffolds and clients.[39] Scaffold molecules are essential for the droplet formation, while client molecules are selectively incorporated into the formed droplets. Fundamental studies to understand the LLPS mechanism have focused on scaffold molecules, especially proteins, and *in vitro* experiments on the phase behavior of purified single proteins suggested that flexible and weak multipoint interactions generally play a crucial role in the generation of LLPS.[40,41] For instance, LAF-1 protein that may serves as a scaffold for P granules, undergoes LLPS through hydrogen

bonding, charge-charge, cation-π, and sp^2/π interactions.[42,43] Pathological tau protein forms droplets through electrostatic interactions completely.[44] In addition, the simulation based on the stickers and spacers model demonstrated that it can accurately predict the *in vitro* phase behavior of proteins acting as scaffolds.[45] Although the LLPS mechanism of single-protein solution is gradually being elucidated, intracellular droplets are often formed by both nucleic acids and proteins acting as scaffolds, and the LLPS mechanism of such multi-components mixtures is more complicated, and therefore poorly understood at present.

1.3. Binary system to explore the LLPS mechanism

Nucleic acids modulate intracellular LLPS through interactions with proteins, which are involved in a variety of biological processes. The interactions between DNA and cyclic GMP-AMP synthase (cGAS) induces droplets formation, which activates the innate immune response.[29] It is also suggested that condensation of DNA with nuclear proteins via LLPS is important for the regulation of gene transcription.[22,23] For the formation of stress granules, multipoint interactions between RNAs and proteins are important, and RNA increases the fluidity of the RNA-binding protein droplets, preventing them from phase transition to solid-like toxic aggregates.[8,40,44] Therefore, DNA and RNA are recognized as key components that play a crucial role in the control of intracellular LLPS.

Binary model systems consisting of anionic nucleic acids and cationic polypeptides including proteins and chemically synthesized polymers have been presented as an effective strategy to understand the LLPS mechanism that driven by the interactions of DNA or RNA with cationic polypeptides. Such model systems have the advantages of systematic control of the physicochemical properties of molecules and solution parameters, which leads to a deeper understanding of LLPS phenomena that are ambiguous in complex intracellular systems. For instance, the LLPS system of single- or double-stranded DNA and poly-l-lysine showed that sequence-dependent flexibility of the DNA strand affects phase behaviors.[45,46] The higher-order structure of RNA contribute to LLPS via specific and non-specific interactions with SARS-CoV2 nucleocapsid protein.[47] It has been also reported that chemical modifications of the side chains of polypeptides such as methylation,[48] phosphorylation,[49,50] and acetylation,[51] affect their phase behavior with nucleic acids. While it is generally believed that anionic nucleic acids induce LLPS mainly driven by non-specific electrostatic interactions with cationic polypeptides, previous studies have been suggested that not only the electrical

properties of nucleic acids and polypeptides but also their other physicochemical properties play an important role in the controlling LLPS. However, there is a substantial lack of knowledge about what properties of nucleic acids and polypeptides affect the phase behavior of multi-components mixtures, and therefore their LLPS mechanism is still a mystery.

1.4. Objective of this study

This thesis focused on the mechanisms of LLPS driven by the interactions between DNA and histone proteins involved in the chromatin organization, and systematically investigated the effect of the physicochemical properties of DNA and cationic polypeptides on the phase behavior using a binary system. Chapters 2 and 3 describe the effect of the chemical and higher-order structures of DNA on the LLPS with linker histone H1, respectively. Chapter 4 presents the effect of the acetylation site of histone H3 tail peptide on the phase behavior with DNA. Chapter 5 provides an overview, perspectives, and discussion of this study, and concludes with a summary of this thesis in Chapter 6.

1.5. References

(1) Zimmerman, S. B.; Trach, S. O. Estimation of Macromolecule Concentrations and Excluded Volume Effects for the Cytoplasm of Escherichia Coli. *J. Mol. Biol.* **1991**, *222* (3), 599–620.

(2) Knockenhauer, K. E.; Schwartz, T. U. The Nuclear Pore Complex as a Flexible and Dynamic Gate. *Cell* **2016**, *164* (6), 1162–1171.

(3) Yoshizawa, T.; Nozawa, R.-S.; Jia, T. Z.; Saio, T.; Mori, E. Biological Phase Separation: Cell Biology Meets Biophysics. *Biophys. Rev*. **2020**, *12* (2), 519–539.

(4) Babinchak, W. M.; Dumm, B. K.; Venus, S.; Boyko, S.; Putnam, A. A.; Jankowsky, E.; Surewicz, W. K. Small Molecules as Potent Biphasic Modulators of Protein Liquid-Liquid Phase Separation. *Nat. Commun.* **2020**, *11* (1), 5574.

(5) Brangwynne, C. P.; Eckmann, C. R.; Courson, D. S.; Rybarska, A.; Hoege, C.; Gharakhani, J.; Jülicher, F.; Hyman, A. A. Germline P Granules Are Liquid Droplets That Localize by Controlled Dissolution/Condensation. *Science* **2009**, *324* (5935), 1729–1732.

(6) Fare, C. M.; Villani, A.; Drake, L. E.; Shorter, J. Higher-Order Organization of Biomolecular Condensates. *Open Biol.* **2021**, *11* (6), 210137.

(7) Razin, S. V.; Gavrilov, A. A. The Role of Liquid–Liquid Phase Separation in the Compartmentalization of Cell Nucleus and Spatial Genome Organization. *Biochemistry (Mosc)* **2020**, *85* (6), 643–650.

(8) Hofmann, S.; Kedersha, N.; Anderson, P.; Ivanov, P. Molecular Mechanisms of Stress Granule Assembly and Disassembly. *Biochim. Biophys. Acta Mol. Cell Res.* **2021**, *1868* (1), 118876.

(9) Neugebauer, K. M. Special Focus on the Cajal Body. *RNA Biol.* **2017**, *14* (6), 669–670.

(10) Lafontaine, D. L. J.; Riback, J. A.; Bascetin, R.; Brangwynne, C. P. The Nucleolus as a Multiphase Liquid Condensate. *Nat. Rev. Mol. Cell Biol*. **2021**, *22* (3), 165–182.

(11) Strom, A. R.; Emelyanov, A. V.; Mir, M.; Fyodorov, D. V.; Darzacq, X.; Karpen, G. H. Phase Separation Drives Heterochromatin Domain Formation. *Nature* **2017**, *547* (7662), 241–245.

(12) Larson, A. G.; Elnatan, D.; Keenen, M. M.; Trnka, M. J.; Johnston, J. B.; Burlingame, A. L.; Agard, D. A.; Redding, S.; Narlikar, G. J. Liquid Droplet Formation by HP1α Suggests a Role for Phase Separation in Heterochromatin. *Nature* **2017**, *547* (7662), 236–240.

(13) Fox, A. H.; Nakagawa, S.; Hirose, T.; Bond, C. S. Paraspeckles: Where Long Noncoding RNA Meets Phase Separation. *Trends Biochem. Sci*. **2018**, *43* (2), 124–135.

(14) Franzmann, T. M.; Jahnel, M.; Pozniakovsky, A.; Mahamid, J.; Holehouse, A. S.; Nüske, E.; Richter, D.; Baumeister, W.; Grill, S. W.; Pappu, R. V.; Hyman, A. A.; Alberti, S. Phase Separation of a Yeast Prion Protein Promotes Cellular Fitness. *Science* **2018**, *359* (6371), eaao5654.

(15) Riback, J. A.; Katanski, C. D.; Kear-Scott, J. L.; Pilipenko, E. V.; Rojek, A. E.; Sosnick, T. R.; Drummond, D. A. Stress-Triggered Phase Separation Is an Adaptive, Evolutionarily Tuned Response. *Cell* **2017**, *168* (6), 1028–1040.e19.

(16) Kilic, S.; Lezaja, A.; Gatti, M.; Bianco, E.; Michelena, J.; Imhof, R.; Altmeyer, M. Phase Separation of 53BP1 Determines Liquid-like Behavior of DNA Repair Compartments. *EMBO J.* **2019**, *38* (16), e101379.

(17) Kato, M.; Yang, Y.-S.; Sutter, B. M.; Wang, Y.; McKnight, S. L.; Tu, B. P. Redox State Controls Phase Separation of the Yeast Ataxin-2 Protein via Reversible Oxidation of Its Methionine-Rich Low-Complexity Domain. *Cell* **2019**, *177* (3), 711–721.e8.

(18) Alberti, S. Phase Separation in Biology. *Curr. Biol.* **2017**, *27* (20), R1097–R1102.

(19) Riback, J. A.; Brangwynne, C. P. Can Phase Separation Buffer Cellular Noise? *Science* **2020**, *367* (6476), 364–365.

(20) O'Flynn, B. G.; Mittag, T. The Role of Liquid–Liquid Phase Separation in Regulating Enzyme Activity. *Curr. Opin. Cell Biol.* **2021**, *69*, 70–79.

(21) Ura T.; Tomita S.; Shiraki K. Dynamic Behavior of Liquid Droplets with Enzyme Compartmentalization Triggered by Sequential Glycolytic Enzyme Reactions. *Chem. Commun.* **2021**, *57* (93), 12544–12547.

(22) Yoshikawa M.; Yoshii T.; Ikuta M.; Tsukiji S. Synthetic Protein Condensates That Inducibly Recruit and Release Protein Activity in Living Cells. *J. Am. Chem. Soc.*, **2021**, *143* (17), 6434–6446.

(23) Larson, A. G.; Narlikar, G. J. The Role of Phase Separation in Heterochromatin Formation, Function, and Regulation. *Biochemistry* **2018**, *57* (17), 2540–2548.

(24) Sabari, B. R.; Dall'Agnese, A.; Boija, A.; Klein, I. A.; Coffey, E. L.; Shrinivas, K.; Abraham, B. J.; Hannett, N. M.; Zamudio, A. V.; Manteiga, J. C.; Li, C. H.; Guo, Y. E.; Day, D. S.; Schuijers, J.; Vasile, E.; Malik, S.; Hnisz, D.; Lee, T. I.; Cisse, I. I.; Roeder, R. G.; Sharp, P. A.; Chakraborty, A. K.; Young, R. A. Coactivator Condensation at Super-Enhancers Links Phase Separation and Gene Control. *Science* **2018**, *361* (6400), eaar3958.

(25) Hnisz, D.; Shrinivas, K.; Young, R. A.; Chakraborty, A. K.; Sharp, P. A. A Phase Separation Model for Transcriptional Control. *Cell* **2017**, *169* (1), 13–23.

(26) Prouteau, M.; Loewith, R. Regulation of Cellular Metabolism through Phase Separation of Enzymes. *Biomolecules* **2018**, *8* (4), 160.

(27) Wunder, T.; Mueller-Cajar, O. Biomolecular Condensates in Photosynthesis and Metabolism. *Curr. Opin. Plant Biol.* **2020**, *58*, 1–7.

(28) Su, X.; Ditlev, J. A.; Hui, E.; Xing, W.; Banjade, S.; Okrut, J.; King, D. S.; Taunton, J.; Rosen, M. K.; Vale, R. D. Phase Separation of Signaling Molecules Promotes T Cell Receptor Signal Transduction. *Science* **2016**, *352* (6285), 595–599.

(29) Du, M.; Chen, Z. J. DNA-Induced Liquid Phase Condensation of cGAS Activates Innate Immune Signaling. *Science* **2018**, *361* (6403), 704–709.

(30) Fujioka, Y.; Noda, N. N. Biomolecular Condensates in Autophagy Regulation. *Curr. Opin. Cell Biol.* **2021**, *69*, 23–29.

(31) Quiroz, F. G.; Fiore, V. F.; Levorse, J.; Polak, L.; Wong, E.; Pasolli, H. A.; Fuchs, E. Liquid-Liquid Phase Separation Drives Skin Barrier Formation. *Science* **2020**, *367* (6483), eaax9554.

(32) Spannl, S.; Tereshchenko, M.; Mastromarco, G. J.; Ihn, S. J.; Lee, H. O. Biomolecular Condensates in Neurodegeneration and Cancer. *Traffic* **2019**, *20* (12), 890–911.

(33) Boija, A.; Klein, I. A.; Young, R. A. Biomolecular Condensates and Cancer. *Cancer Cell* **2021**, *39* (2), 174–192.

(34) Ray, S.; Singh, N.; Kumar, R.; Patel, K.; Pandey, S.; Datta, D.; Mahato, J.; Panigrahi, R.; Navalkar, A.; Mehra, S.; Gadhe, L.; Chatterjee, D.; Sawner, A. S.; Maiti, S.; Bhatia, S.; Gerez, J. A.; Chowdhury, A.; Kumar, A.; Padinhateeri, R.; Riek, R.; Krishnamoorthy, G.; Maji, S. K. α-Synuclein Aggregation Nucleates through Liquid–Liquid Phase Separation. *Nat. Chem.* **2020**, *12* (8), 705–716.

(35) Patel, A.; Lee, H. O.; Jawerth, L.; Maharana, S.; Jahnel, M.; Hein, M. Y.; Stoynov, S.; Mahamid, J.; Saha, S.; Franzmann, T. M.; Pozniakovski, A.; Poser, I.; Maghelli, N.; Royer, L. A.; Weigert, M.; Myers, E. W.; Grill, S.; Drechsel, D.; Hyman, A. A.; Alberti, S. A Liquid-to-Solid Phase Transition of the ALS Protein FUS Accelerated by Disease Mutation. *Cell* **2015**, *162* (5), 1066–1077.

(36) Babinchak, W. M.; Haider, R.; Dumm, B. K.; Sarkar, P.; Surewicz, K.; Choi, J.-K.; Surewicz, W. K. The Role of Liquid--Liquid Phase Separation in Aggregation of the TDP-43 Low-Complexity Domain. *J. Biol. Chem.* **2019**, *294* (16), 6306–6317.

(37) Banani, S. F.; Rice, A. M.; Peeples, W. B.; Lin, Y.; Jain, S.; Parker, R.; Rosen, M. K. Compositional Control of Phase-Separated Cellular Bodies. *Cell* **2016**, *166* (3), 651–663.

(38) Das, S.; Lin, Y.-H.; Vernon, R. M.; Forman-Kay, J. D.; Chan, H. S. Comparative Roles of Charge, π, and Hydrophobic Interactions in Sequence-Dependent Phase Separation of Intrinsically Disordered Proteins. *Proc. Natl. Acad. Sci. U. S. A.* **2020**, *117* (46), 28795–28805.

(39) Dignon, G. L.; Best, R. B.; Mittal, J. Biomolecular Phase Separation: From Molecular Driving Forces to Macroscopic Properties. *Annu. Rev. Phys. Chem.* **2020**, *71*, 53–75.

(40) Elbaum-Garfinkle, S.; Kim, Y.; Szczepaniak, K.; Chen, C. C.-H.; Eckmann, C. R.; Myong, S.; Brangwynne, C. P. The Disordered P Granule Protein LAF-1 Drives Phase Separation into Droplets with Tunable Viscosity and Dynamics. *Proc. Natl. Acad. Sci. U. S. A.* **2015**, *112* (23), 7189–7194.

(41) Schuster, B. S.; Dignon, G. L.; Tang, W. S.; Kelley, F. M.; Ranganath, A. K.; Jahnke, C. N.; Simpkins, A.

G.; Regy, R. M.; Hammer, D. A.; Good, M. C.; Mittal, J. Identifying Sequence Perturbations to an Intrinsically Disordered Protein That Determine Its Phase-Separation Behavior. *Proc. Natl. Acad. Sci. U. S. A.* **2020**, *117* (21), 11421–11431.

(42) Boyko, S.; Qi, X.; Chen, T.-H.; Surewicz, K.; Surewicz, W. K. Liquid–Liquid Phase Separation of Tau Protein: The Crucial Role of Electrostatic Interactions. *J. Biol. Chem.* **2019**, *294* (29), 11054–11059.

(43) Martin, E. W.; Holehouse, A. S.; Peran, I.; Farag, M.; Incicco, J. J.; Bremer, A.; Grace, C. R.; Soranno, A.; Pappu, R. V.; Mittag, T. Valence and Patterning of Aromatic Residues Determine the Phase Behavior of Prion-like Domains. *Science* **2020**, *367* (6478), 694–699.

(44) Niaki, A. G.; Sarkar, J.; Cai, X.; Rhine, K.; Vidaurre, V.; Guy, B.; Hurst, M.; Lee, J. C.; Koh, H. R.; Guo, L.; Fare, C. M.; Shorter, J.; Myong, S. Loss of Dynamic RNA Interaction and Aberrant Phase Separation Induced by Two Distinct Types of ALS/FTD-Linked FUS Mutations. *Mol. Cell* **2020**, *77* (1), 82–94.e4.

(45) Shakya, A.; King, J. T. DNA Local-Flexibility-Dependent Assembly of Phase-Separated Liquid Droplets. *Biophys. J.* **2018**, *115* (10), 1840–1847.

(46) Vieregg, J. R.; Lueckheide, M.; Marciel, A. B.; Leon, L.; Bologna, A. J.; Rivera, J. R.; Tirrell, M. V. Oligonucleotide–Peptide Complexes: Phase Control by Hybridization. *J. Am. Chem. Soc.* **2018**, *140* (5), 1632–1638.

(47) Iserman, C.; Roden, C. A.; Boerneke, M. A.; Sealfon, R. S. G.; McLaughlin, G. A.; Jungreis, I.; Fritch, E. J.; Hou, Y. J.; Ekena, J.; Weidmann, C. A.; Theesfeld, C. L.; Kellis, M.; Troyanskaya, O. G.; Baric, R. S.; Sheahan, T. P.; Weeks, K. M.; Gladfelter, A. S. Genomic RNA Elements Drive Phase Separation of the SARS-CoV-2 Nucleocapsid. *Mol. Cell* **2020**, *80* (6), 1078–1091.e6.

(48) Tsang, B.; Arsenault, J.; Vernon, R. M.; Lin, H.; Sonenberg, N.; Wang, L.-Y.; Bah, A.; Forman-Kay, J. D. Phosphoregulated FMRP Phase Separation Models Activity-Dependent Translation through Bidirectional Control of mRNA Granule Formation. *Proc. Natl. Acad. Sci. U. S. A*. **2019**, *116* (10), 4218–4227.

(49) Aumiller, W. M., Jr; Keating, C. D. Phosphorylation-Mediated RNA/Peptide Complex Coacervation as a Model for Intracellular Liquid Organelles. *Nat. Chem.* **2016**, *8* (2), 129–137.

(50) Turner, A. L.; Watson, M.; Wilkins, O. G.; Cato, L.; Travers, A.; Thomas, J. O.; Stott, K. Highly Disordered Histone H1-DNA Model Complexes and Their Condensates. *Proc. Natl. Acad. Sci. U. S. A.* **2018**, *115* (47), 11964–11969.

(51) Wang, S.; Dai, T.; Qin, Z.; Pan, T.; Chu, F.; Lou, L.; Zhang, L.; Yang, B.; Huang, H.; Lu, H.; Zhou, F. Targeting Liquid–Liquid Phase Separation of SARS-CoV-2 Nucleocapsid Protein Promotes Innate Antiviral Immunity by Elevating MAVS Activity. *Nat. Cell Biol.* **2021**, *23* (7), 718–732.

Chapter 2.

Role of components of single-stranded DNA on liquid–liquid phase separation with cationic linker histone H1

2.1. Introduction

Liquid–liquid phase separation (LLPS) triggered by interactions between biomacromolecules has increasingly been recognized as a possible mechanism governing the formation of biomolecular condensates, such as germline P granules[1] and stress granules.[2] These condensates are often referred to as 'liquid droplets' due to their fluidic properties[1,3] and are distinct from the solid-like aggregates.[4] The fluidic properties of liquid droplets enable their reversible and rapid formation in response to various endogenous and exogenous changes in the intracellular environment, as well as the selective concentration or exclusion of particular biomolecules within the droplet phase and the dynamic exchange of biomolecules with the surrounding phase.[5] Therefore, liquid droplets are likely to serve as transient reaction compartments for a wide range of biological processes .[6,7]

Recently, biomolecular condensates between proteins and nucleic acids formed via LLPS have been proposed to be associated not only with the regulation of gene transcription,[8] DNA replication,[9] and DNA damage repair,[10] but also with the organization of specific chromatin domains.[11–13] Although the major factor in the formation of these condensates is the LLPS-prone proteins, the DNA itself is also critical in this event. For example, the droplet formation of heterochromatin protein HP1α is promoted by non-specific electrostatic interactions with DNA.[14] DNA binding is also essential for LLPS of the transcriptional repressor VRN1[15] and the chromatin component histone proteins.[12,16] In many of these examples, the interactions of DNA with nonstructural cationic polypeptide chains are subject to LLPS. The LLPS of cationic peptide-like polymers and nucleic acids proceeds via similar mechanisms, which has attracted attention in the context of investigating the origin of life, where it has been discussed in relation to the enrichment of substances[17] and the expression of catalytic activity during the primitive stages of the earth.[18] Given the potential diverse involvement of DNA in current and primitive biological LLPS, it is crucial to understand which properties of DNA are most involved in the process in order to elucidate the molecular mechanisms of biological LLPS.

LLPS systems of DNA/cationic polypeptides have been used to investigate the contribution of

physicochemical properties of DNA to phase separation. Examples include the use of poly-L-lysine and single- or double-stranded DNA, where differences in local flexibility, depending on DNA sequence and hybridization, have been shown to alter phase behavior.[19,20] To gain insight into the contribution of the chemical structure of DNA in LLPS, here, I examined the role of the constituent components of DNA, i.e., a phosphate group, a deoxyribose sugar, and a nucleobase, in LLPS with cationic polypeptide chains. Here, linker histone H1 (H1), which is a key regulator of chromatin condensation, was chosen as a model polypeptide. Spectroscopic and microscopic observations after mixing H1 with single-stranded DNA (ssDNA)-based oligomers in which one or more of the constituent components of DNA were removed showed that in addition to the expected electrostatic interactions between the anionic phosphate groups of the oligomers and the cationic residues of H1, interactions involving nucleobases and deoxyriboses promoted the generation of LLPS, increased the density of ssDNA in the formed droplets, and simultaneously decreased their fluidity under low-salt conditions. Furthermore, I found that microscopically distinguishable non-spherical assemblies were formed in solutions containing relatively high concentrations of H1 for all the oligomers, and that these assemblies contained both liquid-like mobile and solid-like immobile fractions. This study is thus expected to provide a basic understanding of the phase behavior of DNA/cationic polypeptide mixtures, and may contribute to elucidate, for example, the mechanism governing LLPS-mediated formation of various intracellular biomolecular condensates containing DNA and RNA and the significance of the chemical structure of nucleic acids from an evolutionary perspective.

2.2. Materials and methods

2.2.1. Materials

Tris-EDTA (TE) buffer [10 mM Tris-HCl; 1 mM EDTA; pH = 7.4] was obtained from Takara Bio Inc. (Shiga, Japan). Histone H1 (H1) from bovine thymus was obtained from Signal Chem (Richmond, BC, Canada). Prior to experiments, the buffer of the supplied H1 solution (1.0 mg/mL) was replaced with the TE buffer according to the previously reported procedure.[21] After the replacement, the concentration of H1 was determined from the absorbance at 280 nm using a NanoDrop One^{C} spectrophotometer (Thermo Fisher Scientific Inc., Waltham, MA, USA) and the molar extinction coefficient at 280 nm (4470 M^{-1} cm^{-1}) calculated by the ProtParam tool. The oligo-deoxyribonucleotides with carboxyfluorescein (FAM) at the 3′-terminus and abasic oligo-

deoxyribonucleotides with FAM at the 5′-terminus were synthesized by Eurofins Genomics (Ebersberg, Germany) and Nihon Gene Research Laboratories Inc. (Miyagi, Japan), respectively. The concentration of FAM-labeled oligomers was determined from the absorbance using the molar extinction coefficient of FAM at 490 nm (80,000 M^{-1} cm^{-1}) in Tris-HCl buffer (pH = 9.0).

2.2.2. Turbidity measurements

Turbidity measurements were performed using a spectrophotometer (UV-1800; Shimadzu Co., Tokyo, Japan). A solution (150 μL) containing 5.0 μM oligomer in TE buffer was placed in a 1 cm quartz cell and the absorbance at 500 nm was recorded at 25 °C. Subsequently, the absorbance was acquired consecutively after the addition of 0.2 μL aliquots of 300 μM H1 solution.

2.2.3. Phase-contrast microscopy imaging

To obtain the phase diagrams, solutions (20 μL) containing 1.0–10.0 μM oligomer and 1.0–10.0 μM H1 in TE buffer were prepared in the wells of a 384-well black clear-bottom microplate (Greiner Bio-One, Kremsmüster, Australia) using an Andrew+ liquid handling robot (Andrew Alliance SA, Geneva, Switzerland). After overnight incubation at room temperature with a lid to avoid evaporation, images of the solution were obtained using a phase-contrast microscope (Eclipse Ts2R, Nikon, Japan) equipped with a DS-Fi3 digital camera (Nikon, Japan). The process of fusion between the droplets was observed via time-lapse photography (increments: 0.1 ms) using a phase-contrast microscope after allowing solutions containing 5.0 μM oligomer and 2.5 or 7.5 μM H1 to incubate for 1 h at room temperature.

2.2.4. Fluorescence recovery after photobleaching (FRAP) measurements

Aliquots (50 μL) containing 10.0 μM FAM-labeled oligomer in TE buffer were mixed with solutions (50 μL) containing 5.0 μM or 15.0 μM H1 in TE buffer (pH = 7.4). After 4 h of incubation at room temperature, aliquots (50 μL) of the mixtures were placed on a cell-culture dish, and the samples were imaged using an Olympus FV1000 confocal microscope at 60× with an excitation wavelength of 488 nm. The 488 nm laser was applied to the region of interest at full power for 1.0 s, and the fluorescence recovery was then recorded for 40 s. The fluorescence intensity of the photobleached area was normalized relative to that of the unbleached area and the background. The time course of the normalized fluorescence intensity was fitted to a single exponential function (eq. 1) in order to obtain the recovery time τ.

$$f(t) = f_0 + A(1 - e^{-\frac{t}{\tau}}) \quad \text{(eq. 1)}$$

Where f_0 is the fluorescence intensity at the time of photobleaching, A is an arbitrary constant, and t is the time after photobleaching.

2.3. Results

2.3.1. Experimental design

The role of each constituent components of DNA in LLPS was investigated through the interactions of ssDNA-based oligomers with cationic polypeptide chains. For this purpose, I used a model system in which liquid droplets are formed by mixing linker histone H1 (H1) and ssDNAs (**Figure 2.1A**).[21–23] H1 has a long and a short cationic lysine-rich intrinsically disordered region (IDR) at its C- and N-terminus, respectively (**Figure 2.1B–D)**. The C-terminal IDR has been proposed to play an important role in the organization of chromatin domains via a LLPS process involving interactions with inter-nucleosome linker DNAs.[12,16] Four FAM-labeled 15-unit repeating oligomers consisting of different DNA components were selected as partners of H1 (**Figure 2.1E**): deoxyadenylic acid (oligo(pdA)), deoxythymidylic acid (oligo(pdT)), a deoxyribonucleotide lacking a nucleobase component (oligo(pd)), and a deoxyribonucleotide lacking both nucleobase and deoxyribose components (oligo(p)). These oligomers do not exhibit any specific conformation and have the same total charge and chain length. Thus, I assumed that any differences in the LLPS of these oligomers with H1 would be due to factors other than electrostatic interactions between the positively charged residues of H1 and the negatively charged phosphate groups of the oligomers. Throughout this study, the effects of each component were examined by comparing spectroscopic and microscopic results after mixing H1 and these oligomers at physiological pH (pH = 7.4) under salt-free conditions to maintain the interactions underlying the phase separation.

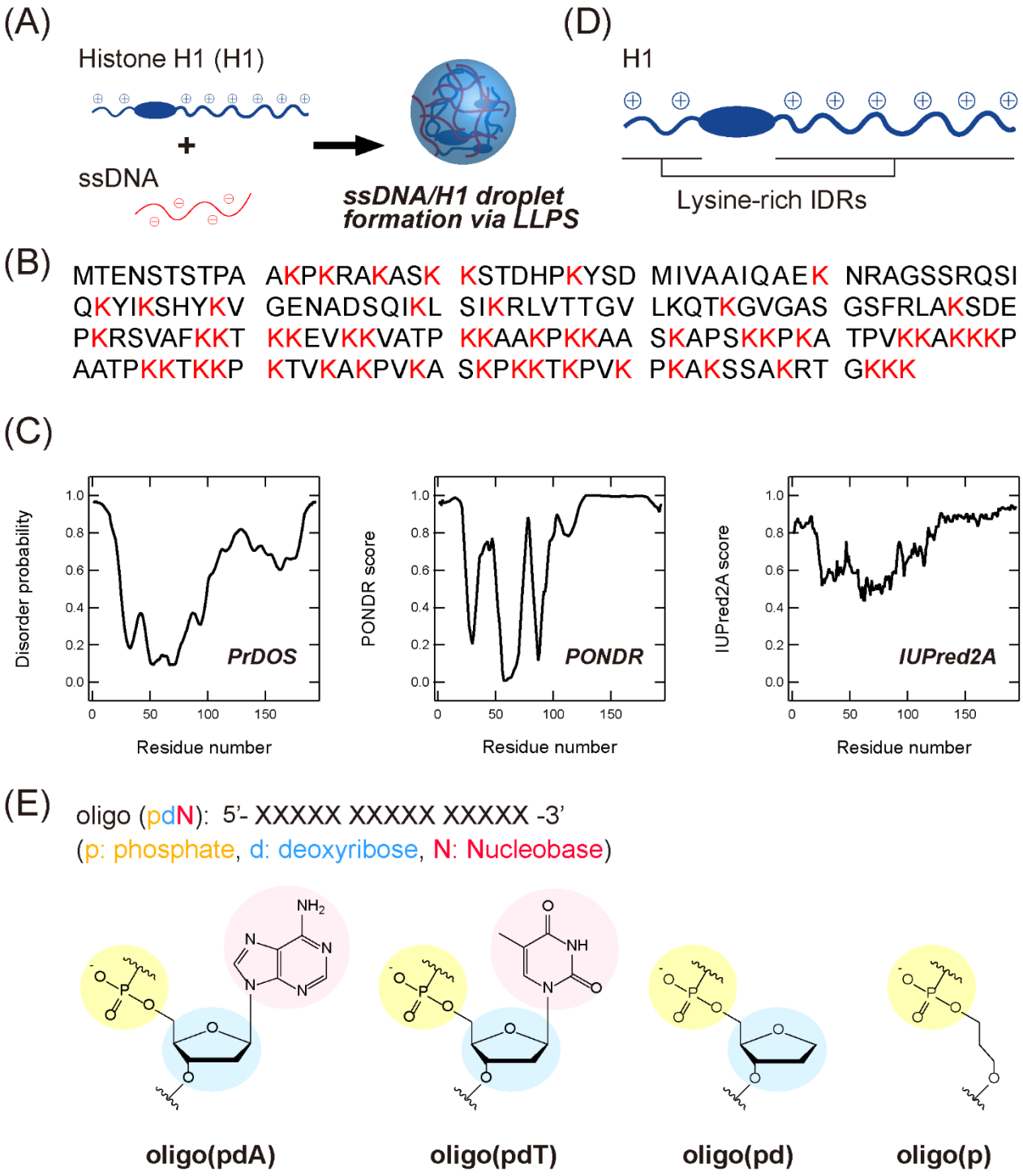

Figure 2.1. LLPS system and molecules used in this study. (A) Schematic illustration of droplet formation in ssDNA/H1 mixtures via LLPS. (B) Sequence of H1 from bovine thymus obtained from Uniprot code Q0IIJ2. (C) Disorder probability of the H1 sequence as predicted using (left) the Protein DisOrder prediction System (PrDOS),[24] (middle) Predictor of Natural Disordered Regions (PONDR),[25] and (right) IUPred2A.[26] Regions of the sequence that exhibit a score greater than 0.5 are defined as intrinsically disordered regions. (D) Structural drawing of histone H1 with lysine-rich IDRs at the N- and C-terminus. (E) Chemical structures of the ssDNA-based oligomers.

2.3.2. LLPS of mixtures of the ssDNA-based oligomers and H1

Initially, the contribution of each DNA component to LLPS was examined by measuring the changes in the turbidity of mixed solutions of the oligomers and H1. When H1 was titrated against solutions containing each of the oligomers (5.0 μM), all the solutions became turbid with increasing H1 concentration, indicating that oligomer/H1 assemblies were formed in all cases **(Figure 2.2)**. The decreases in turbidity that were observed with further increasing the H1 concentration were due to the destabilization of the assemblies by the excess cationic charges, which is often observed in the assembly of oppositely charged polymers and is referred to as the 'charge-inversion mechanism'.[27,28] The H1 concentration at which the maximum turbidity was observed varied slightly among the oligomers depending on whether they contained a nucleobase; this value was 3.0 μM for oligo(pdA) and oligo(pdT) and 2.5 μM for oligo(pd) and oligo(p). Interactions involving the nucleobases likely increased the number of H1 molecules that could bind to one oligomer, similarly to in a previous report.[29] The two nucleobase-containing oligomers exhibited similar maximum turbidity values, i.e., oligo(pdA) and oligo(pdT) both showed maximum turbidities nearly three times greater than those of oligo(pd) and oligo(p), suggesting that the nucleobase moieties may have increased the amount of ssDNA/H1 assemblies. In addition, I found that the solution was not completely transparent in the presence of excess H1 (>6.0 μM); instead, the turbidity gradually increased in a concentration-dependent manner above the charge-inversion threshold (*vide infra*).

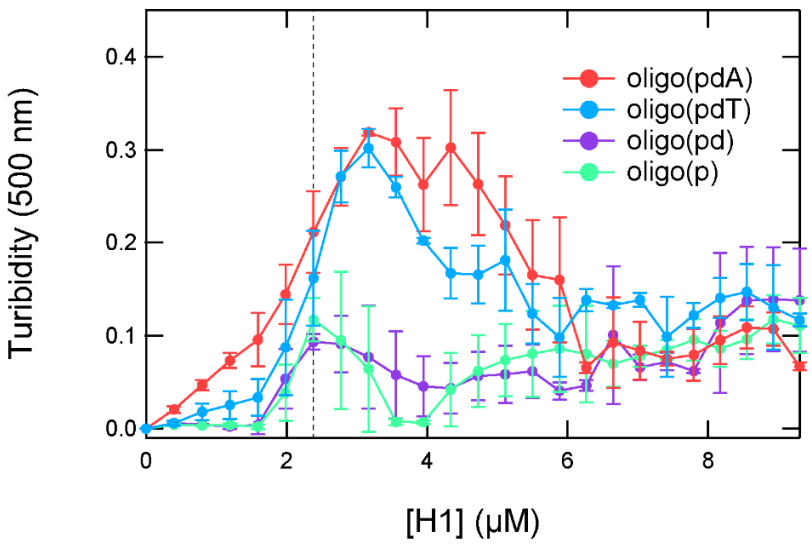

Figure 2.2. Turbidimetric titration curves of H1 against solutions containing 5.0 μM of the oligomers. All experiments were carried out in 10 mM Tris-EDTA buffer (pH = 7.4).

Phase-contrast microscopy images showed the formation of spherical assemblies in solutions containing 5.0 μM oligomer and 2.5 μM H1 (**Figure 2.3A**), i.e., at the H1 concentration where the oligomers without nucleobases exhibited their maximum turbidity (**Figure 2.2**). Consistent with the order of the maximum turbidity values, the oligomers with nucleobases formed larger assemblies than those without (**Figure 2.3B**). These assemblies rapidly fused within seconds upon contact (**Figure 2.4**). This highly fluidic behavior indicates that these assemblies are liquid droplets formed via LLPS.

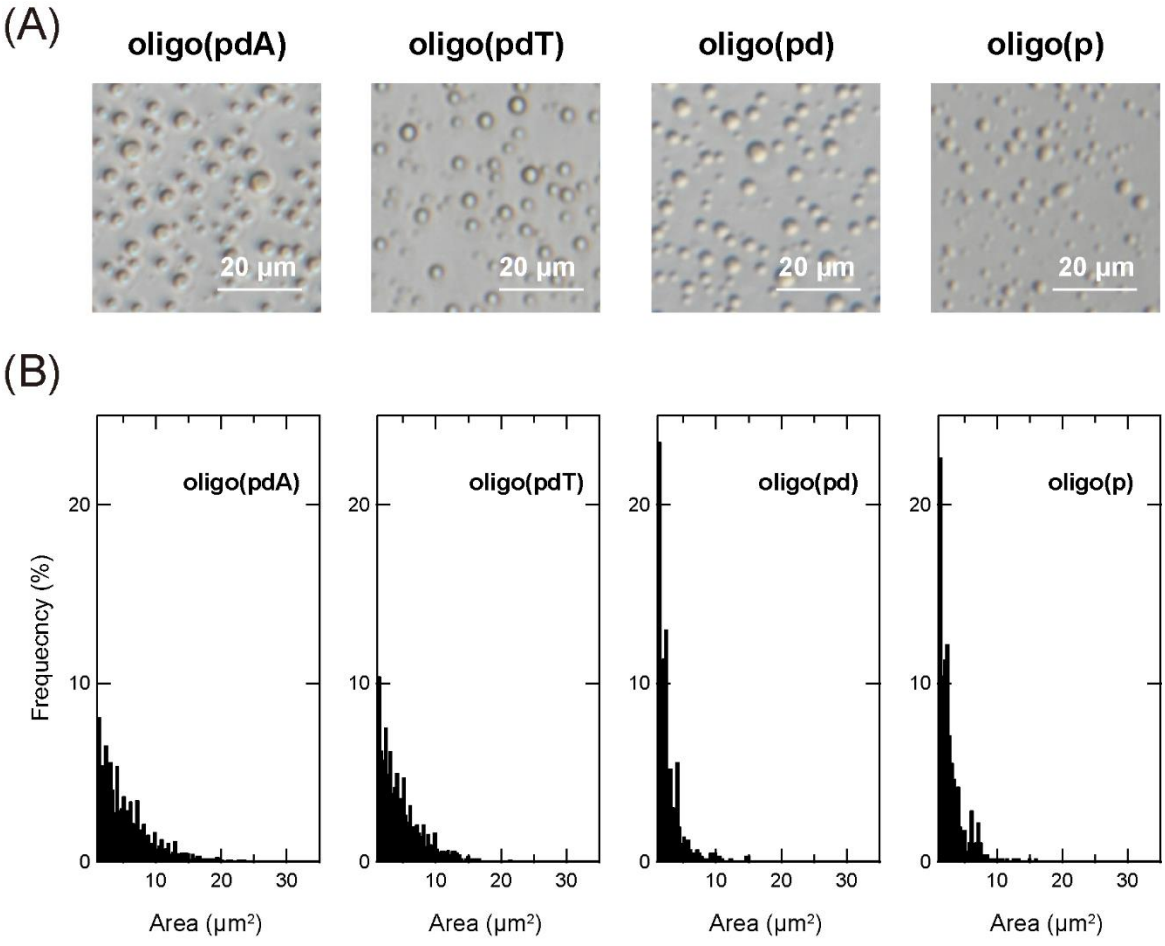

Figure 2.3. Spherical assembly formation by the oligomers and H1. (A) Phase-contrast microscopy images of the solutions under the conditions indicated by the dotted line in Figure 2.2 (5.0 μM oligomer and 2.5 μM H1); scale bar = 20 μm. (B) Size distribution of the spherical assemblies formed in the solutions containing the oligomers (5 μM) and H1 (2.5 μM). Values were obtained by analyzing the fluorescence-microscopy images using the image-processing software *image J*.

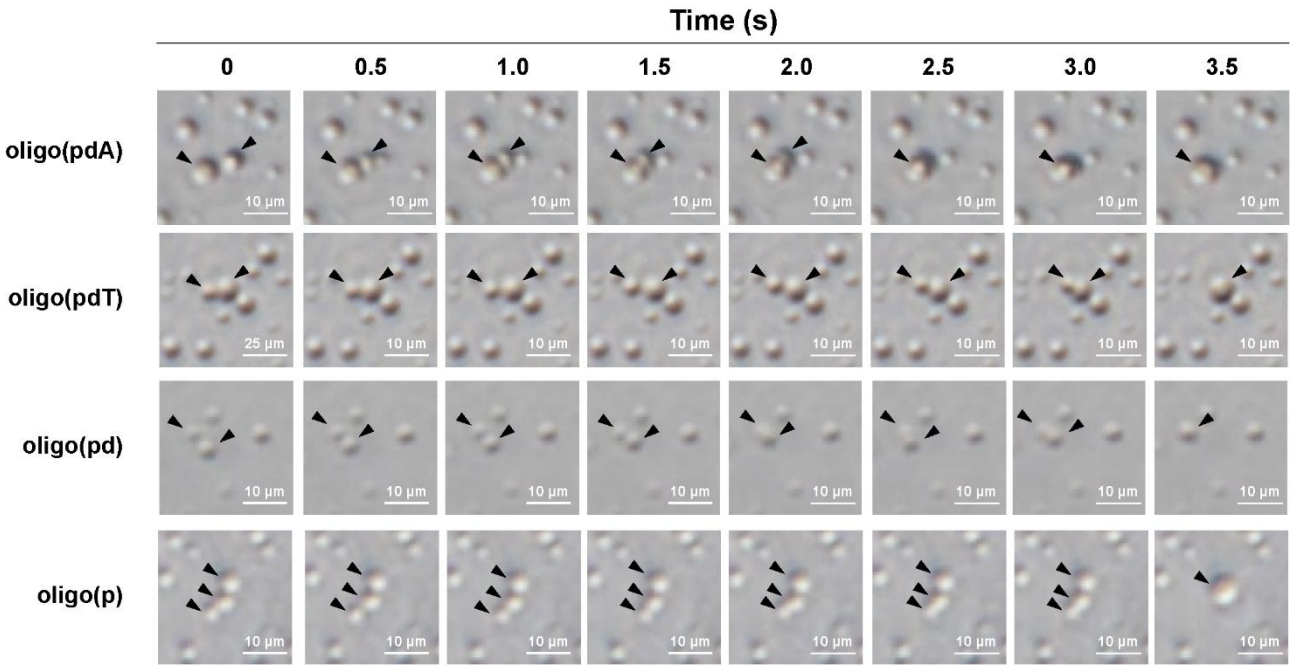

Figure 2.4. Fusion processes of the spherical assemblies formed in the solutions containing the oligomers (5 μM) and H1 (2.5 μM) observed using a phase-contrast microscope; scale bar = 10 μm.

Confocal fluorescence microscopy images confirmed that all the FAM-labeled oligomers were concentrated within the droplet (**Figure 2.5A**). Therefore, the motility of the oligomers within the droplets was compared using fluorescence recovery after photobleaching (FRAP) measurements.[30] The fluorescence intensity inside the droplet recovered within 30 seconds after photobleaching (**Figure 2.5B**), indicating dynamic diffusion of the oligomers within the droplets. The fluorescence recovery time decreased with increasing removal of DNA components [oligo(pdT) ≈ oligo(pdA) > oligo(pd) > oligo(p)]. The density of oligomers inside the droplets followed the same order (**Figure 2.5A**). Therefore, both the nucleobase and deoxyribose moieties likely function as regulators in increasing the density and decreasing the motility of ssDNAs inside droplets.

The phase diagrams for the concentrations of each molecule were constructed based on phase-contrast microscopy images to better understand the binary phase separation systems containing the various oligomers and H1 (**Figure 2.6A**). For all the oligomers, non-spherical assemblies were observed rather than the droplets, i.e., spherical assemblies, under some conditions. Both types of assemblies were the result of phase separation, but have been distinguished in the phase diagrams. Consistent with the turbidity measurements, the area of (i) LLPS and (ii) phase separation including spherical or non-spherical assemblies were larger for oligo(pdA) and

oligo(pdT) than for oligo(pd) and oligo(p). The critical concentration of H1, i.e., the minimum molecular concentration required for LLPS, exhibited a similar trend. Of the oligomers without nucleobases, oligo(pd) appeared to exhibit a slightly lower critical concentration of H1. For instance, 5.0 μM oligo(pd) underwent LLPS with 1.0 μM H1, while oligo(p) did not under the same conditions. These results indicate that not only the nucleobase moieties, but also the deoxyribose moiety, promote phase separation with H1.

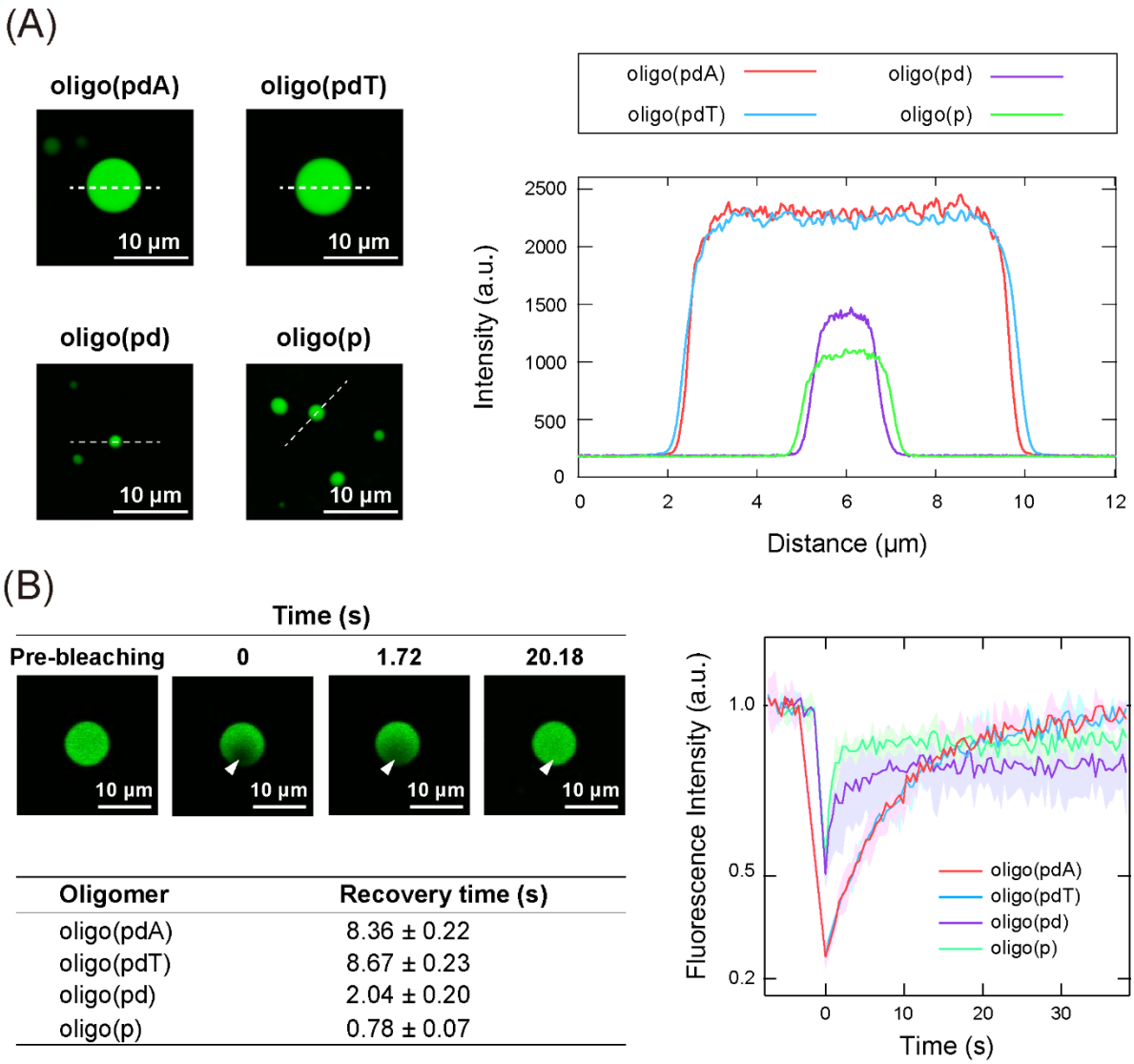

Oligomer	Recovery time (s)
oligo(pdA)	8.36 ± 0.22
oligo(pdT)	8.67 ± 0.23
oligo(pd)	2.04 ± 0.20
oligo(p)	0.78 ± 0.07

Figure 2.5. Distribution and motility of the oligomers inside the droplets. (A) Left: Confocal fluorescence microscopy images of the droplets formed by the oligomers (5 μM) and H1 (2.5 μM); scale bar = 10 μm. Right: Fluorescence intensities along the white dashed lines in each image in left panel. (B) Left: confocal fluorescence microscopic images during FRAP measurements. White arrowhead indicates the bleached area; scale bar = 10 μm. Right: FRAP recovery curves for the oligomers; values shown represent mean values ± standard deviation (n = 3). The table below shows the fluorescence recovery times calculated by single-exponential fitting.

2.3.3. Characterization of non-spherical assemblies formed between ssDNA-based oligomers and H1

The phase diagrams of the concentration of the oligomer vs. that of H1 revealed that non-spherical assemblies, rather than the spherical droplets (**Figure 2.3B**), were formed under certain solution conditions (**Figure 2.6B**). Interestingly, the non-spherical assemblies were only formed at relatively high concentrations of H1 for all the oligomers. For example, at the oligomer concentration used in the turbidity measurements (5.0 μM; **Figure 2.2**), the boundaries for non-spherical assembly formation were approximately 7.5 μM, 5.0 μM, 4.0 μM, and 4.0 μM of H1 for oligo(pdA), oligo(pdT), oligo(pd), and oligo(p), respectively (**Figure 2.6A**). Based on these results, the gradual increase after the decrease in turbidity at higher H1 concentrations (**Figure 2.2**) was attributed to the transition from spherical droplets to non-spherical assemblies. It should be noted here that spherical droplets were not formed at an oligomer concentration of 1.0 μM for the oligomers with nucleobases.

More specifically, when relatively low (2.5 μM) or high (7.5 μM) concentrations of H1 were mixed with 5.0 μM oligomer solutions, the circularity of the assemblies differed significantly, with values of ~0.9 and ~0.5, respectively, for all oligomers (**Figure 2.6C**). Since assemblies formed via LLPS exhibit a spherical morphology (i.e., the circularity is close to 1.0) to minimize their surface energy, the observed non-spherical assemblies are generally regarded as 'aggregates' formed via so-called liquid–solid phase separation.[1,31] Thus, the observed decrease in the circularity of the assemblies suggests a transition from liquid droplets to aggregates or gels. Such transitions have previously been observed in protein-[4,32] and DNA-related assemblies.[20] As a related example, liquid droplets of the protein HP1α on heterochromatin domains decrease in circularity as the cell cycle progresses, and the internal molecules become immobile.[33] In light of these phenomena, I further examined whether the observed non-spherical assemblies of the ssDNA-based oligomers and H1 also have aggregate-like properties.

Time-lapse images of the collision process of the non-spherical assemblies showed that none of the oligomer/H1 assemblies fused via so-called Ostwald ripening,[34] but instead simply remained adsorbed while retaining their shape (**Figure 2.7**). There was therefore a possibility that the non-spherical assemblies had gel- or aggregate-like properties, unlike the spherical droplets, which can fuse rapidly (**Figure 2.4**).

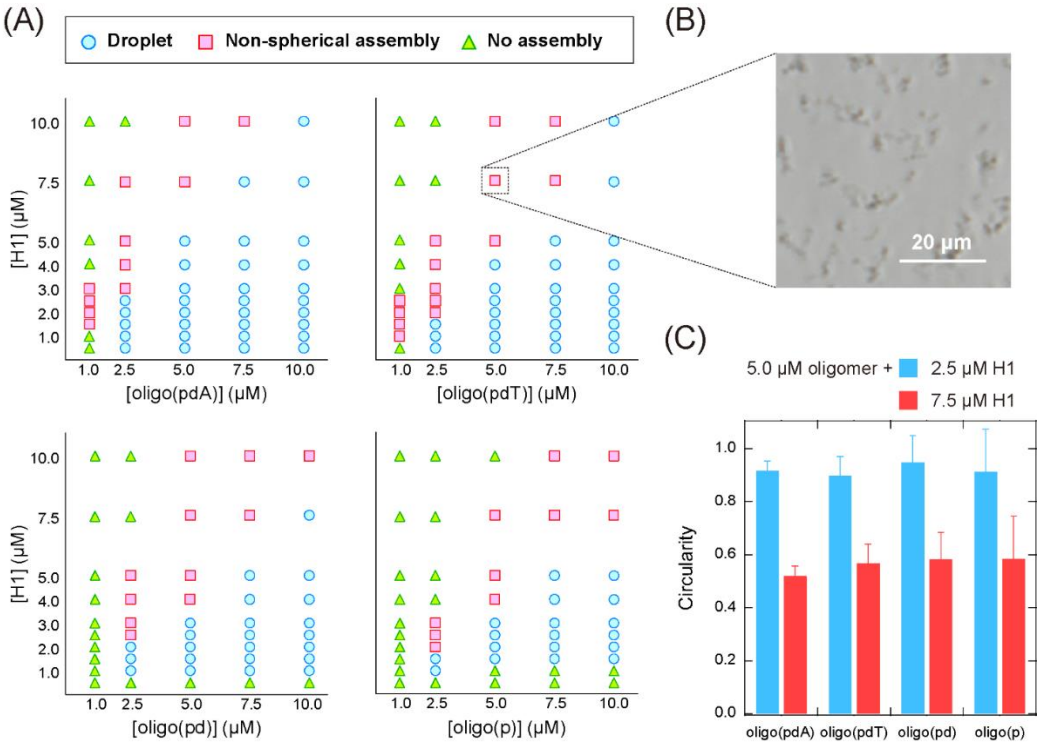

Figure 2.6. (A) Phase diagrams of aqueous mixtures of oligomers and H1. (B) Phase-contrast microscopy image of typical non-spherical assemblies; 5.0 μM poly(pdT) and 7.5 μM H1; scale bar = 20 μm. (C) Circularity of the assemblies formed in solutions containing 5.0 μM oligomer and 2.5 or 7.5 μM H1. The values were obtained by analyzing the fluorescence microscopy images of the solutions under the indicated conditions using the image processing software *image J*.

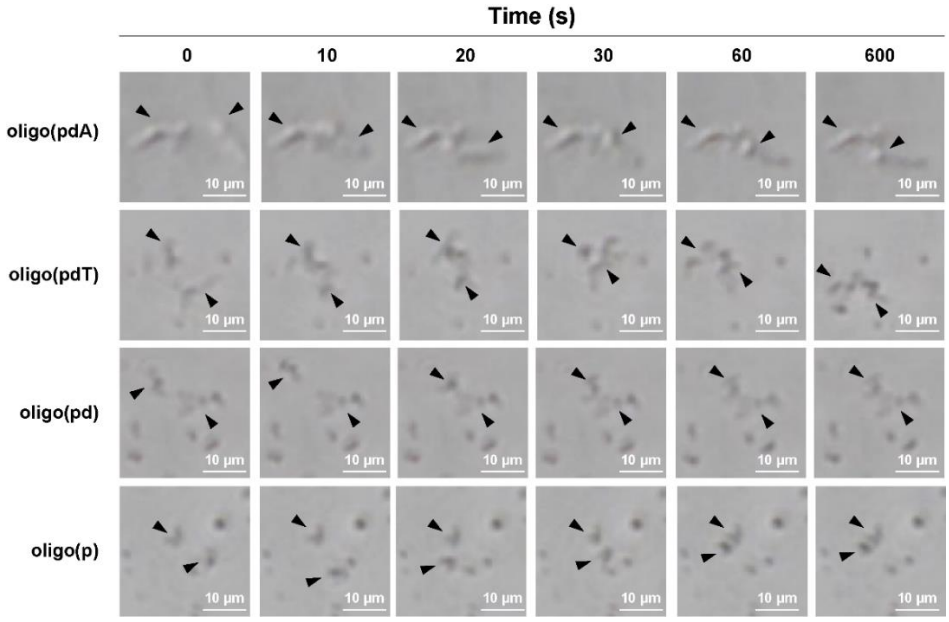

Figure 2.7. Collision processes of the non-spherical assemblies formed in the solutions containing oligomers (5 μM) and H1 (7.5 μM) observed by phase-contrast microscopy; scale bar = 10 μm.

Confocal fluorescence microscopy images of the non-spherical assemblies revealed a cluster-like morphology, which consisted of many small near-spherical particulates (2–3 μm in diameter) adhered to one another (**Figure 2.8**), as have been seen for protein–polyelectrolyte complexes or protein aggregates.[35–37] FRAP measurements were then carried out on these assemblies to investigate the fluidity of the internal oligomers. Unexpectedly, the fluorescence of the photobleached region of the assemblies was recovered over time (**Figure 2.8**). The degree of fluorescence recovery, i.e., the mobile fraction,[38] was about 50% regardless of the oligomer structure. Interestingly, the calculated fluorescence recovery times were comparable to those of the spherical droplets (**Figure 2.5B**), although no clear trend with regard to the presence or absence of DNA components could be discerned (**Figure 2.8B**). These FRAP results suggest that a fraction of the oligomers inside the small particulates diffuse like in the spherical droplets; consistent with this result, the non-spherical assemblies dissolved upon adding salt (**Figure 2.9**). The remaining immobile solid-like fraction may have prevented the fusion of the small particulates, but diffusion of the oligomers may be possible between the adhered particulates, as has been observed in protein–RNA condensates.[39]

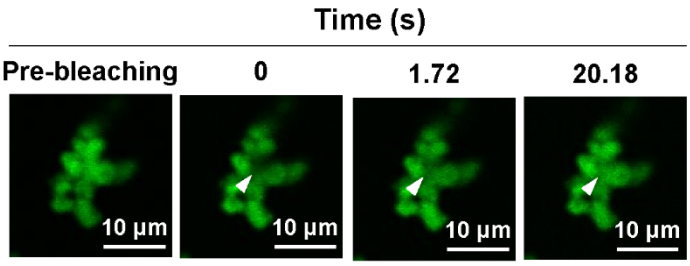

Oligomer	Recovery time (s)
oligo(pdA)	6.80 ± 0.43
oligo(pdT)	17.72 ± 1.02
oligo(pd)	2.95 ± 0.46
oligo(p)	6.64 ± 0.60

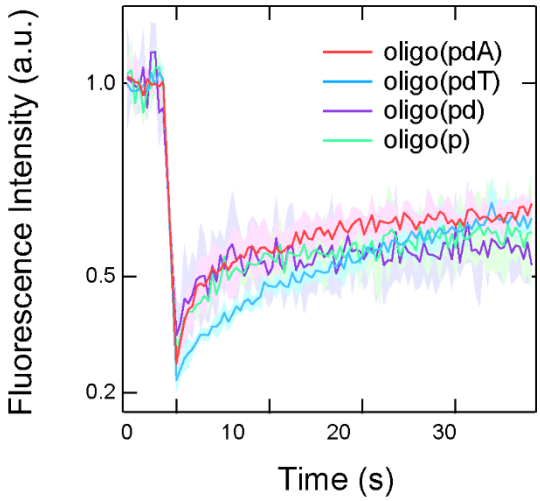

Figure 2.8. Physical properties of the non-spherical assemblies. Left: confocal fluorescence microscopy images during the FRAP measurements. White arrowheads indicate the bleached areas; scale bar = 10 μm. Right: FRAP recovery curves for the oligomers; values shown represent mean values ± standard deviation (n = 3). The table below lists the fluorescence-recovery times calculated by single-exponential fitting.

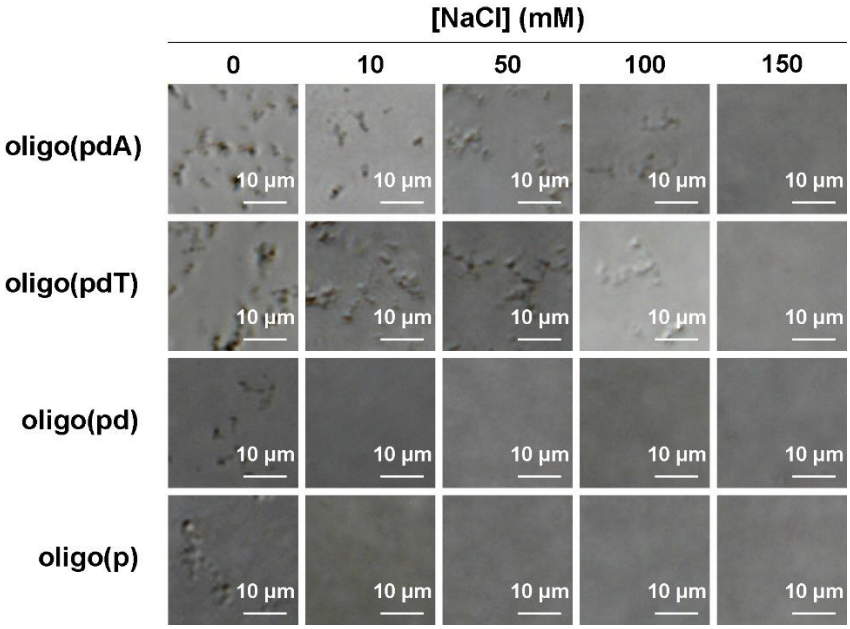

Figure 2.9. Effect of adding NaCl (0-150 mM) on the formation/dissolution of non-spherical assemblies in the solutions containing oligomers (5.0 μM) and H1 (7.5 μM) observed by phase-contrast microscopy; scale bar = 10 μm.

2.4. Discussion

In this study, I showed that the constituent components of DNA, i.e., nucleobase and deoxyribose moieties, as well as anionic phosphate groups, promote both liquid–liquid and liquid–solid phase separation with cationic histone H1. When liquid droplets are formed, these moieties regulate the density and motility of the ssDNAs inside the droplet. In the following sections, I discuss the mechanisms by which phase separation occurs and the biological significance of the phase-separation state in terms of the DNA components.

2.4.1. Interactions between each DNA component and H1 in the promotion of LLPS

A comparison of the four model oligomers with different DNA components but the same charge revealed that the nucleobase components markedly promoted LLPS with H1. Electrostatic interactions are the primary driving force for biological LLPS,[40] including that of the duplex DNA/H1 system[23]; however, interactions related to π-electrons are also significant. For example, π–π interactions also play a major role in the formation of various biomolecular condensates.[41,42] It is therefore plausible that π–π interactions between the aromatic amino acids of H1 (3 Tyr and 2 Phe in 194 aa; for the sequence of H1, see **Figure 2.1B**) and the nucleobases

and/or those between nucleobases promoted LLPS, as has been previously suggested.[21] Cation–π interactions may also be involved.[42,43] H1 contains 55 Lys and 7 Arg residues. Although cation–π interactions related to biological LLPS are often mediated by Arg, Lys can also promote LLPS with nucleobases via cation–π interactions.[22,44] These π-electron-related interactions should be responsible for the high LLPS potential of the nucleobase components of DNA.

The introduction of the deoxyribose moiety into the phosphate groups of oligo(p) also slightly promoted phase separation with H1 (**Figure 2.6A**). The deoxyribose in DNA tends to exhibit van der Waals interactions with amino acids such as Lys, Thr, and Ser,[45] which are abundant in H1. In addition, sugar–π interactions between deoxyribose sugars and amino acids are found in the crystal structures of protein–DNA complexes,[46] and thus, this type of interactions could potentially promote the LLPS of DNA/H1 mixtures. Another possibility is that since changes in the flexibility of DNA contribute entropically to LLPS with cationic polymers,[19,20] an increase in DNA rigidity due to the introduction of the deoxyribose moieties may also be involved.

2.4.2. Physical properties of the assemblies and their possible relevance to biological events

In the phase-separation systems of the DNA-based oligomers and H1, spherical droplets were formed via LLPS when the concentration of H1 was relatively low compared to that of the oligomers, while relatively high concentrations of H1 induced the formation of non-spherical assemblies. When droplets were formed, the presence of nucleobase and deoxyribose moieties increased the density and decreased the diffusion rate of the oligomers inside the droplets (**Figure 2.5**). These were correlated with the effect of the moieties on the critical concentration at which LLPS occurs (**Figure 2.6A**).

The non-spherical assemblies are more complicated. The cluster-like assemblies, which were formed via the adhesion of small near-spherical particulates, did not undergo fusion upon contact (**Figure 2.7**); similar phenomena have been observed in chromatin[47] and RNA condensates with gel-like properties.[48] Although these assemblies appear to exhibit solid-like properties, FRAP measurements demonstrated that they consist in part of liquid-like mobile fractions (**Figure 2.8**). The cell nucleus contains loosely condensed euchromatin regions where gene transcription is active and highly condensed heterochromatin regions where it is inactive. As the depletion of H1 triggers chromatin de-condensation in the nucleus, H1 is thought to play an integral role in heterochromatin formation.[49,50] The addition of H1 to nucleosome array droplets reduces their fluidity,

resulting in heterochromatin-like properties.[12] Taking these facts into account, H1 may form immobilized fractions by reducing the fluidity of DNA-containing droplets in a concentration-dependent manner, as observed in this study. The IDR at the N-terminus of H1 does not have a high affinity for chromatin, but does toward heterochromatin proteins.[51,52] This difference in affinity may cause local deviations in the concentration of H1 in the nucleus and subsequent interaction of the C-terminal IDR with DNA, possibly contributing to the formation of cluster-like heterochromatin.

The results of the present study suggest that the constituent components of DNA may commonly promote phase separation with cationic polypeptide chains related to biological LLPS. However, in general, the experiments of this study were performed under low-ionic-strength conditions to facilitate the observation of phase separation. Therefore, it could be argued that evidence is still insufficient to support a strong case for a direct relationship with biological events as described above. Although electrostatic interactions are weakened at high ionic strength, which often leads to a dissolution of the liquid droplets, phase separation can occur if the concentrations of DNA and proteins are sufficiently high or if a crowded environment, such as the inside of a cell, is reproduced.[53] Under conditions where such electrostatic interactions are suppressed, the contribution of uncharged components revealed in this study may become high in comparison. Nevertheless, the states of phase separation, such as the droplets or non-spherical assemblies, should be governed by the balance of interactions, and therefore, studies under conditions closer to the physiological environment should be conducted to provide a more accurate understanding.

Chemical modifications of biomolecules involved in the epigenetics, such as post-translational modifications[12,54] and DNA modifications,[55] have been shown to regulate the biological LLPS and prebiotic-relevant coacervation.[56] The strategies to systematically design constituent units through chemical approaches can be expected to provide valuable insights into the complicated phase-separation mechanisms of biomacromolecules, which are polymer chains of amino acids and nucleic acids composed of diverse elements.

2.5. Conclusions

In summary, this study using single-stranded DNA-based oligomers in which one or more of the constituent DNA components had been removed revealed that the nucleobase and deoxyribose DNA moieties (i) promote the LLPS with H1 and (ii) control the motility and density of the oligomers inside the droplets under low-salt

conditions. In addition, I observed the formation of non-spherical assemblies with mobile and immobile fractions when the concentration of H1 was higher than that of the oligomers, which could potentially be related to the role of H1 in chromatin organization. This study may thus provide fundamental insight into the formation mechanisms of various biomolecular condensates containing nucleic acids, such as chromatin, and may also contribute to the understanding of biomacromolecules in the context of the origin of life.

2.6. References

(1) Brangwynne, C. P.; Eckmann, C. R.; Courson, D. S.; Rybarska, A.; Hoege, C.; Gharakhani, J.; Jülicher, F.; Hyman, A. A. Germline P Granules Are Liquid Droplets That Localize by Controlled Dissolution/Condensation. *Science* **2009**, *324* (5935), 1729–1732.

(2) Boeynaems, S.; Alberti, S.; Fawzi, N. L.; Mittag, T.; Polymenidou, M.; Rousseau, F.; Schymkowitz, J.; Shorter, J.; Wolozin, B.; Van Den Bosch, L.; Tompa, P.; Fuxreiter, M. Protein Phase Separation: A New Phase in Cell Biology. *Trends Cell Biol.* **2018**, *28* (6), 420–435.

(3) Uversky, V. N. Intrinsically Disordered Proteins in Overcrowded Milieu: Membrane-Less Organelles, Phase Separation, and Intrinsic Disorder. *Curr. Opin. Struct. Biol.* **2017**, *44*, 18–30.

(4) Patel, A.; Lee, H. O.; Jawerth, L.; Maharana, S.; Jahnel, M.; Hein, M. Y.; Stoynov, S.; Mahamid, J.; Saha, S.; Franzmann, T. M.; Pozniakovski, A.; Poser, I.; Maghelli, N.; Royer, L. A.; Weigert, M.; Myers, E. W.; Grill, S.; Drechsel, D.; Hyman, A. A.; Alberti, S. A Liquid-to-Solid Phase Transition of the ALS Protein FUS Accelerated by Disease Mutation. *Cell* **2015**, *162* (5), 1066–1077.

(5) Nakashima, K. K.; Vibhute, M. A.; Spruijt, E. Biomolecular Chemistry in Liquid Phase Separated Compartments. *Front. Mol. Biosci.* **2019**, *6*, 21.

(6) Kamimura, Y. R.; Kanai, M. Chemical Insights into Liquid-Liquid Phase Separation in Molecular Biology. *Bull. Chem. Soc. Jpn.* **2021**, *94* (3), 1045–1058.

(7) Yoshizawa, T.; Nozawa, R.-S.; Jia, T. Z.; Saio, T.; Mori, E. Biological Phase Separation: Cell Biology Meets Biophysics. *Biophys. Rev.* **2020**, *12* (2), 519–539.

(8) Hnisz, D.; Shrinivas, K.; Young, R. A.; Chakraborty, A. K.; Sharp, P. A. A Phase Separation Model for Transcriptional Control. *Cell* **2017**, *169* (1), 13–23.

(9) Parker, M. W.; Bell, M.; Mir, M.; Kao, J. A.; Darzacq, X.; Botchan, M. R.; Berger, J. M. A New Class of

Disordered Elements Controls DNA Replication through Initiator Self-Assembly. *eLife* **2019**, *8*, e48562.

(10) Laflamme, G.; Mekhail, K. Biomolecular Condensates as Arbiters of Biochemical Reactions inside the Nucleus. *Commun. Biol.* **2020**, *3* (1), 773.

(11) Erdel, F.; Rippe, K. Formation of Chromatin Subcompartments by Phase Separation. *Biophys. J.* **2018**, *114* (10), 2262–2270.

(12) Gibson, B. A.; Doolittle, L. K.; Schneider, M. W. G.; Jensen, L. E.; Gamarra, N.; Henry, L.; Gerlich, D. W.; Redding, S.; Rosen, M. K. Organization of Chromatin by Intrinsic and Regulated Phase Separation. *Cell* **2019**, *179* (2), 470-484.e21.

(13) Larson, A. G.; Narlikar, G. J. The Role of Phase Separation in Heterochromatin Formation, Function, and Regulation. *Biochemistry* **2018**, *57* (17), 2540–2548.

(14) Larson, A. G.; Elnatan, D.; Keenen, M. M.; Trnka, M. J.; Johnston, J. B.; Burlingame, A. L.; Agard, D. A.; Redding, S.; Narlikar, G. J. Liquid Droplet Formation by HP1α Suggests a Role for Phase Separation in Heterochromatin. *Nature* **2017**, *547* (7662), 236–240.

(15) Zhou, H.; Song, Z.; Zhong, S.; Zuo, L.; Qi, Z.; Qu, L.; Lai, L. Mechanism of DNA-induced Phase Separation for Transcriptional Repressor VRN1. *Angew. Chem. Int. Ed. Engl*. **2019**, *58* (15), 4858-4862.

(16) Shakya, A.; Park, S.; Rana, N.; King, J. T. Liquid-Liquid Phase Separation of Histone Proteins in Cells: Role in Chromatin Organization. *Biophys. J.* **2020**, *118* (3), 753–764.

(17) Poudyal, R. R.; Pir Cakmak, F.; Keating, C. D.; Bevilacqua, P. C. Physical Principles and Extant Biology Reveal Roles for RNA-Containing Membraneless Compartments in Origins of Life Chemistry. *Biochemistry* **2018**, *57* (17), 2509–2519.

(18) Poudyal, R. R.; Guth-Metzler, R. M.; Veenis, A. J.; Frankel, E. A.; Keating, C. D.; Bevilacqua, P. C. Template-Directed RNA Polymerization and Enhanced Ribozyme Catalysis inside Membraneless Compartments Formed by Coacervates. *Nat. Commun.* **2019**, *10* (1), 490.

(19) Shakya, A.; King, J. T. DNA Local-Flexibility-Dependent Assembly of Phase-Separated Liquid Droplets. *Biophys. J.* **2018**, *115* (10), 1840–1847.

(20) Vieregg, J. R.; Lueckheide, M.; Marciel, A. B.; Leon, L.; Bologna, A. J.; Rivera, J. R.; Tirrell, M. V. Oligonucleotide–Peptide Complexes: Phase Control by Hybridization. *J. Am. Chem. Soc.* **2018**, *140* (5), 1632–1638.

(21) Mimura, M.; Tomita, S.; Shinkai, Y.; Hosokai, T.; Kumeta, H.; Saio, T.; Shiraki, K.; Kurita, R. Quadruplex Folding Promotes the Condensation of Linker Histones and DNAs via Liquid-Liquid Phase Separation. *J. Am. Chem. Soc.* **2021**, *143* (26), 9849–9857.

(22) Shakya, A.; King, J. T. Non-Fickian Molecular Transport in Protein–DNA Droplets. *ACS Macro Lett.* **2018**, *7* (10), 1220–1225.

(23) Turner, A. L.; Watson, M.; Wilkins, O. G.; Cato, L.; Travers, A.; Thomas, J. O.; Stott, K. Highly Disordered Histone H1-DNA Model Complexes and Their Condensates. *Proc. Natl. Acad. Sci. U. S. A.* **2018**, *115* (47), 11964-11969.

(24) Ishida, T.; Kinoshita, K. PrDOS: Prediction of Disordered Protein Regions from Amino Acid Sequence. *Nucleic Acids Res.* **2007**, *35*, W460-464.

(25) Linding, R.; Jensen, L. J.; Diella, F.; Bork, P.; Gibson, T. J.; Russell, R. B. Protein Disorder Prediction: Implications for Structural Proteomics. *Structure* **2003**, *11* (11), 1453–1459.

(26) Mészáros, B.; Erdős, G.; Dosztányi, Z. IUPred2A: Context-Dependent Prediction of Protein Disorder as a Function of Redox State and Protein Binding. *Nucleic Acids Res.* **2018**, *46* (W1), W329–W337.

(27) Nguyen, T. T.; Rouzina, I.; Shklovskii, B. I. Reentrant Condensation of DNA Induced by Multivalent Counterions. *J. Chem. Phys.* **2000**, *112* (5), 2562–2568.

(28) Banerjee, P. R.; Milin, A. N.; Moosa, M. M.; Onuchic, P. L.; Deniz, A. A. Reentrant Phase Transition Drives Dynamic Substructure Formation in Ribonucleoprotein Droplets. *Angew. Chem. Int. Ed. Engl.* **2017**, *56* (38), 11354–11359.

(29) Chollakup, R.; Smitthipong, W.; Eisenbach, C. D.; Tirrell, M. Phase Behavior and Coacervation of Aqueous Poly(Acrylic Acid)−Poly(Allylamine) Solutions. *Macromolecules* **2010**, *43* (5), 2518–2528.

(30) Taylor, N. O.; Wei, M.-T.; Stone, H. A.; Brangwynne, C. P. Quantifying Dynamics in Phase-Separated Condensates Using Fluorescence Recovery after Photobleaching. *Biophys. J.* **2019**, *117* (7), 1285–1300.

(31) Yamasaki, A.; Alam, J. M.; Noshiro, D.; Hirata, E.; Fujioka, Y.; Suzuki, K.; Ohsumi, Y.; Noda, N. N. Liquidity Is a Critical Determinant for Selective Autophagy of Protein Condensates. *Mol. Cell* **2020**, *77* (6), 1163-1175.e9.

(32) Matsuda, A.; Mimura, M.; Maruyama, T.; Kurinomaru, T.; Shiuhei, M.; Shiraki, K. Liquid Droplet of Protein-Polyelectrolyte Complex for High-Concentration Formulations. *J. Pharm. Sci.* **2018**, *107* (10),

2713–2719.

(33) Strom, A. R.; Emelyanov, A. V.; Mir, M.; Fyodorov, D. V.; Darzacq, X.; Karpen, G. H. Phase Separation Drives Heterochromatin Domain Formation. *Nature* **2017**, *547* (7662), 241–245.

(34) Voorhees, P. W. Ostwald Ripening of Two-Phase Mixtures. *Annu. Rev. Mater. Sci.* **1992**, *22* (1), 197–215.

(35) Krebs, M. R. H.; Devlin, G. L.; Donald, A. M. Protein Particulates: Another Generic Form of Protein Aggregation? *Biophys. J.* **2007**, *92* (4), 1336–1342.

(36) Cousin, F.; Gummel, J.; Combet, S.; Boué, F. The Model Lysozyme–PSSNa System for Electrostatic Complexation: Similarities and Differences with Complex Coacervation. *Adv. Colloid Interface Sci.* **2011**, *167* (1–2), 71–84.

(37) Tomita, S.; Yoshikawa, H.; Shiraki, K. Arginine Controls Heat-Induced Cluster-Cluster Aggregation of Lysozyme at around the Isoelectric Point. *Biopolymers* **2011**, *95* (10), 695–701.

(38) Zhu, L.; Richardson, T. M.; Wacheul, L.; Wei, M.-T.; Feric, M.; Whitney, G.; Lafontaine, D. L. J.; Brangwynne, C. P. Controlling the Material Properties and rRNA Processing Function of the Nucleolus Using Light. *Proc. Natl. Acad. Sci. U. S. A.* **2019**, *116* (35), 17330–17335.

(39) Boeynaems, S.; Holehouse, A. S.; Weinhardt, V.; Kovacs, D.; Van Lindt, J.; Larabell, C.; Van Den Bosch, L.; Das, R.; Tompa, P. S.; Pappu, R. V.; Gitler, A. D. Spontaneous Driving Forces Give Rise to Protein-RNA Condensates with Coexisting Phases and Complex Material Properties. *Proc. Natl. Acad. Sci. U. S. A.* **2019**, *116* (16), 7889–7898.

(40) Boyko, S.; Qi, X.; Chen, T.-H.; Surewicz, K.; Surewicz, W. K. Liquid–Liquid Phase Separation of Tau Protein: The Crucial Role of Electrostatic Interactions. *J. Biol. Chem.* **2019**, *294* (29), 11054–11059.

(41) Vernon, R. M.; Chong, P. A.; Tsang, B.; Kim, T. H.; Bah, A.; Farber, P.; Lin, H.; Forman-Kay, J. D. Pi-Pi Contacts Are an Overlooked Protein Feature Relevant to Phase Separation. *eLife* **2018**, *7*, e31486.

(42) Chong, P. A.; Vernon, R. M.; Forman-Kay, J. D. RGG/RG Motif Regions in RNA Binding and Phase Separation. *J. Mol. Biol.* **2018**, *430* (23), 4650–4665.

(43) Qamar, S.; Wang, G.; Randle, S. J.; Ruggeri, F. S.; Varela, J. A.; Lin, J. Q.; Phillips, E. C.; Miyashita, A.; Williams, D.; Ströhl, F.; Meadows, W.; Ferry, R.; Dardov, V. J.; Tartaglia, G. G.; Farrer, L. A.; Kaminski Schierle, G. S.; Kaminski, C. F.; Holt, C. E.; Fraser, P. E.; Schmitt-Ulms, G.; Klenerman, D.; Knowles,

T.; Vendruscolo, M.; St George-Hyslop, P. FUS Phase Separation Is Modulated by a Molecular Chaperone and Methylation of Arginine Cation-π Interactions. *Cell* **2018**, *173* (3), 720-734.e15.

(44) Biot, C.; Buisine, E.; Kwasigroch, J.-M.; Wintjens, R.; Rooman, M. Probing the Energetic and Structural Role of Amino Acid/Nucleobase Cation-Pi Interactions in Protein-Ligand Complexes. *J. Biol. Chem.* **2002**, *277* (43), 40816–40822.

(45) Luscombe, N. M.; Laskowski, R. A.; Thornton, J. M. Amino Acid–Base Interactions: A Three-Dimensional Analysis of Protein–DNA Interactions at an Atomic Level. *Nucleic Acids Res.* **2001**, *29* (13), 2860–2874.

(46) Wilson, K. A.; Wells, R. A.; Abendong, M. N.; Anderson, C. B.; Kung, R. W.; Wetmore, S. D. Landscape of π–π and Sugar–π Contacts in DNA–Protein Interactions. *J. Biomol. Struct. Dyn.* **2016**, *34* (1), 184–200.

(47) Li, Y.; Eshein, A.; Virk, R. K. A.; Eid, A.; Wu, W.; Frederick, J.; VanDerway, D.; Gladstein, S.; Huang, K.; Shim, A. R.; Anthony, N. M.; Bauer, G. M.; Zhou, X.; Agrawal, V.; Pujadas, E. M.; Jain, S.; Esteve, G.; Chandler, J. E.; Nguyen, T.-Q.; Bleher, R.; de Pablo, J. J.; Szleifer, I.; Dravid, V. P.; Almassalha, L. M.; Backman, V. Nanoscale Chromatin Imaging and Analysis Platform Bridges 4D Chromatin Organization with Molecular Function. *Sci. Adv.* **2021**, *7* (1), eabe4310.

(48) Roden, C.; Gladfelter, A. S. RNA Contributions to the Form and Function of Biomolecular Condensates. *Nat. Rev. Mol. Cell Biol.* **2021**, *22* (3), 183–195.

(49) Izquierdo-Bouldstridge, A.; Bustillos, A.; Bonet-Costa, C.; Aribau-Miralbés, P.; García-Gomis, D.; Dabad, M.; Esteve-Codina, A.; Pascual-Reguant, L.; Peiró, S.; Esteller, M.; Murtha, M.; Millán-Ariño, L.; Jordan, A. Histone H1 Depletion Triggers an Interferon Response in Cancer Cells via Activation of Heterochromatic Repeats. *Nucleic Acids Res.* **2017**, *45* (20), 11622–11642.

(50) Izzo, A.; Schneider, R. The Role of Linker Histone H1 Modifications in the Regulation of Gene Expression and Chromatin Dynamics. *Biochim. Biophys. Acta Gene Regul. Mech.* **2016**, *1859* (3), 486–495.

(51) Daujat, S.; Zeissler, U.; Waldmann, T.; Happel, N.; Schneider, R. HP1 Binds Specifically to Lys26-Methylated Histone H1.4, Whereas Simultaneous Ser27 Phosphorylation Blocks HP1 Binding. *J. Biol. Chem.* **2005**, *280* (45), 38090–38095.

(52) Sarg, B.; Lopez, R.; Lindner, H.; Ponte, I.; Suau, P.; Roque, A. Identification of Novel Post-Translational Modifications in Linker Histones from Chicken Erythrocytes. *J. Proteomics* **2015**, *113*, 162–177.

(53) André, A. A. M.; Spruijt, E. Liquid–Liquid Phase Separation in Crowded Environments. *Int. J. Mol. Sci.* **2020**, *21* (16), 5908.

(54) Aumiller, W. M., Jr; Keating, C. D. Phosphorylation-Mediated RNA/Peptide Complex Coacervation as a Model for Intracellular Liquid Organelles. *Nat. Chem.* **2016**, *8* (2), 129–137.

(55) Wang, L.; Hu, M.; Zuo, M.-Q.; Zhao, J.; Wu, D.; Huang, L.; Wen, Y.; Li, Y.; Chen, P.; Bao, X.; Dong, M.-Q.; Li, G.; Li, P. Rett Syndrome-Causing Mutations Compromise MeCP2-Mediated Liquid–Liquid Phase Separation of Chromatin. *Cell Res.* **2020**, *30* (5), 393–407.

(56) Ukmar-Godec, T.; Hutten, S.; Grieshop, M. P.; Rezaei-Ghaleh, N.; Cima-Omori, M.-S.; Biernat, J.; Mandelkow, E.; Söding, J.; Dormann, D.; Zweckstetter, M. Lysine/RNA-Interactions Drive and Regulate Biomolecular Condensation. *Nat. Commun.* **2019**, *10* (1), 2909.

(57) Bhamla, M. S.; Benson, B.; Chai, C.; Katsikis, G.; Johri, A.; Prakash, M. Hand-Powered Ultralow-Cost Paper Centrifuge. *Nat. Biomed. Eng.* **2017**, *1* (1), 0009.

Chapter 3.

Quadruplex folding promotes the condensation of linker histones and DNAs via liquid–liquid phase separation

3.1. Introduction

Genomic DNA in eukaryotic cells wraps around histone protein cores to form nucleosomes, which are further compacted into chromatin.[1] The level of chromatin condensation is closely related to gene transcription;[2] heterochromatin is a tightly packed form that is inaccessible to polymerases and thus inactivates gene transcription, whereas gene transcription is activated in euchromatin, in which the nucleosomes are loosely packed.[3] Chromatin undergoes highly dynamic changes in its condensed structure during a cell cycle. However, the mechanisms that govern the organization of chromatin remain largely unknown.

Liquid-liquid phase separation (LLPS) has emerged as a possible mechanism for the control of chromatin organization through the promotion of nucleosome packing.[4] Biological LLPS is a process in which solutions of biomacromolecules spontaneously separate into two phases.[5,6] In such events, one phase is usually a small-volume droplet-like phase in which the biomacromolecules are concentrated in aqueous media, while the other is the surrounding phase, which is depleted of the biomacromolecules.[7] Multivalent weak intermolecular interactions involving intrinsically disordered regions (IDRs) of proteins, such as electrostatic, cation-π, and π-π interactions, play crucial roles in LLPS.[5,6] For instance, binding of the IDR-containing heterochromatin protein HP1α to the histone H3K9 methylation site induces LLPS in specific domains of heterochromatin.[8,9] LLPS also occurs in euchromatin regions that are rich in acetylated histone tails when the transcriptional regulator protein BRD4, which contains a long IDR, is co-localized.[10,11] Thus, the nature of the relationship between LLPS-mediated chromatin-condensation and proteins is gradually determined.

Several reports have indicated that DNA is also involved in the LLPS associated with chromatin condensation. The length of the inter-nucleosome linker DNA strongly affects the LLPS of nucleosome arrays.[10] Double-stranded DNA induces LLPS in the presence of histone H1,[12] which is capable of regulating

chromatin organization via binding to inter-nucleosome linker DNA. However, knowledge regarding the structure of the DNA involved in LLPS-mediated chromatin-condensation is still very limited. Therefore, in this work, I have focused on the secondary structures of DNA, especially the most common G-quadruplex structure.[13]

G-quadruplex is a stacking planar structure formed through Hoogsteen hydrogen bonds between four guanine residues (**Figure 3.1**).[13] Guanine-rich sequences with the potential to fold into the G-quadruplex structure are frequently observed in oncogene promoter sequences and telomere regions, which are known as quadruplex clusters or G4 clusters,[14,15] where they may promote or inhibit the access of transcriptional factors or telomere binding proteins.[16,17] Recently, it has been revealed that G-quadruplex sequences are also abundant in heterochromatin region;[18] however, the role of these sequences on chromatin condensation has not been clarified. Thus, I attempted to elucidate the relationship between the G-quadruplex DNA structure and the LLPS of chromatin constituents using a variety of sequences that are capable of forming quadruplex structures. The presented findings will facilitate the understanding of the role of G-quadruplex structures in the cell nucleus and chromatin condensation.

3.2. Materials and methods

3.2.1. Materials

Tris-EDTA (TE) buffer [10 mM Tris-HCl; 1 mM EDTA; pH = 7.4] was obtained from Takara Bio Inc. (Shiga, Japan). Thioflavin T, sodium chloride (NaCl), ethanol (EtOH), methanol (MeOH), 2-propanol, dimethyl sulfoxide (DMSO) and acetone were obtained from Wako Pure Chemical Ind. (Osaka, Japan). Cytidine 5′-monophosphate disodium (CMP), thymidine 5′-monophosphate disodium (TMP), 8-anilino-1-naphthalenesulfonic acid ammonium salt (ANS), Nile red (NR), rhodamine 6G (R6G) and carboxy-terminated polyamidoamine (PAMAM) dendrimer (generation 3.5, 64 carboxyl groups) were obtained from Sigma Chemical Co. (St. Louis, MO, USA). Guanosine 5′-monophosphate disodium (GMP) was obtained from Combi-Blocks Inc (San Diego, CA, USA). Adenosine 5′-monophosphate (AMP) and 1,6-hexanediol were obtained from Tokyo Chemical Industry Co., Ltd (Tokyo, Japan). *N*-mesoporphyrin IX (NMM) was obtained from Frontier Scientific, Inc (Logan, USA). Poly-L-lysine hydrobromide (PLL; degree of polymerization: 50) and methoxy-poly (ethylene glycol)-*block*-poly(L-lysine trifluoroacetate) (PEG-*b*-PLL; degree of

polymerization PEG: 113, degree of polymerization PLL: 50) were obtained from Alamanda Polymers, Inc. (Huntsville, AL, USA). Acetonitrile was obtained from Merck Millipore Ltd. (Darmstadt, Germany). Histone H1 (H1) from bovine thymus, obtained from Signal Chem (Richmond, BC, Canada).

Prior to the experiments, a 1.0 mg/mL H1 solution containing 150 mM NaCl, and 50 mM Tris-HCl (pH = 7.5) was desalted using the following procedure. The solution was thawed at 37 °C, transferred to a 10,000 MWCO Amicon Ultra centrifugal filter unit (Merck Millipore Ltd., Darmstadt, Germany), centrifuged (10,000 *g*), and diluted with distilled water. The centrifugation/dilution cycle was repeated five times. After purification, the concentration of H1 was determined from the absorbance at 280 nm using a NanoDrop 1000 spectrophotometer (Thermo Fisher Scientific Inc., Waltham, MA, USA).

The single-strand DNA (ssDNA) sequences with and without a carboxyfluorescein (FAM) label at the 3′-terminus were synthesized and purified by Eurofins Genomics (Ebersberg, Germany). The ssDNAs were dissolved in TE buffer (pH = 7.4) and annealed as follows: 100 μM of ssDNA in TE buffer (pH = 7.4) was heated to 95 °C for 5 minutes and then cooled to 25 °C at a rate of 1 °C/min using a PCR thermal cycler (TP-600; Takara Bio Inc., Shiga, Japan).

3.2.2. Circular dichroism measurements

Circular dichroism (CD) measurements were performed using a spectropolarimeter (J-720; Japan Spectroscopic Co., Ltd., Tokyo, Japan). Basically, solutions containing 50 μM of ssDNA in TE buffer (pH = 7.4) were placed in a 1 mm or 1 cm quartz cuvette, and the spectra were recorded at 25 °C. The CD spectra of the samples were corrected by subtracting the corresponding spectra of the buffer solution in the absence of ssDNA. CD spectra of ssDNA during droplet formation were obtained by titrating 2 μL of 60 μM H1 solution against 300 μL of 10 μM DNA solution in TE buffer (pH = 7.4). CD spectra of the H1 solution at the same concentration as each titration condition were subtracted as background. To prepare condensed phase samples, a solution containing 2 mM DNA and 0.4 mM H1 in TE buffer (pH = 7.4) was centrifuged at 10,000 *g* for 10 min. After removing the supernatant, the condensed phases were transferred between two quartz plates to make thin condensed samples, and the CD spectra of these samples were measured.

3.2.3. Turbidity measurements

In the wells of a 96-well microplate (clear bottom, non-treated; Corning Inc., NY, USA), solutions (30 μL) of 20 μM of ssDNA in TE buffer (pH = 7.4) were mixed with solutions (30 μL) of 0-20 μM H1 in TE buffer

(pH = 7.4). After incubation (15 min, 30 °C), their absorbance at 400 nm was recorded using a microplate reader (Cytation 5; BioTek Instruments, Inc., Winooski, VT, USA).

3.2.4. Phase-contrast microscopy imaging

Solutions (60 μL) containing 2 μM H1 and 10 μM ssDNA in TE buffer (pH = 7.4) were prepared in the wells of a 96-well plate. After incubation for 2 h at room temperature, images of the solution were obtained using a phase-contrast microscope (Primo Vert; Carl Zeiss, Germany) equipped with an AxioCam ERc5s camera (Carl Zeiss) and Axio Vision software (Carl Zeiss). After allowing the solutions containing 10 μM ssDNA and 2 μM H1 to incubate for 1 h at room temperature, the process of fusion between the DNA/H1 liquid droplets was observed by time-lapse photography (increments: 0.1 ms) using a phase-contrast microscope (Eclipse Ts2R, Nikon, Japan) equipped with a digital camera (CAMEDIA C-5060, Olympus, Japan). To image the LLPS of the nucleotide monophosphates, solutions containing 0-20 mM nucleotide monophosphate, 2 μM H1, and 15% PEG4000 in TE buffer (pH = 7.4) were prepared. After incubation for 5 h at room temperature, phase-contrast images of each solution were obtained.

3.2.5. Fluorescence microscopy imaging

Solutions (50 μL) containing 2 μM H1 and 10 μM ssDNAs in TE buffer (pH = 7.4) were incubated for 2 h at room temperature and then mixed with solutions (5 μL) containing 5.5 μM fluorescent probes (ThT, NMM, NR, R6G, or ANS) in TE buffer (pH = 7.4). The fluorescence images were obtained using a fluorescence cell imager (ZOE^{TM}; Bio-Rad Laboratories Inc., California, USA). To investigate the effect of the ssDNA sequences on the formation of droplets with H1, solutions (60 μL) containing 4 μM H1, 10 μM Pu22, and poly(dA) (with either Pu22 or poly(dA) being labeled with FAM at 3'-terminus) in TE buffer (pH = 7.4) were prepared. After incubation for 2 h at room temperature, fluorescence images of the solutions were obtained. The fluorescence intensities inside and outside the liquid droplets (for **Figure 3.7**) were quantified by analyzing the optical density distribution of the pixels along the straight line indicated in each image using image processing software (image J, National Institutes of Health).

3.2.6. Fluorescence spectra of ThT and NMM

Solutions (50 μL) containing 10 μM ssDNA and 0.5 μM ThT or 10 μM NMM in TE buffer (pH = 7.4) in the presence or absence of 2 μM H1 were placed in a sub-micro fluorometer cell (Tosoh Quartz Co., Tokyo,

Japan). After incubation for 5 min at 25 °C, the fluorescence spectra were recorded using a JASCO FP-8300 spectrofluorometer (ThT: λ_{ex} = 445 nm, λ_{em} = 460–700 nm; NMM: λ_{ex} = 400 nm, λ_{em} = 550–700 nm). Fluorescence spectra of 10 μM NMM in various solvents (water, DMSO, acetonitrile, MeOH, EtOH, acetone, 2-propanol) were obtained under the same conditions.

3.2.7. Fluorescence titration experiment

Fluorescence titration measurements were performed on a JASCO FP-8300 spectrofluorometer. 50 μL of solutions containing fluorogenic probe (ThT; 0.05 μM or 0.5 μM, NMM; 1.0 μM or 10 μM) in TE buffer (pH = 7.4) were placed in a sub-micro fluorometer cell. The fluorescence spectra were recorded at 25 °C (ThT: λ_{ex} = 445 nm, λ_{em} = 460-700 nm; NMM: λ_{ex} = 400 nm, λ_{em} = 550-700 nm). Subsequently, fluorescence spectra were acquired consecutively after addition of 0.2-1.0 μL aliquots of 150 or 450 μM Pu22 solution.

3.2.8. Effect of NaCl and 1,6-hexanediol on the stability of the droplets

Solutions (50 μL) containing 2 μM H1 and 10 μM ssDNA in TE buffer (pH = 7.4) were prepared in the wells of a 96-well plate (clear bottom, non-treated). After incubation for 2 h at room temperature, solutions (50 μL) containing 0-600 mM NaCl or 0-40% 1,6-hexanediol in TE buffer (pH = 7.4) were added; turbidity measurements at 400 nm and phase-contrast images were then recorded as described above.

3.2.9. Fluorescence recovery after photobleaching (FRAP) measurement

Solutions (25 μL) containing 60 μM FAM-modified ssDNA (Pu22, Pu22-1, Pu22-2, or poly(dA)) in TE buffer (pH = 7.4) were mixed with solutions (25 μL) containing 12 μM H1 in TE buffer (pH = 7.4). The concentration conditions were optimized so that poly(dA) formed liquid droplets of sufficient size for FRAP measurements. An aliquot (20 μL) was placed on a cover slip attached to a glass slide, and then the liquid droplets were imaged with an Olympus FV1000 confocal microscope at 60× using a detection wavelength of 488 nm. The 488 nm laser was applied to the region of interest at full power for 10 s (for Pu22, Pu22-1, and Pu22-2) or 5 s (for poly(dA)), before the fluorescence recovery was recorded for 5 min (for Pu22, Pu22-1, and Pu22-2) or 1 min (for poly(dA)). The fluorescence intensity of the photobleached area was normalized relative to that of the unbleached area. The time lapse of the fluorescence intensity was fitted to a single exponential function (eq. 1) in order to obtain the recovery time τ, as described in a previous report.[19]

$$f(t) = A(1 - e^{-\frac{t}{\tau}}) \qquad \text{(eq. 1)}$$

3.2.10. Fluorescence lifetime measurement

The fluorescence lifetime was counted on a time-correlated single-photon-counting spectrometer (FluoroCube, HORIBA) with a 410 nm pulsed laser diode for excitation (NanoLED; a pulse width of ~200 ps; a pulsed power 11 pJ/pulse; repetition rate 1 MHz). The wavelength resolution was set to be 2 nm. The scattered light of the excitation light source was cut by a long-pass filter of 430 nm. The solution (50 μL) containing 10 μM DNA and 3 μM ThT or NMM in TE buffer were prepared in a sub-micro fluorometer cell. The droplet phase samples were prepared by centrifuging the turbid solution (480 μL) obtained by mixing 480 μM DNA solution containing 144 μM ThT or NMM and 96 μM H1 solution in equal amounts in a PCR tube for 5 min at 1000 *g*. After removing the supernatant, the droplet phases were transferred between two glass slides to make thin condensed samples, and the fluorescence lifetime measurements were conducted.

3.2.11. High-resolution magic angle spinning nuclear magnetic resonance (HR-MAS-NMR) measurements

^{1}H detected HR-MAS-NMR measurements were recorded on a Bruker (Karlsruhe, Germany) AVANCE NEO 800 spectrometer equipped with a 4 mm H/C/D/N DVT HR-MAS probe. The temperature was maintained at 25 °C throughout the acquisition time in order to avoid clouding of the retrieved droplet phase. A one-dimensional (1D) proton spectrum using watergate for water suppression was acquired, with shaped pulse power optimized to 4.5 mW. The MAS spinning rates of 4000, 5000, and 7000 Hz were tested to distinguish spinning side bands and the final data were collected with 7000 Hz MAS spinning. The droplet phase was prepared by centrifuging the turbid solution obtained by mixing 2 mM DNA solution and 0.5 mM H1 solution in equal amounts in a PCR tube for 5 min at 1000 *g*. All of this droplet phase was transferred to the rotor by hand-powered centrifuge[57] and then HR-MAS-NMR measurements were performed

3.3. Results and discussion

3.3.1. Experimental design

To investigate the effect of G-quadruplex formation on LLPS in the context of chromatin condensation, I chose histone H1 (H1) and various single-stranded DNA (ssDNA) sequences. H1 controls the packing density of nucleosomes via non-specific electrostatic interactions between its positively charged lysine-rich

IDR at its C-terminal and negatively charged DNA.[21] Shakya *et al*. recently reported that among histone proteins, H1 has the highest ability to form droplets with DNA via LLPS.[22] Eight 22 nt ssDNA sequences were initially prepared (**Table 3.1**): an oncogene *c-myc* promoter sequence that can fold into a parallel G-quadruplex structure (Pu22)[23]; a telomere sequences that can fold into an antiparallel G-quadruplex structure (22AG)[24]; sequences in which one or two of the successive guanines of these G-quadruplex sequences were replaced with adenine (Pu22-1, Pu22-2, 22AG-1 and 22AG-2); and a simple repeat of deoxyadenylic acid (poly(dA)) and deoxythymidylic acid (poly(dT)) with a random coil structure. The nucleotides are arranged an all-anti configuration in the parallel forms of G-quadruplexes, while the antiparallel forms contain nucleotides in both *syn* and *anti* configurations (**Figure 3.1**).

Table 3.1. Sequences and structures of the DNA used in this study.

Name	Sequence (5'→3')	Structure
Pu22	TGAGGGTGGGTAGGGTGGGTAA	Parallel G-quadruplex
Pu22-1	TGAGGATGGATAGGATGGATAA	Parallel G-quadruplex (partial)
Pu22-2	TGAGAATGAATAGAATGAATAA	Random
22AG	AGGGTTAGGGTTAGGGTTAGGG	Anti-parallel G-quadruplex
22AG-1	AGGATTAGGATTAGGATTAGGA	Anti-parallel G-quadruplex (partial)
22AG-2	AGAATTAGAATTAGAATTAGAA	Random
poly(dA)	AAAAAAAAAAAAAAAAAAAAA	Random
poly(dT)	TTTTTTTTTTTTTTTTTTTTT	Random
$dsDNA_{11}$	TGAGGGTGGGT*	Double helix

* One of the sequences constituting the duplex is shown.

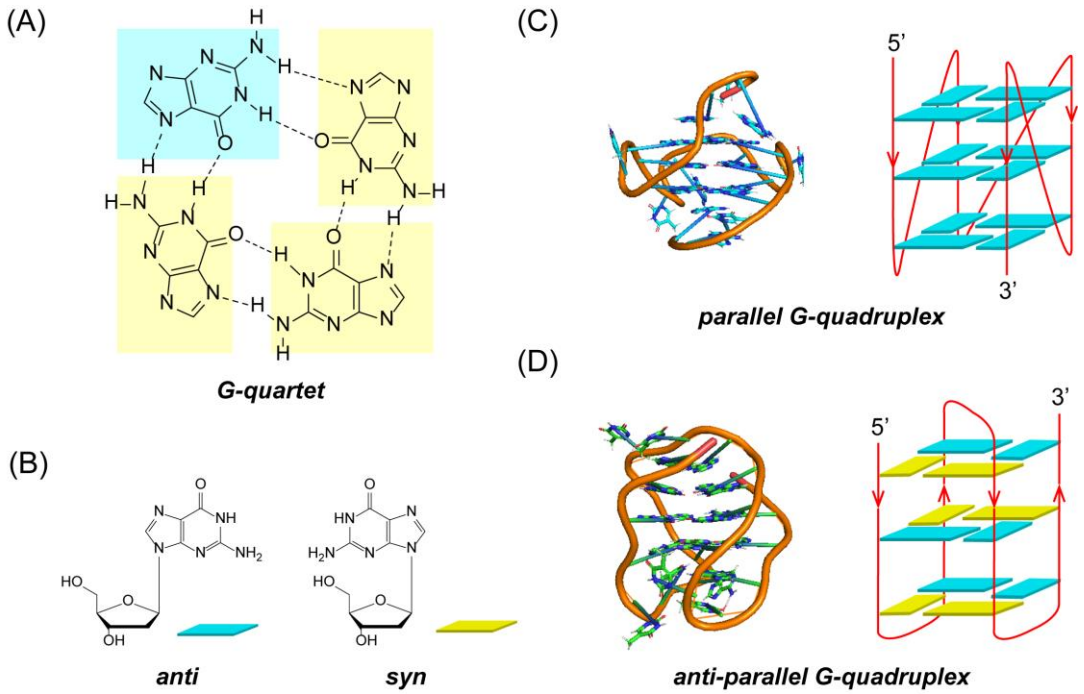

Figure 3.1. Schematic illustration of the G-quadruplex DNA structures. (A) G-quartets, consisting of four guanin bases, stack to form a G-quadruplex. (B) Nucleotide with *anti* (blue square) and *syn* (yellow square) configurations. G-quadruplex structures are classified into (C) parallel and (D) anti-parallel types based on the direction of 4 strands. Crystal structures of G-quadruplexes are obtained from Protein Data Bank (PDB ID: 1XAV for parallel G-quadruplex; and 143D for anti-parallel G-quadruplex).

3.3.2. Secondary structures of ssDNAs

To validate the secondary structures of the ssDNA sequences used in this study, I conducted far-UV CD measurements. Pu22 and Pu22-1 showed a positive peak at 260 nm and a negative peak at 245 nm, which indicates the formation of parallel G-quadruplex structures (**Figure 3.2A**).[25] The lower intensity of these characteristic peaks for Pu22-1 suggested a decrease in the amount of G-quadruplex structures. The spectrum of Pu22-2 differed greatly from that of Pu22 and Pu22-1, and indicated that this sequence exhibited a random coil structure. 22AG showed a positive peak at 290 nm and a negative peak at 260 nm, indicating that anti-parallel G-quadruplex structures had been formed (**Figure 3.2B**).[25] The CD spectra of 22AG-1 and 22AG-2 were clearly different from that of 22AG, indicating that both sequences exhibit random coil structures. However, ThT fluorescence was observed from 22AG-1 (**Figure 3.9**, *vide infra*), implying that the solution of 22AG-1 contained some G-quadruplex structures. The spectra of poly(dA) and poly(dT) are consistent with previous reports that indicate a random coil structure (**Figure 3.2C**).[26]

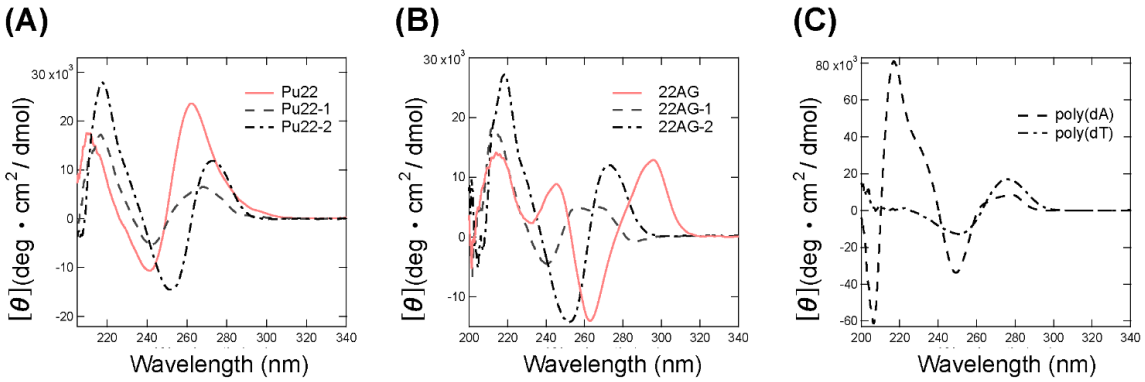

Figure 3.2. Secondary structure of the ssDNA sequences used in this study. CD spectra of solutions containing ssDNA (50 μM) in TE buffer (pH = 7.4): (A and B) An oncogene c-myc promoter sequence (Pu22, A), a telomeric sequence (22AG, B), sequences in which one or two of the successive guanines of these ssDNA sequences were replaced with adenine (Pu22-1, Pu22-2, 22AG-1, and 22AG-2), and (C) simple repeat sequences (poly(dA) and poly(dT)).

3.3.3. LLPS of G-quadruplex-forming ssDNA with H1

The turbidity of the aqueous solutions of the guanine-containing sequences (Pu22, Pu22-1, and Pu22-2) increased upon addition of H1 up to a certain concentration ([H1]/[ssDNA] = 0.2-0.4) (**Figure 3.3A**), indicating that interactions between the ssDNA sequences and H1 resulted in the formation of large assemblies. Interestingly, the maximum turbidity values of the solutions increased with the number of continuous guanines in the ssDNA sequence (Pu22 > Pu22-1 > Pu22-2). The decreased turbidity at high concentrations of H1 probably results from repulsive forces that arise from the excess of positive charge;[12,27] thus, electrostatic interactions between the cationic H1 and anionic ssDNA are presumably a dominant force in the formation of the assemblies. However, although poly(dA), like the other ssDNA sequences, is anionic, the poly(dA) solution did not exhibit an apparent increase in turbidity upon addition of H1 (**Figure 3.3C**).

Spherical assemblies were observed via phase-contrast microscopy for all turbid ssDNA solutions ([H1]/[ssDNA] = 0.2; **Figure 3.4A**), similarly to my recent studies of cationic protein/anionic polymer pairs.[28,29] Time-lapse images showed rapid, sub-millisecond fusion of the assemblies (**Figure 3.4B**). This behavior indicates that these assemblies are not gel-like aggregates, but instead liquid-like droplets with highly fluid properties, as have been observed for other phase-separating proteins.[30] Consistent with the turbidity measurements (**Figure 3.3**), the size of the observed droplets decreased with decreasing number of continuous guanines in the ssDNA sequence. In the case of poly(dA), only small droplets (diameter < 1.0

μm) were formed. Similar behavior was observed for 22AG, its derivatives, and a poly(dT) (**Figures 3.3B and 3.4A**). Thus, ssDNA sequences capable of forming G-quadruplex are likely to have a high ability to form droplets with H1.

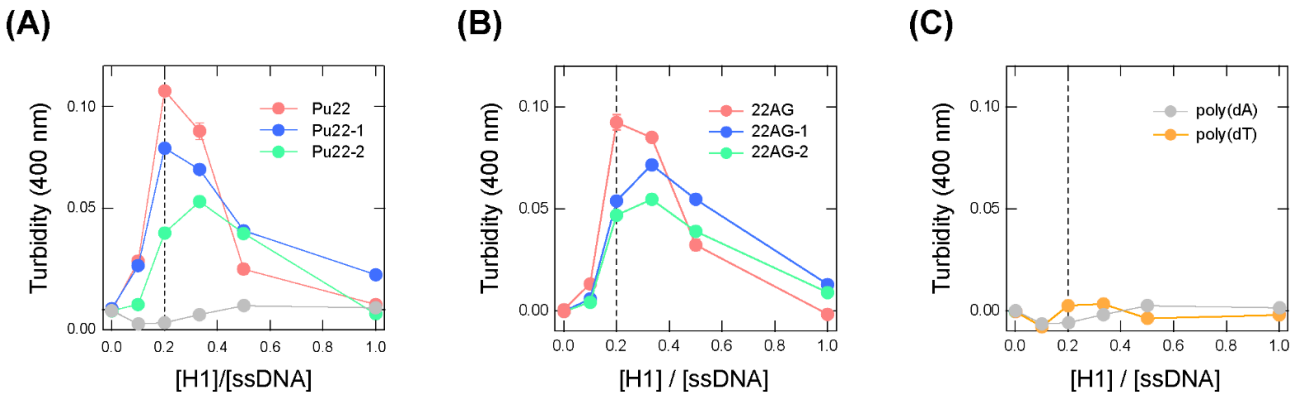

Figure 3.3. Turbidity of solutions that contain H1 (0-10 μM) and various ssDNA sequences (10 μM): (A) Pu22 and its derivatives; (B) 22AG and its derivatives; and (C) poly(dA) and poly(dT).

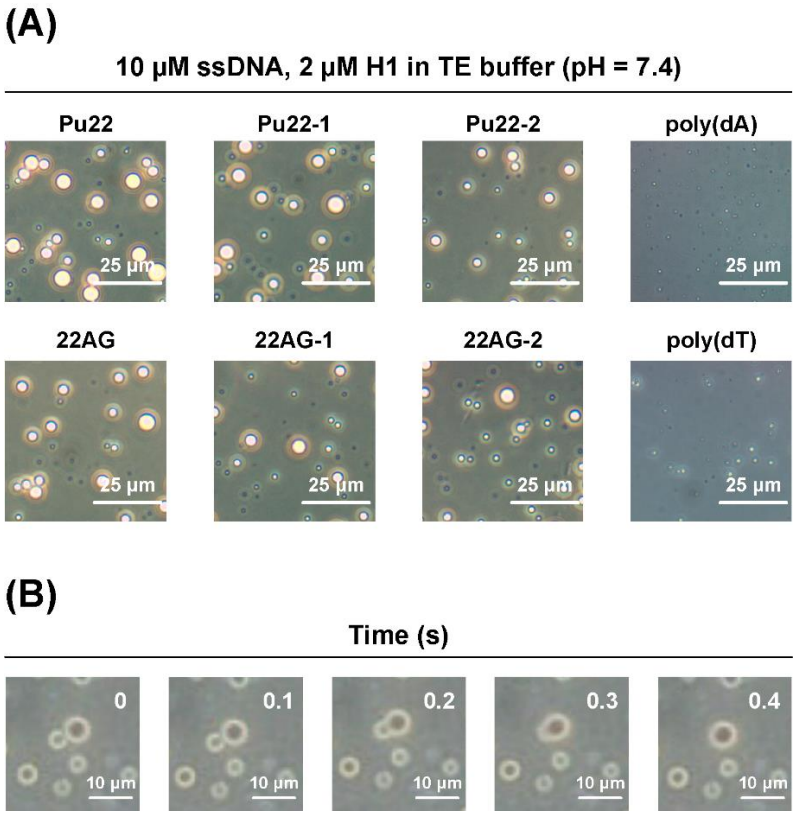

Figure 3.4. Liquid-like droplets of G-quadruplex-forming ssDNA with H1. (A) Phase-contrast-microscopy images of solutions under the conditions indicated by the dotted line in Figure 3.3 (10 μM ssDNA and 2 μM H1); scale bar = 25 μm. (C) Fusion process of the Pu22/H1 droplets; scale bar = 10 μm.

The effect of the ssDNA sequence on the fluidity inside the droplet was compared using fluorescence recovery after photobleaching (FRAP), which is a common method for evaluating the motility of molecules inside the droplets.[31] The diffusion rate of the carboxyfluorescein (FAM)-modified ssDNA sequences increased with decreasing number of continuous guanines [poly(dA) > Pu22-2 > Pu22-1 > Pu22], i.e., in the opposite order of the content of quadruplex structures (**Figure 3.5**). Interestingly, the density of the ssDNAs inside the droplet was correlated with their motility (**Figure 3.6**), i.e., the higher the G-quadruplex content, the lower the density inside the droplet, despite the stronger intermolecular interactions inside the droplet. Therefore, the G-quadruplex folding also controls the motility and density of the molecules inside the resulting droplets, which could potentially affect cellular functions such as the inhibition of gene transcription.

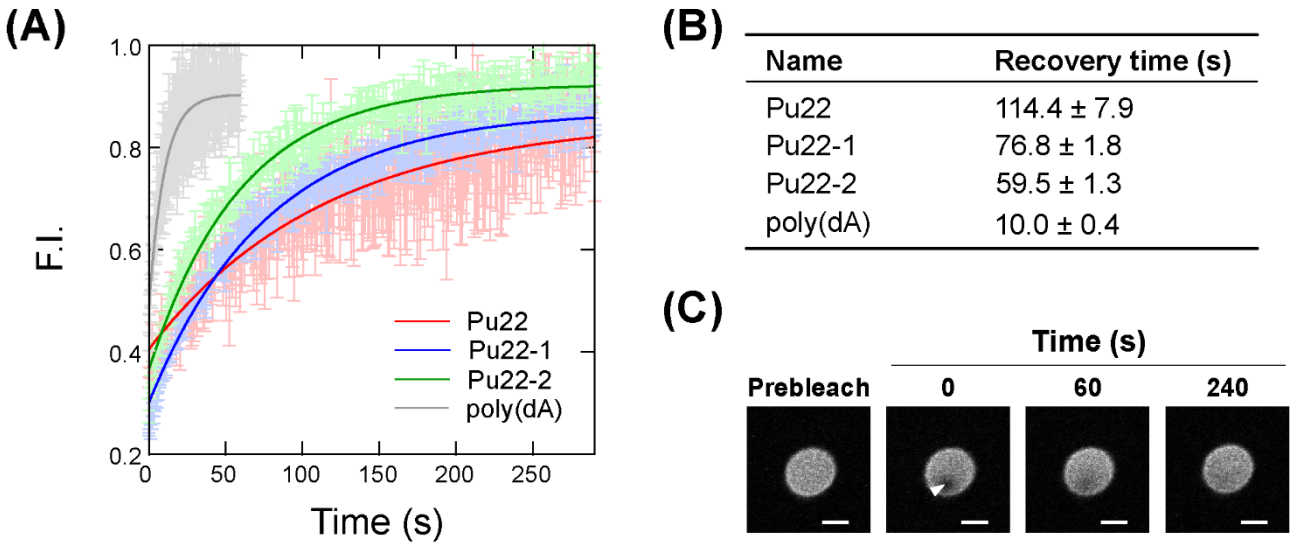

Figure 3.5. Motility of ssDNA within the droplet. (A) FRAP recovery curves for the different ssDNA structures. (B) recovery times of fluorescence calculated by exponential fitting (colored lines; N = 3), and (C) confocal fluorescence microscopy images obtained during the FRAP measurement of a Pu22/H1 liquid droplet. The white arrowhead indicates the bleaching site; scale bar = 5 μm.

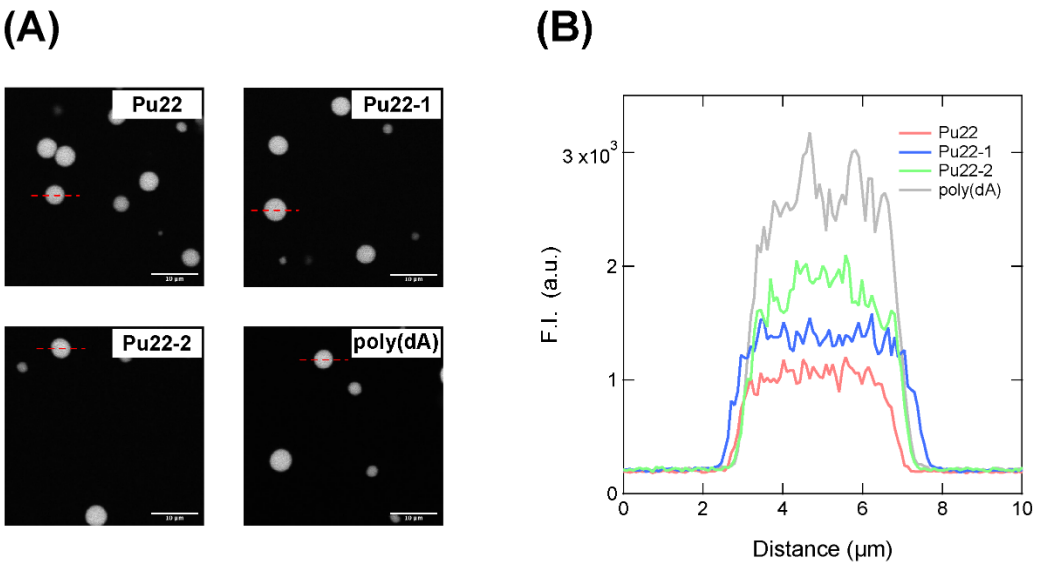

Figure 3.6. Distribution of ssDNAs inside and outside the droplets. (A) Confocal fluorescence microscopy images of droplets formed by 20 μM FAM-modified ssDNA and 4 μM H1 in TE buffer; scale bar = 10 μm. The concentration of molecules was higher than those in Figure 3.4A to compare the effect of the sequence differences using droplets of sufficient size. (B) Fluorescence intensity along the red dashed line in each of the images in (A). Based on this result and that shown in Figure 3.5, poly(dA) formed droplets with high density but high fluidity, while Pu22 formed droplets with low density but low fluidity. This shows a correlation between the density and the motility of the ssDNAs inside the droplet, which seems counterintuitive. As reported for the LAF-1/RNA system, however, the concentration, motility, and interaction strength of molecules inside a droplet are not proportional and are difficult to predict.[32] As can be inferred from the discussion relating to Figures 3.26 and 3.27, Pu22 has unique interfaces and thus may be an efficient structure for forming droplets.

To study the sequence selectivity of the droplet formation, either Pu22 or poly(dA) was labeled with FAM, and then both were mixed with H1. When Pu22 was labeled, the inside of the droplet emitted strong fluorescence, whereas the fluorescence inside and outside of the droplet was comparable for labeled poly(dA) (**Figure 3.7**), suggesting sequence selectivity not only in the formation of droplets with H1, but also in the incorporation of ssDNA into the resulting droplets.

Based on these results, it seems feasible to conclude that ssDNA sequences that can fold into G-quadruplex structures plays a significant role in (i) the generation of LLPS through interactions with H1, (ii) the motility and density of the molecules inside the formed droplets, and (iii) the ability of the droplets to incorporate other ssDNAs.

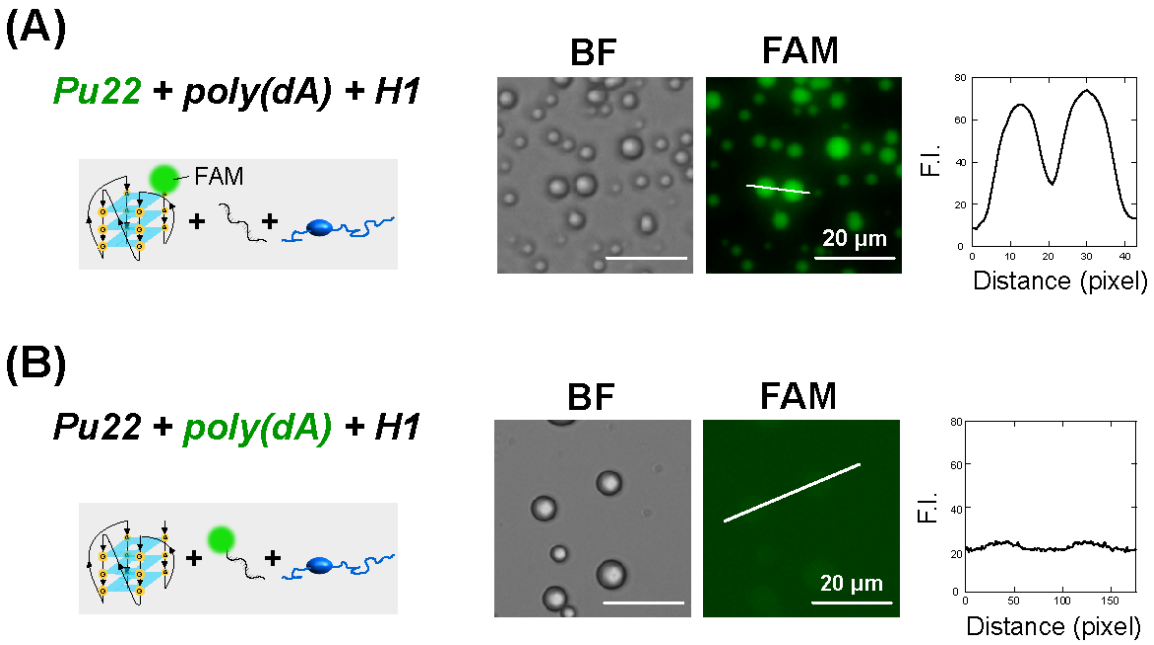

Figure 3.7. Selectivity of the ssDNA sequences for the droplet formation with H1. Either Pu22 or poly(dA) was modified with FAM, and both (10 μM) were mixed with H1 (2 μM). The fluorescence intensity along the white line was quantified from the brightness of each pixel; scale bar = 20 μm. All experiments were carried out in 10 mM Tris-EDTA buffer (pH = 7.4).

3.3.4. G-quadruplex folding within liquid-like droplets

The stability of the G-quadruplex structure is affected by protein binding.[17] The occurrence of LLPS was triggered by the interaction of ssDNAs and H1, and the components of the droplets are generally concentrated within the droplets by a factor of several to several hundred compared to the surrounding phase.[10,33] Therefore, the G-quadruplex content might fluctuate due to the high concentration of H1 inside the droplets. Therefore, I investigated the folding state of the ssDNA within the droplet using two fluorogenic probes that selectively bind to G-quadruplex structures, thioflavin T (ThT) and *N*-methylmesoporphyrin IX (NMM) (**Figure 3.8A**). ThT binds to G-quadruplex structures regardless of their configuration,[34] while NMM recognizes only parallel-folded G-quadruplexes (**Figure 3.8B**).[35] These probes are almost nonfluorescent in aqueous solution, but exhibit strong emission when bound to G-quadruplex structures.

(A)

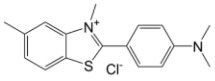

Thioflavin T (ThT)

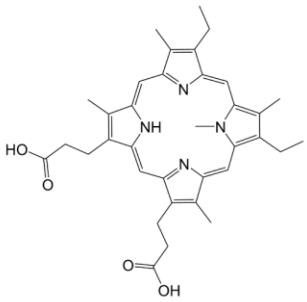

N-methylmesoporphyrin IX (NMM)

(B)

Binding selectivity

DNA structures	ThT	NMM
Parallel G-quadruplex	○	○
Anti-parallel G-quadruplex	○	×
Random coil	×	×

Figure 3.8. Fluorogenic probes that selectively bind to G-quadruplexes. (A) Chemical structures of the fluorescent probes ThT and NMM, which exhibit greatly enhanced fluorescence upon their selective binding to G-quadruplex structures. (B) The binding selectivity of ThT and NMM is taken from refs 34 and 35, respectively.

In the absence of H1, the overall fluorescence intensity of the solutions in the presence of ThT follows the order Pu22 > Pu22-1 > Pu22-2 >> Poly(dA), i.e., the abundance of G-quadruplex structures increases with increasing number of successive guanines in the ssDNA sequence (**Figure 3.9**). The maximum fluorescence intensity of ThT after the droplet formation is comparable for the Pu22-2/H1 or poly(dA)/H1 solutions, while that of the Pu22/H1 and Pu22-1/H1 solutions increases 1.5- and 1.6-fold, respectively. This result implies that G-quadruplex folding of Pu22 and Pu22-1 may be promoted during the droplet formation process. Fluorescence microscopy images of the Pu22 and Pu22-1 solutions showed significant fluorescence inside the droplets (**Figure 3.10**), demonstrating that the binding of ThT to the G-quadruplex occurred mainly inside the droplets. In contrast, the Pu22-2 and poly(dA) solutions exhibited very weak fluorescence.

In the case of a telomere-derived sequence (22AG) that is capable of folding into an anti-parallel G-quadruplex structure, ThT gave results similar to Pu22 (**Figure 3.9**), whereas NMM exhibited interesting behavior. Aqueous solutions of Pu22 showed similar strong fluorescence with or without H1 after the addition of NMM, which is specific to parallel-type G-quadruplexes (**Figure 3.11A**), indicating that the parallel G-quadruplex structure of Pu22 is not significantly denatured by H1. On the other hand, substantial NMM emission was observed from the entire solution of anti-parallel 22AG only after droplets were formed by the addition of H1. Similar to the emission of ThT, that of NMM was concentrated inside the droplets for both ssDNA sequences (**Figure 3.11B**). The enhancement in the fluorescence after droplet formation for 22AG suggests that the G-quadruplex structures of 22AG transitioned from the anti-parallel to the parallel

form. It has been reported that the anti-parallel to parallel transition in telomere-derived ssDNA inhibits telomerase processability.[36] Thus, if transition of the G-quadruplex structures of 22AG is coupled to the droplet-formation-inducing interaction with H1, it may be involved in the telomere activity switching mechanism in the cell nucleus.

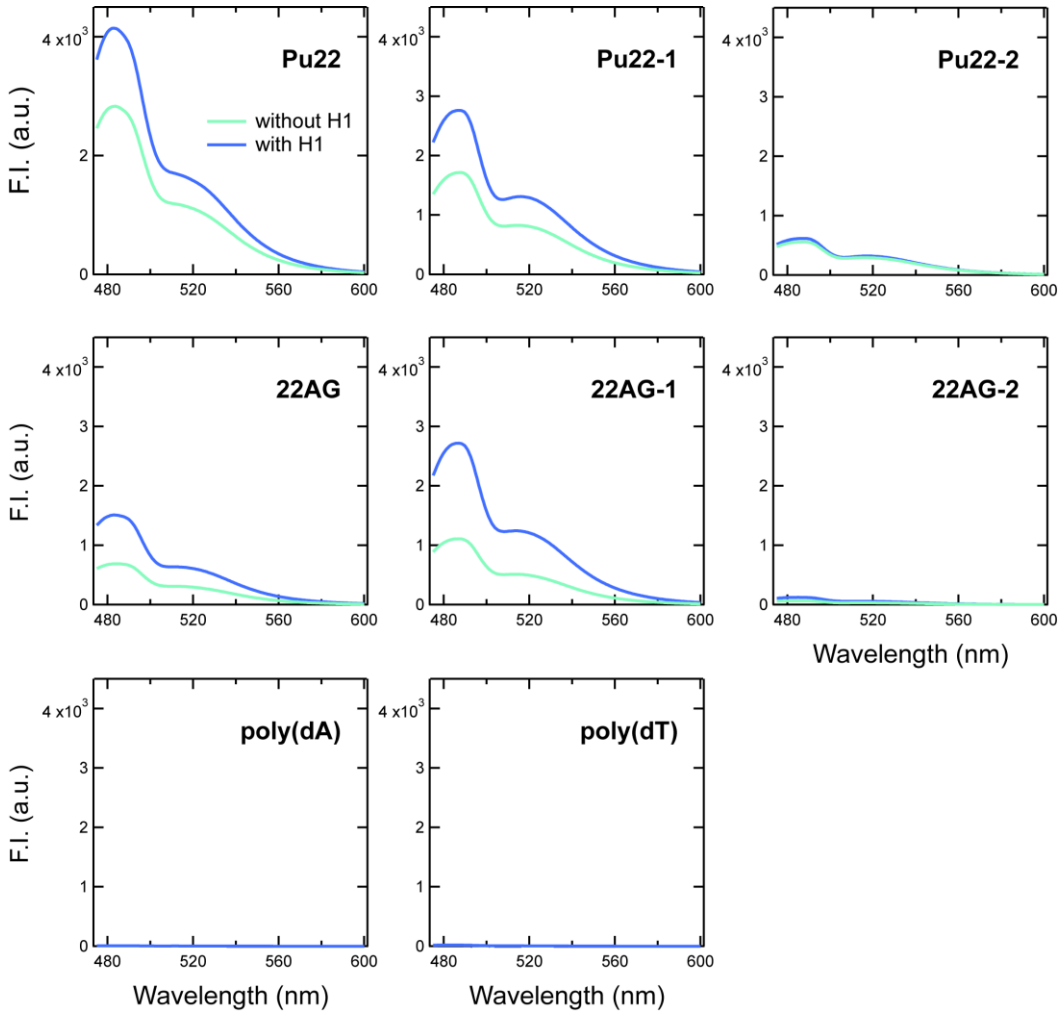

Figure 3.9. G-quadruplex formation of the ssDNA in the presence of H1. Fluorescence spectra of ThT in the presence of ssDNA (10 μM) with (dark blue) and without (light blue) H1 (2 μM); $\lambda_{ex}/\lambda_{em}$ = 445 nm / 460-700 nm.

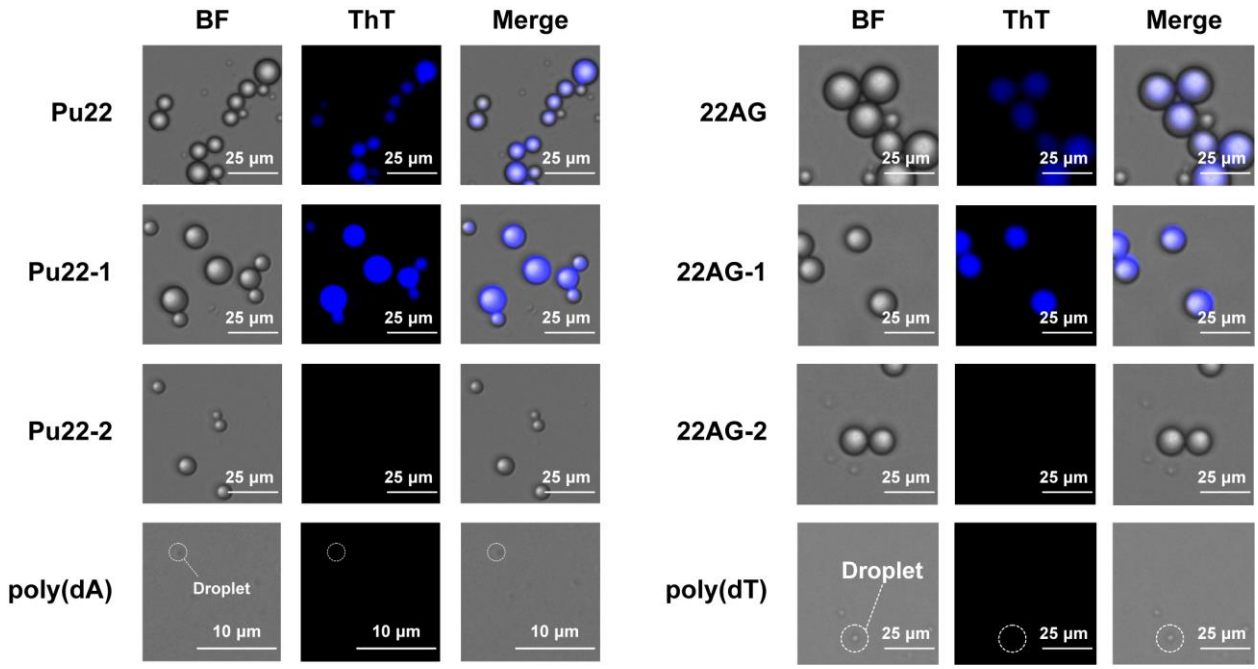

Figure 3.10. Fluorescence microscopy images of ssDNA/H1 liquid droplets after the addition of ThT; scale bar = 25 μm (10 μm for poly(dA)).

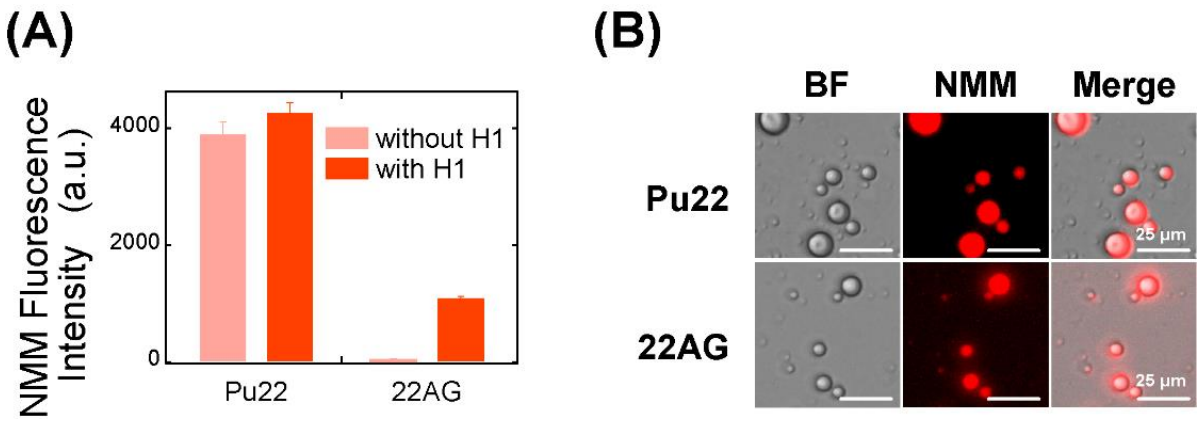

Figure 3.11. (A) Fluorescence intensity of NMM in solutions that contain ssDNA (10 μM) with or without H1 (2 μM). (B) Fluorescence microscopy images of ssDNA/H1 liquid droplets after the addition of NMM; scale bar = 25 μm (10 μm for poly(dA)).

3.3.5. Emission mechanism of probes when added to droplet suspension

When H1 was added to solutions containing G-quadruplex ssDNAs and the probes (ThT and NMM) to induce droplet formation, the fluorescence of the probes was enhanced, which was observed only from the interior of the droplets (**Figures 3.10 and 3.11B**). I found that both polarity-responsive fluorogenic probes (8-anilino-1-naphthalenesulfonic acid (ANS) and NR) and a fluorescent molecule insensitive to polarity (R6G) produced strong fluorescence from the interior of the droplets, regardless of whether ssDNA formed a G-quadruplex structure (**Figure 3.12**), suggesting that the probes used were concentrated inside the droplet regardless of the DNA sequence, and the dielectric constant inside the droplet was lower than that of the bulk solution. Environmental factors within such droplets can influence the fluorescence properties of the probes. This fact may lead to uncertainty in the interpretation of the experimental results for comparing the fluorescence intensities of G-quadruplex-specific probes during droplet formation and non-formation. In this section, I investigated the possibilities of other effects on fluorescence properties of the probes, especially focusing on dielectric constants, other than the binding of the probes to the G-quadruplex structures.

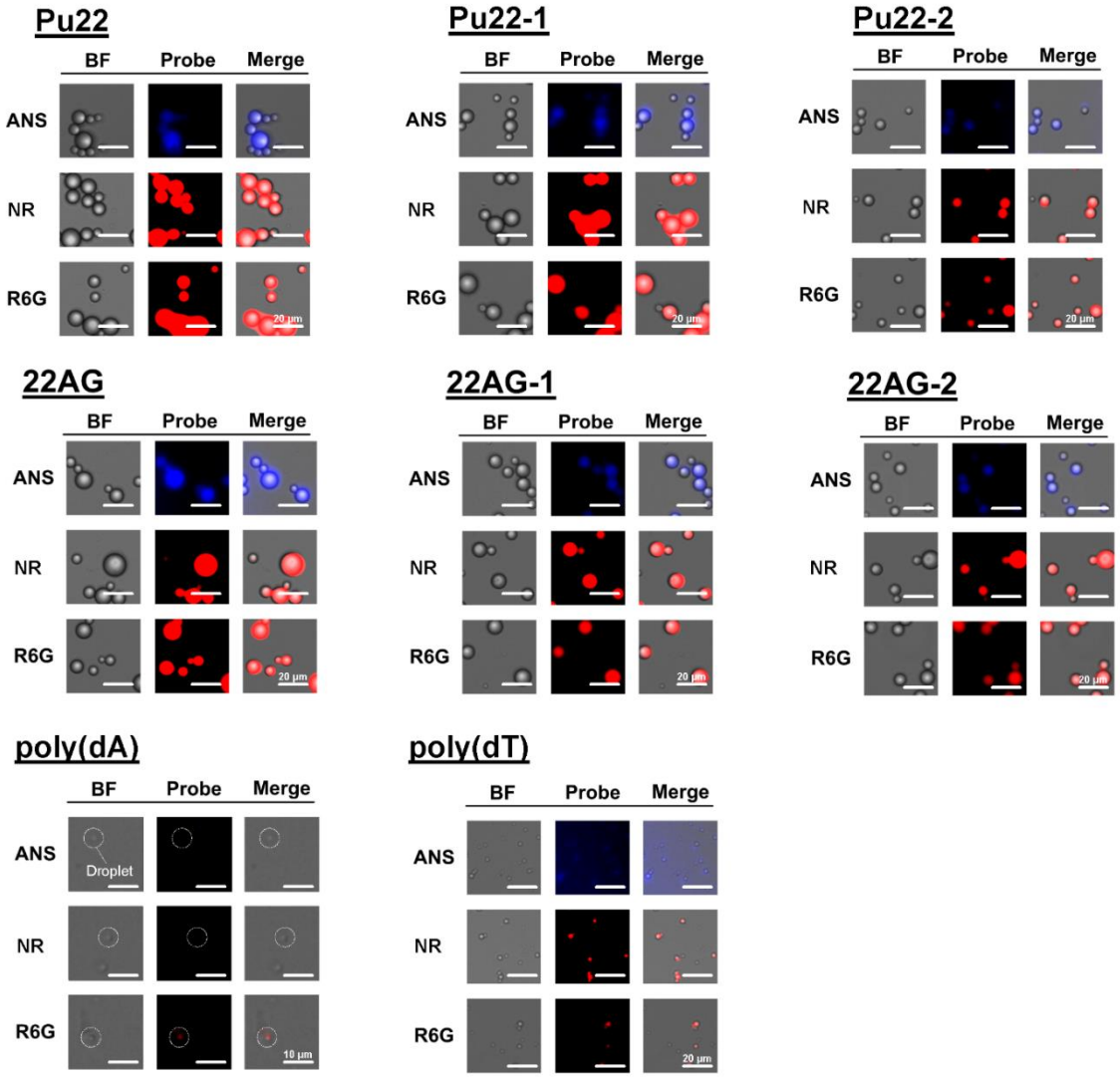

Figure 3.12. Non-specific fluorescence probes incorporated into the ssDNA/H1 droplets. Fluorescence microscopy images of ssDNA/H1 droplets in the presence of 0.5 μM probes that are not specific to G-quadruplex structures (ANS, NR, and R6G); scale bar = 20 μm (10 μm for poly(dA)). For all ssDNA sequences, the constantly fluorescent R6G was concentrated inside rather than outside the droplets. The polarity-responsive fluorescent probes (ANS and NR) fluoresced inside the droplet, except for poly(dA), which showed lower dielectric constant inside the droplet than outside. These common enrichment trends suggest that ThT and NMM may also be concentrated inside the droplets, but fluorescence enhancement should be induced only when G-quadruplex structures are present.

3.3.5.1. Effect of the dielectric constant on the fluorescence intensity of the probes

As reported previously,[37] the dielectric constant inside the droplets is generally lower than that of water, which is consistent with the fluorescence enhancement of NR and ANS (**Figure 3.12**). Therefore, I

considered the possibility that the fluorescence intensity of the 'free probes' not bound to the G-quadruplex structure could be enhanced inside the droplet. It is known that the fluorescence intensity of ThT is only very slightly affected by the dielectric constant.[38] For NMM, my experiments showed that the fluorescence intensity of NMM increased up to 6.6-fold in organic solvents with various dielectric constants relative to that in water (**Figure 3.13**). Considering the fact that the fluorescence intensity of NMM increased 140.3- and 27.9-fold in the presence of Pu22 and 22AG, respectively, the increase in the fluorescence intensities of free ThT and NMM due to the decrease in the dielectric constant would most likely be negligible.

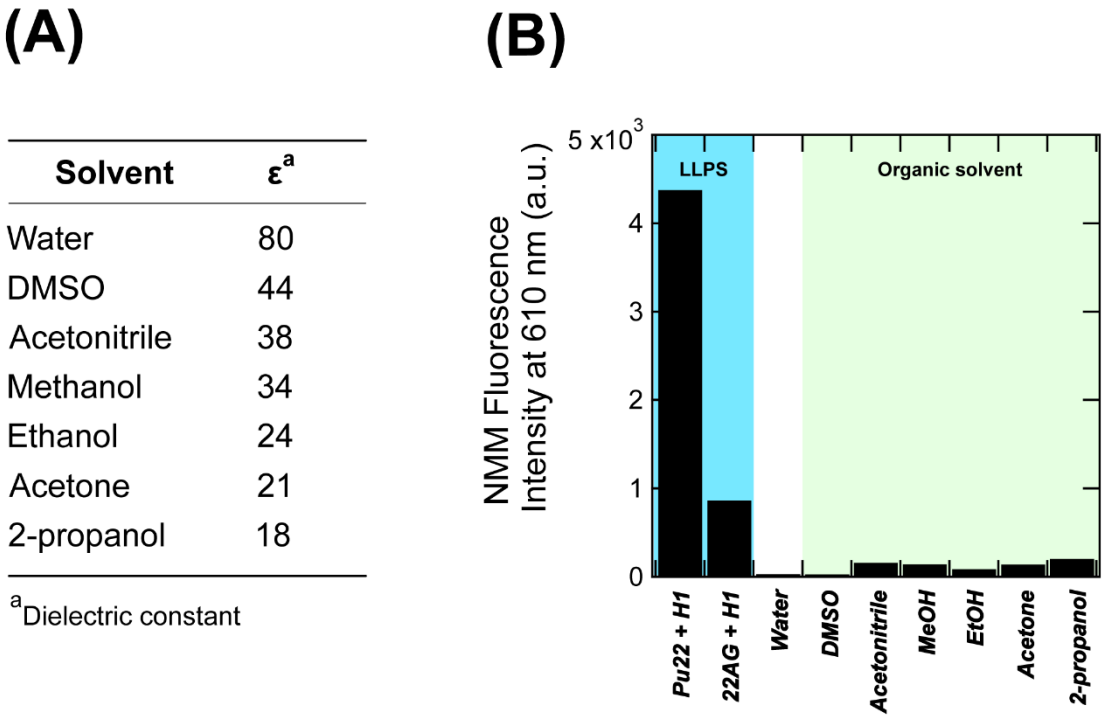

Figure 3.13. Effect of the dielectric constant on the fluorescence intensity of NMM. (A) Dielectric constants of the various solvents used this study [taken from ref. 39]. (B) Fluorescence intensity of 10 μM NMM in the various organic solvents, in water, and in water under LLPS conditions (in the presence of 10 μM Pu22 or 22AG with 2 μM H1).

3.3.5.2. Maximum excitation / emission wavelengths of the bound fluorogenic probes in two phases

I confirmed that the change in the fluorescence intensity of the 'free probes' in low dielectric constant

environments, such as that of the droplets, was negligible. However, it remained unclear whether the droplet environment could affect the fluorescence of 'probes bound to the G-quadruplex'. The change in the dielectric constant of the solvent could potentially result in a shift in the maximum excitation (Ex)/emission (Em) wavelengths. Such spectral shifts could be related to the fluorescence of the probes inside the droplet. Thus, I measured the excitation and emission spectra of ThT and NMM in solutions containing Pu22 with or without H1 (i.e., under conditions in which droplets are formed or are not formed, respectively). The results showed that the maximum Ex/Em wavelengths of the two probes did not change regardless of whether droplets were formed (**Figure 3.14**). Therefore, the effect of peak shift can be excluded as a cause of the fluorescence enhancement.

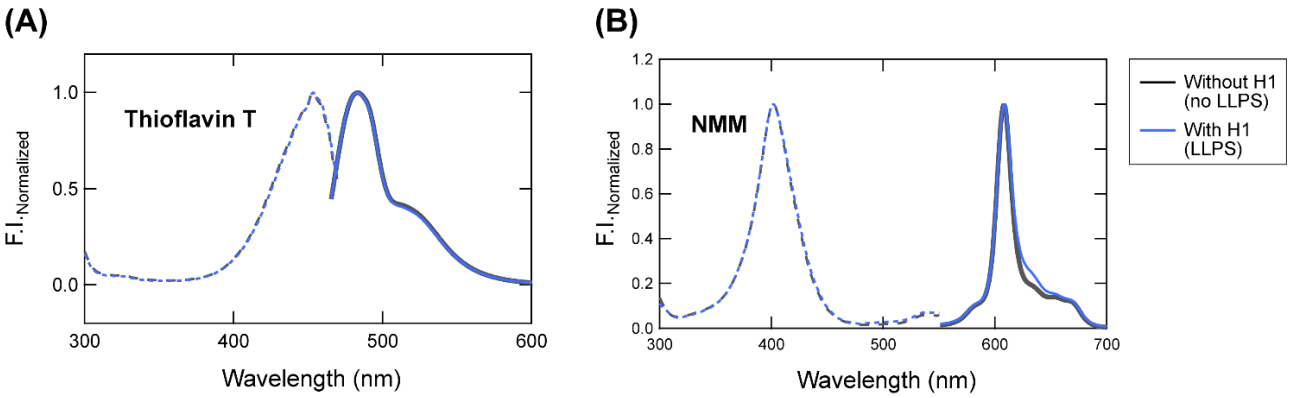

Figure 3.14. Excitation and emission spectra of fluorogenic probes with or without LLPS. Normalized excitation and emission spectra of solutions containing 10 μM Pu22 in the absence or presence of 2.0 μM H1 in TE buffer (pH = 7.5) after the addition of (A) 0.5 μM ThT or (B) 10 μM NMM. The fluorescence spectra were recorded at 25 °C (ThT: λ_{ex} = 445 nm for excitation spectra, λ_{em} = 490 nm for emission spectra; NMM: λ_{ex} = 400 nm for excitation spectra, λ_{em} = 610 nm for emission spectra).

3.3.5.3. Effect of the environment inside the droplets on the fluorescence intensity of 'probes bound to G-quadruplexes'

Having confirmed that the incorporation of the bound probes into the droplet did not cause a shift in their fluorescence wavelength, I then focused on the fluorescence intensity. I carried out experiments using the probes at different concentrations to examine their behavior under saturated and non-saturated binding conditions. I hypothesized that the quantum yield of probes bound to G-quadruplexes does not depend on whether the ssDNA/probe complex is incorporated into the droplet. If this is correct, when the probes (ThT and NMM) are first mixed with an excess of G-quadruplex ssDNA (Pu22) sufficient for almost all the probes to bind, the subsequent addition of H1 to form droplets should not change the fluorescence intensity (**Figure 3.15A**).

The binding isotherm of Pu22 to 0.05 μM ThT shows that almost all the ThT was bound to Pu22 in the presence of 10 μM Pu22 (**Figure 3.15B**). When 2 μM H1 was then added to a solution containing 0.05 μM ThT and 10 μM Pu22 to form droplets, the fluorescence of ThT showed little change (**Figure 3.15F**). This result suggested that, as hypothesized, the fluorescence of ThT bound to Pu22 was independent of droplet formation. On the other hand, when 0.5 μM ThT was used, free ThT was present even in the presence of 10 μM Pu22 (**Figure 3.15C**). Under these conditions, the addition of 2 μM H1 increased the fluorescence intensity of ThT (**Figure 3.15G**), suggesting that the folding of Pu22 into G-quadruplexes was promoted with the formation of droplets, and that the remaining ThT was able to bind to the newly formed G-quadruplexes, as suggested by the results of Figures 3.9 and 3.10. Similar results were obtained in the case of NMM (**Figures 3.15D, E, H and I**).

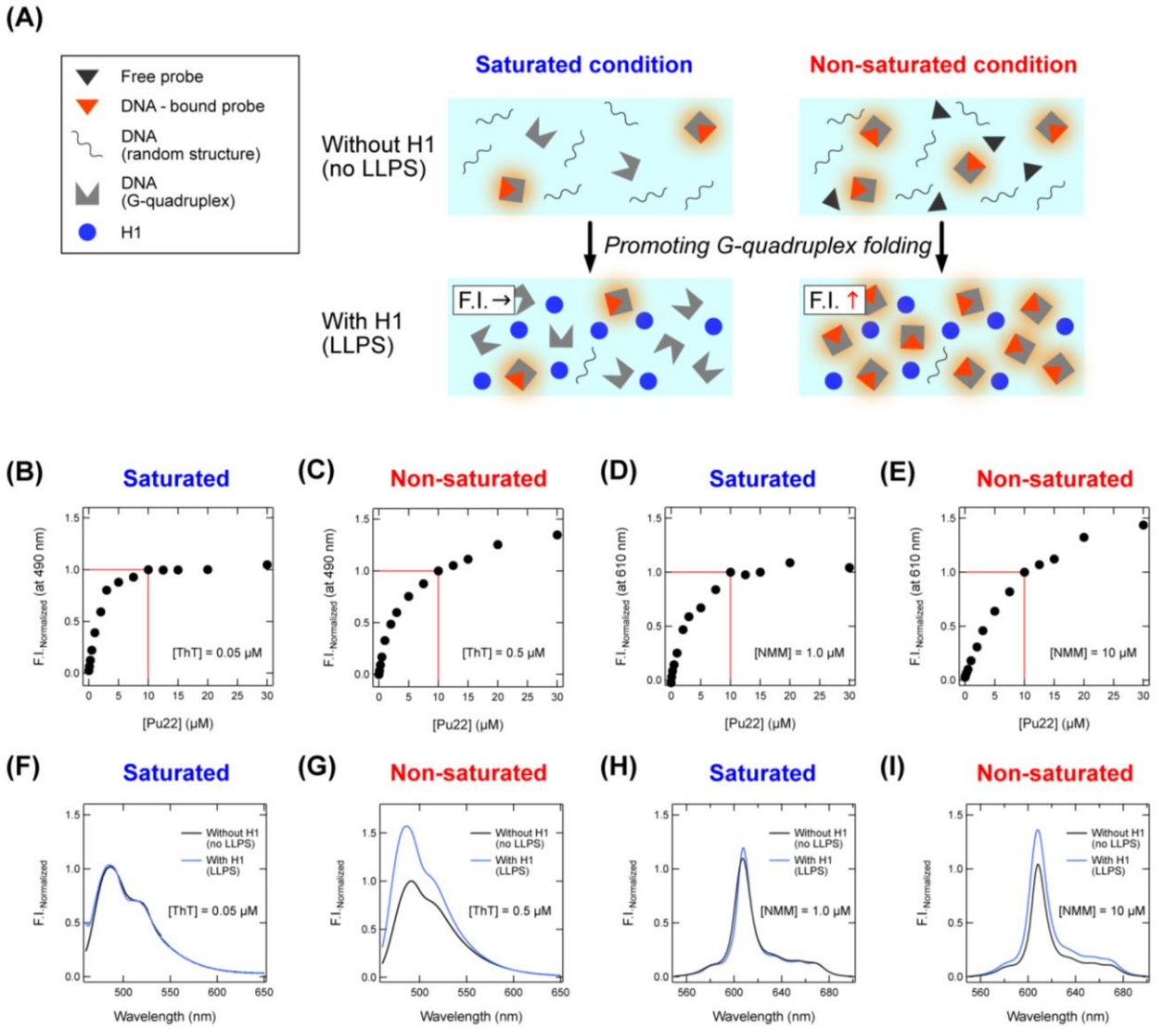

Figure 3.15. Relationship between the binding state of the fluorogenic probes to Pu22 and the fluorescence change before and after droplet formation. (A) Schematic illustration of scenarios in which two different concentrations of the probes are mixed with G-quadruplex-forming ssDNAs. One is the 'saturated condition', in which the probe concentration is sufficiently lower than that of Pu22, and hence, the binding is saturated. The other is a 'non-saturated condition', in which the probe concentration is sufficiently high for free probes to remain in the solution. Fluorescence intensity of 0.05 μM (B) or 0.5 μM (C) ThT and 1.0 μM (D) or 10 μM (E) NMM upon the addition of 0–30 μM Pu22 in TE buffer (pH = 7.4). The fluorescence intensity in each plot was normalized by that for 10 μM Pu22. Fluorescence spectra of 0.05 μM (F) or 0.5 μM ThT (G) and 10 μM (H) or 1.0 μM NMM (I) with 10 μM Pu22 in TE buffer (pH = 7.4) in the presence (blue) and absence (black) of 2 μM H1; λ_{ex} = 445 nm (ThT), λ_{ex} = 400 nm (NMM). The fluorescence intensity was normalized by that in the absence of H1 at 490 nm (ThT) or 610 nm (NMM).

To obtain further evidence that the fluorescence of the G-quadruplex-bound probes is not affected under LLPS conditions, measurements of the fluorescence lifetimes of the probes were performed for both 'dilute samples' containing Pu22 and 'condensed phase samples' containing Pu22 and H1. The condensed phase samples were the lower fraction obtained by centrifuging a suspension containing H1 and Pu22. Two fluorescence lifetime components were observed for ThT in a dilute sample (**Figure 3.16A**); one was less than 1 ns and was derived from free ThT, and the other was ~3 ns and was derived from ThT bound to the G-quadruplexes.[40] In the condensed phase sample, only the latter (~3 ns) was observed. The nearly identical fluorescence lifetimes in the two samples suggest that the fluorescence properties of ThT bound to G-quadruplex are not significantly affected by the surrounding environment. Similarly, the fluorescence lifetime of NMM was almost the same for dilute samples containing Pu22 and condensed phase samples containing Pu22 and H1 (**Figure 3.16B**).

Summarizing this section, I have shown that (i) the solution environments inside the droplet did not affect the fluorescence properties of the ThT and NMM probes bound to G-quadruplex ssDNAs, and (ii) the enhancement of the probe fluorescence observed under LLPS condition was due to an increase in the amount of G-quadruplex folding. Therefore, I consider that my two insights obtained from the probe responses are plausible; the interaction with H1 to induce droplet formation (i) facilitated parallel G-quadruplex folding of Pu22 and (ii) switched the G-quadruplex folding from the anti-parallel to parallel form of 22AG.

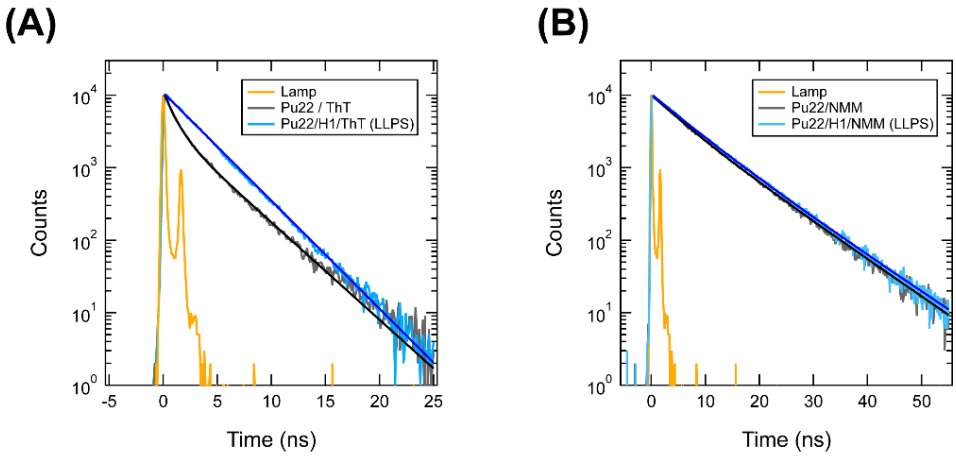

(C)

Sample	τ_1 (ns)	τ_2 (ns)	R^2
Pu22/ThT	3.23	0.91	0.9961
Pu22/H1/ThT	2.84	—	0.9963
Pu22/NMM	6.99	—	0.9961
Pu22/H1/NMM	7.42	—	0.9877

Figure 3.16. Fluorescence lifetimes of the probes in the dilute and droplet phases. Fluorescence decay traces of ThT (A) and NMM (B) in the presence of 10 µM Pu22 with (blue) and without (black) 2 µM H1 in TE buffer (pH = 7.4); $\lambda_{ex}/\lambda_{em}$ = 410 nm/490 nm for ThT, $\lambda_{ex}/\lambda_{em}$ = 410 nm/610 nm for NMM. (C) The τ values of ThT and NMM obtained by a reasonable fitting procedure based on the double-exponential function, supported by the high R^2 values (>0.98).

3.3.6. Spectroscopic investigation of quadruplex structures within droplets

Fluorescence measurements using G-quadruplex-specific probes suggested that the interactions between DNA and H1 to form droplets promoted the folding of parallel G-quadruplex structures (**Figures 3.9-11**, and the results shown in the Sections 3.3.4 and 3.3.5). In this section, to provide further support this interpretation, I investigated the structures of ssDNAs in the presence of H1, which induces droplet formation, by spectroscopic analyses.

3.3.6.1. Far UV CD measurements

First, I performed H1 titration experiments using the far-UV CD spectra of DNA solutions. These measurements were carried out only at relatively low H1 concentrations, as the turbidity of the solution caused by the formation of droplets increases the photomultiplier voltage, hampering the acquisition of the

signal. With the titration of H1, both Pu22 and Pu22-1 exhibited an increase in the negative peak at approximately 240 nm and the positive peak at approximately 260 nm, which represent parallel G-quadruplex folding (**Figure 3.17**). These results indicate that interaction with H1 promoted the folding of Pu22 and Pu22-1 into the G-quadruplex, which seems to be consistent with the results obtained using ThT.

As most of the ssDNAs were concentrated in the droplets (**Figure 3.6**), the CD spectra of the suspensions most likely derived from the ssDNAs inside the droplets. However, I further attempted to measure condensed phase samples prepared by centrifugation of the droplet suspensions in order to demonstrate more directly that the higher-order structures were maintained or promoted in the droplets. CD spectra of the condensed phase samples sandwiched between quartz plates provided a partial but qualitative understanding. Both the CD spectrum of Pu22 in the condensed phase sample and that of the H1-free TE buffer showed a positive peak at approximately 260 nm and a negative peak at approximately 245 nm, which implies the presence of parallel G-quadruplexes (**Figure 3.18A**). The slight peak shift observed was probably due to the stabilization of the G-quadruplex structure.[41] The CD spectrum of 22AG in the condensed phase was characterized by a negative peak at approximately 230 nm, a broad part at approximately 260 nm, and a positive peak at approximately 300 nm (**Figure 3.18B**). A comparison between a dilute solution in which antiparallel folding is dominant (with 50 mM NaCl) and one in which antiparallel and parallel folding coexist (with 50 mM KCl)[42] suggested that the CD spectrum in the condensed phase sample includes not only antiparallel but also some parallel structures, which is consistent with the insights gained from the experiments using fluorescent probes (**Figures 3.9-11** and the results shown in Sections 3.3.4 and 3.3.5).

These results suggest that, although not yet quantitatively understood, the formation of droplets with H1 maintained or promoted quadruplex folding, as was suggested by the results of the fluorescent probe experiments.

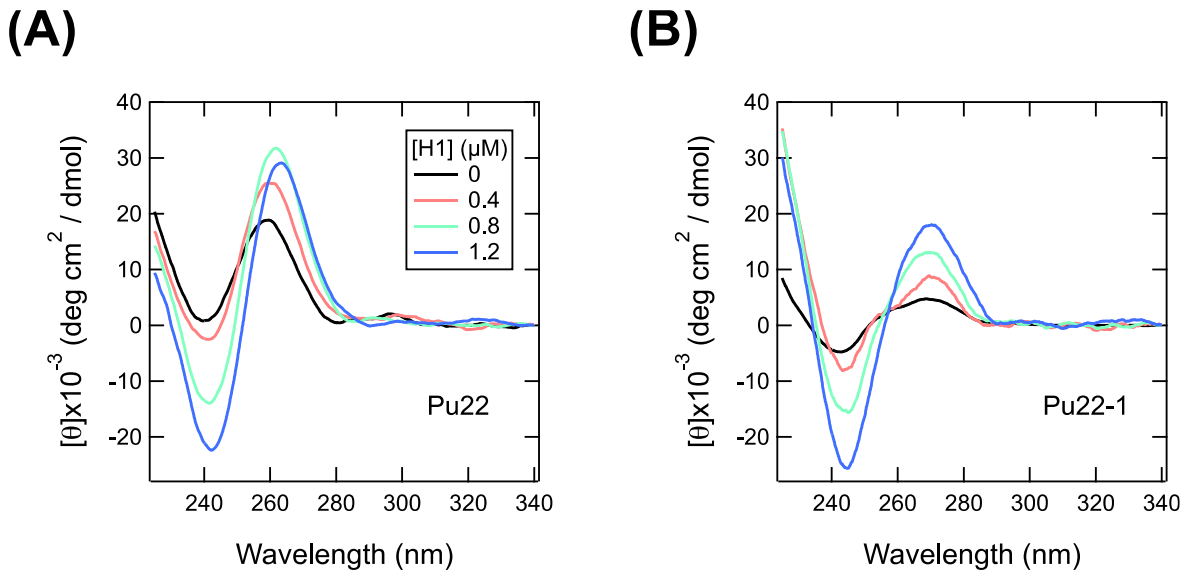

Figure 3.17. G-quadruplex folding via interaction with H1. CD spectra of solutions containing 10 μM ssDNAs [(A) Pu22 and (B) Pu22-1] with 0–1.2 μM H1 in TE buffer (pH = 7.4). CD spectra of solutions of H1 at the concentration corresponding to each spectrum were used for background subtraction.

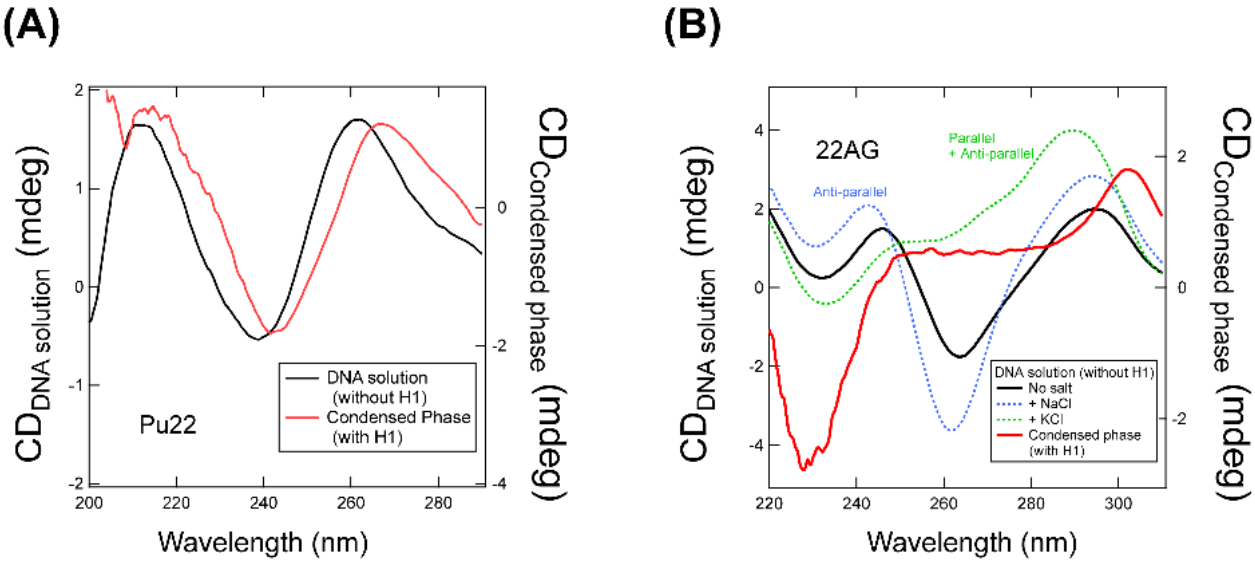

Figure 3.18. Structure of ssDNA sequences in the condensed phase. CD spectra of Pu22 (A), 22AG (B) in the condensed phase and various dilute solutions. Raw data is shown for the condensed phases due to the indefinite optical path length.

3.3.6.2. HR-MAS-NMR measurements

In order to observe the DNA structure inside the condensed phase from a different viewpoint, a condensed phase sample was measured using HR-MAS-NMR, which is a suitable technique for samples with high viscosity.[43] However, in the NMR spectrum of the obtained Pu22/H1 condensed phase, many peaks were remarkably broadened or disappeared, including in the region reflecting the G-quadruplex structure (10.5–12.0 ppm) (**Figure 3.19**). As similar broadening or disappearance of peaks was observed in other regions (e.g., 6.0–7.5 ppm), these results were likely caused by a decrease in the signals due to polymorphism of the G-quadruplex structure, exchange broadening induced by the interaction with H1, and/or an increase in the viscosity in the condensed phase.[44] Therefore, even if the G-quadruplex structure is maintained inside the droplet (as indicated in the fluorescence probe assays and CD spectra), it is highly likely that no clear signals will be generated in the HR-MAS-NMR spectrum.

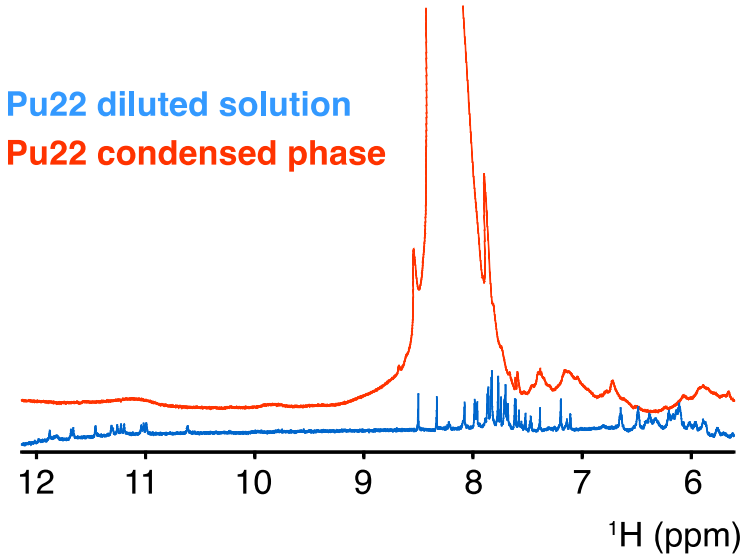

Figure 3.19. HR-MAS-NMR spectra of Pu22 in diluted and condensed phases.

In summary of this section, the CD spectra of the droplet suspensions and condensed phases supported the possibility of the promotion and maintenance of G-quadruplex folding inside the droplets. The measurements of the condensed phase using high-resolution magic angle spinning nuclear magnetic resonance (HR-MAS-NMR), which is a suitable technique for the NMR measurement of samples with high viscosity,[43] suggested that the conformation of quadruplex Pu22 inside the droplets may be polymorphic within the range to which G-quadruplex specific probes can bind.

3.3.7. Mechanism of the promotion of quadruplex folding during LLPS generation

The results of my fluorescence measurements (**Figure 3.9-11** and Sections 3.3.4) and the spectroscopic analyses in Section 3.3.6 suggested that G-quadruplex folding was promoted by the formation of DNA/H1 droplets. However, the mechanism by which G-quadruplex folding was promoted during droplet formation remains unclear. It has been reported that G-quadruplex folding is promoted by charge neutralization by cations,[45] which suggests that interaction with the lysine-rich cationic tail of H1 might have promoted G-quadruplex folding. G-quadruplex folding can also be promoted by solvents with low dielectric constant[46] or high viscosity,[47] such as the interior of liquid droplets. To examine whether the contribution of charge neutralization or solvent effects predominate in the enhanced G-quadruplex folding during droplet formation, I used two model cationic polymers: (i) poly-L-lysine (PLL), which is a simple repetitive sequence and was used to examine the role of charge neutralization by H1 and (ii) PEG-*block*-poly-L-lysine (PEG-*b*-PLL), which has a PEG chain that inhibits LLPS and was used to examine the role of a droplet environment.

Like H1, PLL formed droplets when mixed with Pu22, and in the case of Pu22-1, aggregation occurred (**Figure 3.20A**). In contrast to this result, PEG-*b*-PLL did not form visible assemblies when mixed with DNA due to the PEG segment. In ssDNA solutions in the absence and presence of both cationic polymers, ThT and NMM showed comparable fluorescence responses to those observed when H1 was used (**Figures 3.20B and 3.20C**). That is, both polymers promoted the folding of Pu22 and Pu22-1 into the G-quadruplex structure and induced the structural transition of 22AG from anti-parallel to parallel. Although it has been reported that dehydration due to the addition of crowder molecules affects the folding, it is likely that the main factor in my case is the stability change due to the nonspecific interactions with polycationic tails of H1. This action of H1 seems to resemble that of the chaperone-like surfaces of other proteins that facilitate the folding of the G-quadruplex, such as HIV-1 nucleocapsid proteins.[48]

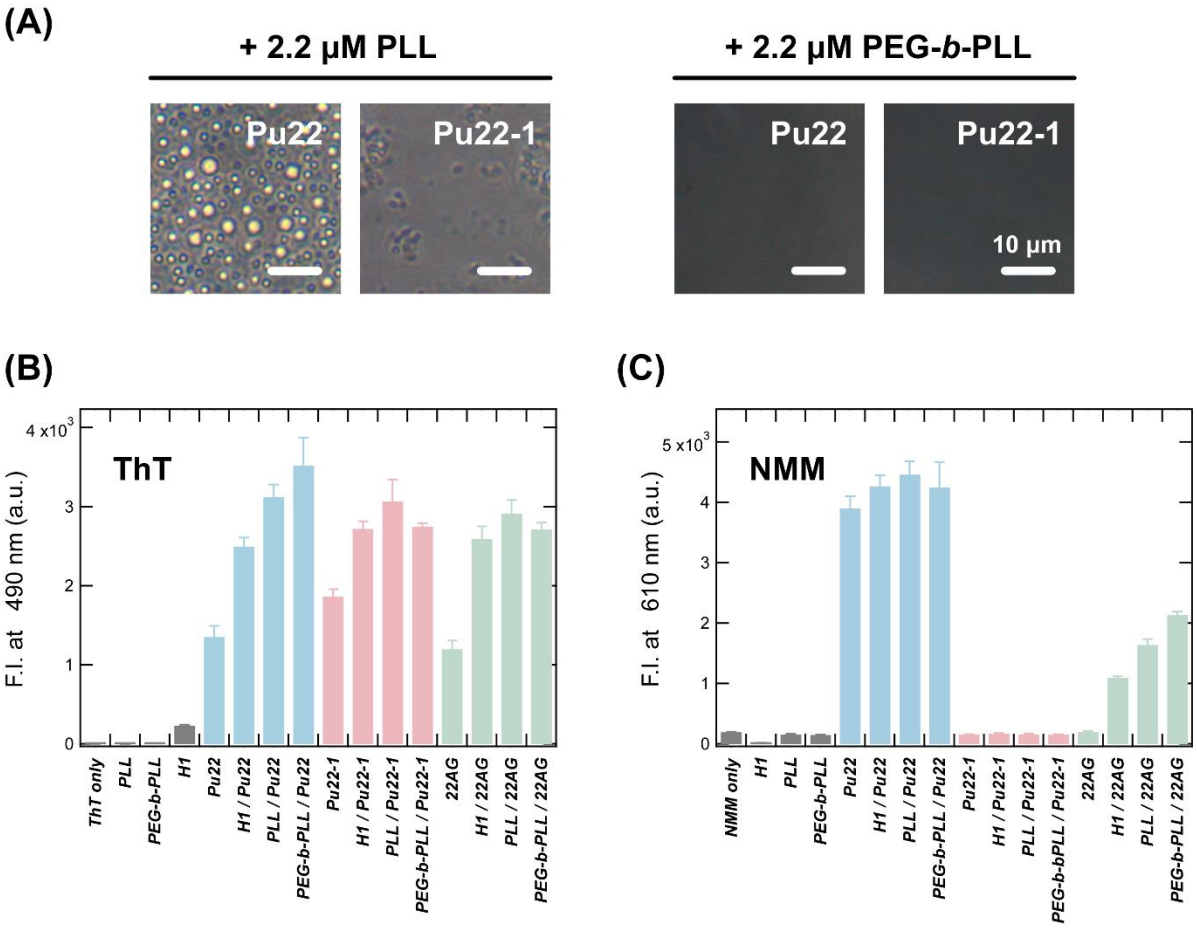

Figure 3.20. Comparison of the effects of H1 and cationic synthetic polymers on probe binding to ssDNAs. (A) Phase contrast microscopic images of solutions containing 10 μM ssDNA and 2.2 μM PLL or PEG-*b*-PLL in TE buffer (pH = 7.4). Fluorescence intensity of (B) 0.5 μM ThT and (C) 10 μM NMM in solutions that contain ssDNAs (10 μM) with or without H1 (2.0 μM), PLL or PEG-*b*-PLL (2.2 μM).

3.3.8. Generality of the promotion of LLPS by the quadruplex conformation

To clarify the generality of the promotion of LLPS by quadruplex structures in ssDNA, I tested another quadruplex structure formed by successive cytosine bases, the so-called i-motif (**Figure 3.21A**).[49] As in the case of G-quadruplex, the increase in turbidity upon addition of H1 was greater for an i-motif-forming sequence (22CT) than for a shuffled variant of this sequence in which the cytosines are not successive ($22CT_{shuffle}$) (**Figure 3.21B**). Consistent with the turbidity results, the droplets formed by 22CT were significantly larger than those formed by $22CT_{shuffle}$ (**Figure 3.21B**). The CD spectrum of 22CT in the absence of H1 showed that the i-motif structure is unstable at neutral pH, but is stabilized at acidic pH, producing a broad positive peak at approximately 290 nm (**Figure 3.21C**).[50] The spectrum of the condensed

phase sample is similar to that at acidic pH, suggesting that that the folding of 22CT into the i-motif was promoted by the process of H1 binding coupled to the droplet formation (**Figure 3.21C**).

Thus, the dependence of the phase separation behavior on the arrangement of the ssDNA suggests that the quadruplex structure is important in promoting LLPS with H1, regardless of the kind of constituent nucleobases. In addition, I found that the droplet formation between quadruplex-forming ssDNAs and polycationic chains such as H1 was synchronized with structural stabilization or transition.

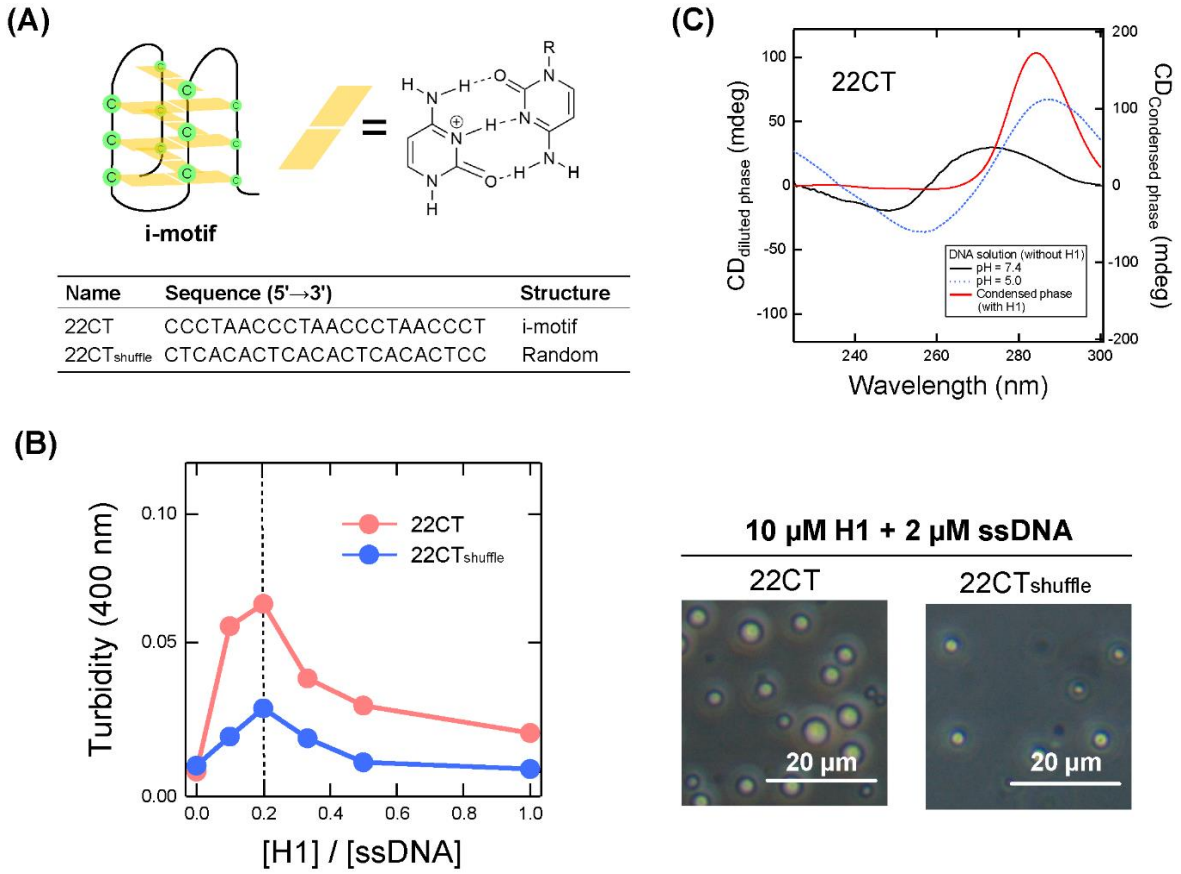

Name	Sequence (5'→3')	Structure
22CT	CCCTAACCCTAACCCTAACCCT	i-motif
$22CT_{shuffle}$	CTCACACTCACACTCACACTCC	Random

Figure 3.21. Droplet formation in a solution that contains cytosine-based quadruplex structures and H1. (A) Schematic illustration of the i-motif structure and the DNA sequences used in this experiment. (B) Formation of liquid droplets in solutions of i-motif DNA (22CT) or a shuffled sequence ($22CT_{shuffle}$) with H1 (2 μM); scale bar = 20 μm. (C) CD spectra of 22CT in the condensed phase and various dilute solutions.

3.3.9. Driving forces for the formation of droplets between DNAs and H1

Subsequently, I investigated the reason that the quadruplex structures promote droplet formation between H1 and ssDNA. To gain further insight into the driving forces of droplet formation, I examined the effects of additives (NaCl and 1,6-hexanediol) that can inhibit electrostatic and hydrophobic interactions, respectively,[51] by adding them to solutions containing the DNA/H1 liquid droplets. For comparison, I also used 11-base pairs of double-stranded DNA ($dsDNA_{11}$; for DNA sequence, see in **Table 3.1**), which had the same total number of nucleobases as the other ssDNAs. The duplex structure has some features similar to those of the quadruplex structure: (i) nucleobases embedded by base pairing, (ii) a relatively rigid structure, and (iii) LLPS occurs when mixed with H1.[12,52]

NaCl markedly reduced both the turbidity of the solution and the droplet size (**Figure 3.22**). In all DNAs, the droplets disappeared completely at higher-than-physiological NaCl concentrations (~300 mM), as observed previously.[12] This result demonstrates that the electrostatic interactions between the cationic C-terminus of H1 and the anionic phosphate groups of DNAs are the dominant driving force in the generation of LLPS.

Unexpectedly, the droplets consisting of the various G-quadruplex-forming ssDNAs gradually dissolved as the 1,6-hexanediol concentration was increased, whereas the turbidity of the solutions containing droplets formed by $dsDNA_{11}$ did not change at all, even in the presence of 20% 1,6-hexanediol (**Figure 3.23**). This result suggests that hydrophobic interactions contribute substantially to the stabilization of the droplets of G-quadruplex-forming ssDNAs, but not those of $dsDNA_{11}$. To better understand the nature of these hydrophobic interactions, the relationship between LLPS and the nucleotide-monophosphate (NMP), DNA structural units, was examined. Among the four NMPs, only guanine monophosphate (GMP) caused droplet formation in the presence of both H1 and high concentrations of PEG, which is known to promote the generation of LLPS (**Figure 3.24**).[53]

Guanine has the lowest energy of stacking interaction with both aromatic amino acids[54] and nucleobases[55] among the nucleobases. Considering the fact that H1 contains only several aromatic amino acids (only two Phe and three Tyr in 194 aa), more stable stacking of the guanine bases may explain the results observed for the various NMPs, i.e., it is plausible that the hydrophobic π-π stacking of guanine bases is a significant factor for the LLPS of G-quadruplexes.

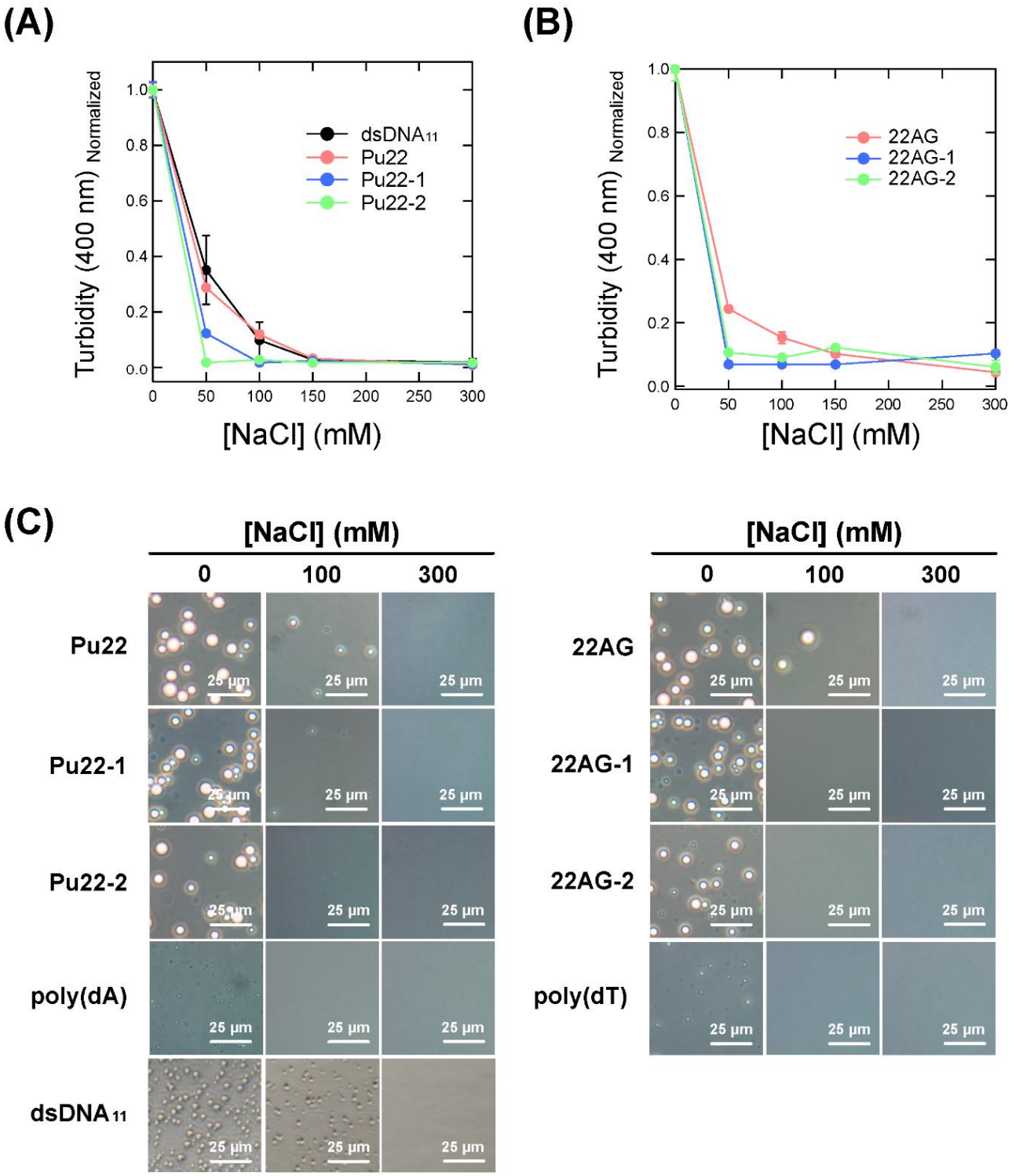

Figure 3.22. (A, B) Turbidity of solutions that contain ssDNA (10 μM) and H1 (0-10 μM) in the presence of the 0-300 mM NaCl (B) Phase-contrast microscopy images of the ssDNA / H1 solutions in the presence of NaCl; scale bar = 25 μm.

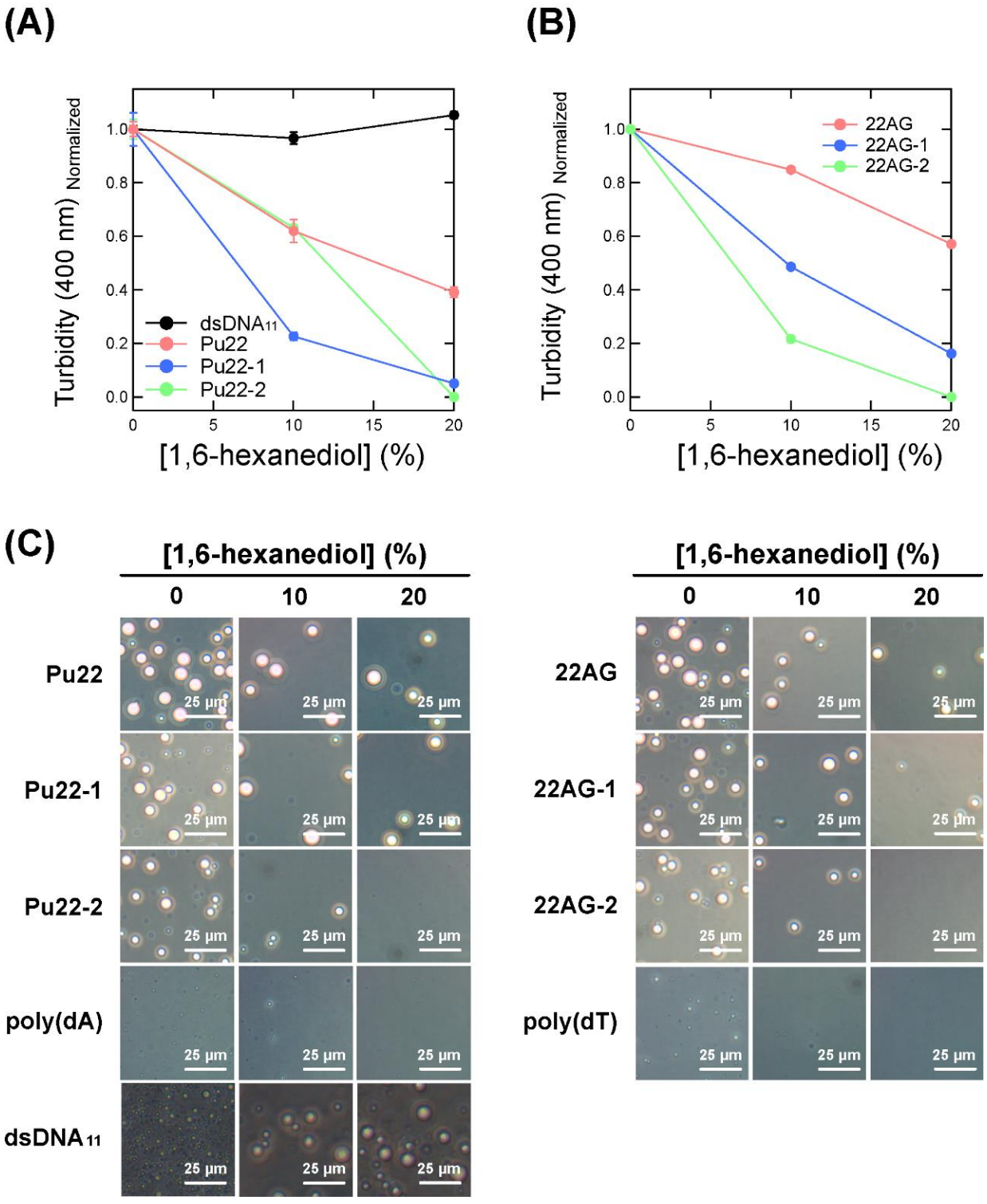

Figure 3.23. (A, B) Turbidity of solutions of the ssDNA/H1 liquid droplets in the presence of 0-20% 1,6–hexanediol. (B) Phase-contrast microscopy images of the ssDNA / H1 solutions in the presence of 1,6–hexanediol; scale bar = 25 μm.

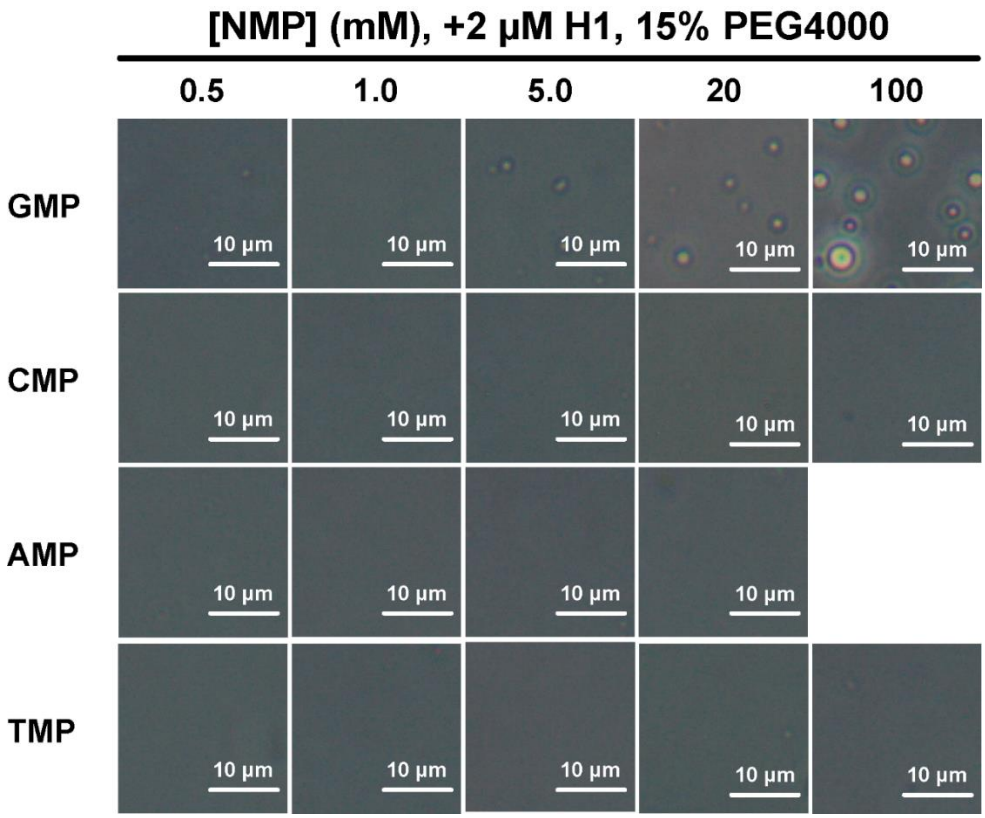

Figure 3.24. Droplet formation of nucleoside monophosphates (NMP) with H1. Phase-contrast microscopy images of solutions that contain 0-100 mM NMP, 2 μM H1, and 15% PEG4000; scale bar = 10 μm. Due to the low solubility of AMP, only data up to 20 mM are shown.

Taken together, (i) electrostatic interactions between the DNAs and the intrinsically disordered region of H1 and (ii) π-π stacking between quadruplex DNAs drove droplet formation between G-quadruplex DNA and H1, unlike in the electrostatically driven LLPS of duplex DNA and H1. In addition to electrostatic interactions, π-π interactions are known to be significant in protein phase separation to direct the state of the assembly towards liquid-like droplets rather than gel-like aggregates.[56] Hydrogen-bonding interactions between partially exposed guanine bases and lysine residues[57] of H1, and cation-π interactions, which stabilize a wide variety of intracellular droplets,[58,59] between the same pairs may also contribute to the stability of the DNA/H1 droplets.

3.3.10. Role of structural rigidity on the formation of droplets between DNAs and H1

Although the key driving forces have been identified, the effects of the structuring of ssDNA on the formation of droplets are still puzzling. It is generally believed that biological LLPS requires flexible sequences (e.g., IDR).[60] It has been reported that when DNAs are stiffened by the formation of secondary structures such as double strands or loops, they form gel-like aggregates rather than liquid-like droplets in the presence of cationic polymers,[61,62] or are excluded from protein droplets.[63] The high droplet formation ability of the compact and rigid quadruplex folding structure seems to be inconsistent with these findings.

Therefore, the effect of structuring was investigated by comparing the LLPS of flexible poly(dA) and a highly rigid, hydrophilic, spherical poly(amidoamine) (PAMAM) dendrimer with 64 carboxyl groups on its surface. According to the phase diagrams of H1 vs. NaCl concentration (**Figures 3.25 and 3.26**), Pu22, whose rigidity is intermediate between those of dsDNA[64] and the PAMAM dendrimer,[65] clearly exhibited the highest phase separation ability (**Figure 3.26**). This result implies that structural flexibility is not necessarily an essential factor for LLPS with H1. The PAMAM dendrimer can also be considered to be a model of polyanionic proteins, such as the histone chaperone prothymosin alpha, which can bind and condense H1 without LLPS,[66] and my result may be similar to the behavior of such proteins.

The observed high LLPS ability of quadruplex folding structures is possibly due to the formation of interfaces consisting of organized top/bottom planes of guanine bases and the interactions between interfaces formed by structuring can promote LLPS.[67] Short dsDNAs also undergo hierarchical self-assembly by end-to-end stacking of base pairs at the terminal interfaces upon droplet formation with polycations.[68] The G-quadruplex exhibits more open and wider stacking interfaces compared to the duplex, and DNAs with quadruplex structures tend to stack intermolecularly in the longitudinal direction at high concentrations.[69,70] These characteristics explain the smaller contribution of hydrophobic interactions in the duplexes compared to that in the G-quadruplexes. Indeed, the phase diagrams showed that Pu22 droplets appeared to be more tolerant to salts than $dsDNA_{11}$ droplets (**Figures 3.26**). This difference should be attributed to improved stability due to hydrophobic inter-nucleobase stackings provided by the upper and lower surfaces of G-quartets. Turbidity measurements (**Figure 3.3**) showed that one H1 molecule bound to multiple ssDNAs. This bridging of ssDNAs by H1 likely contributed to the facilitation of the stacking, and eventually stabilized the intermolecular G-quadruplex formation.

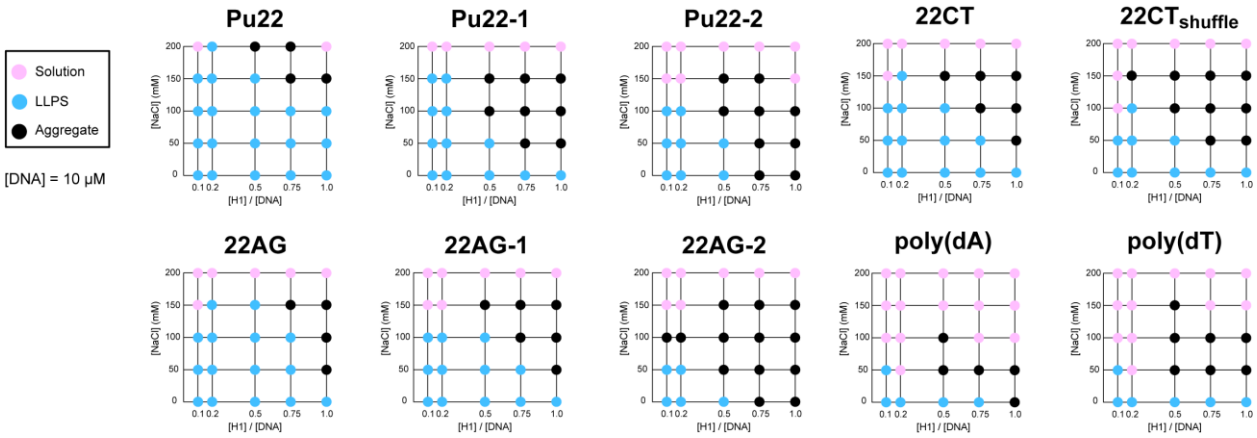

Figure 3.25. Phase diagrams of the DNA/H1 complexes as a function of NaCl concentration (0–200 mM) and molar mixing ratio of DNA (10 μM) and H1 (1–10 μM).

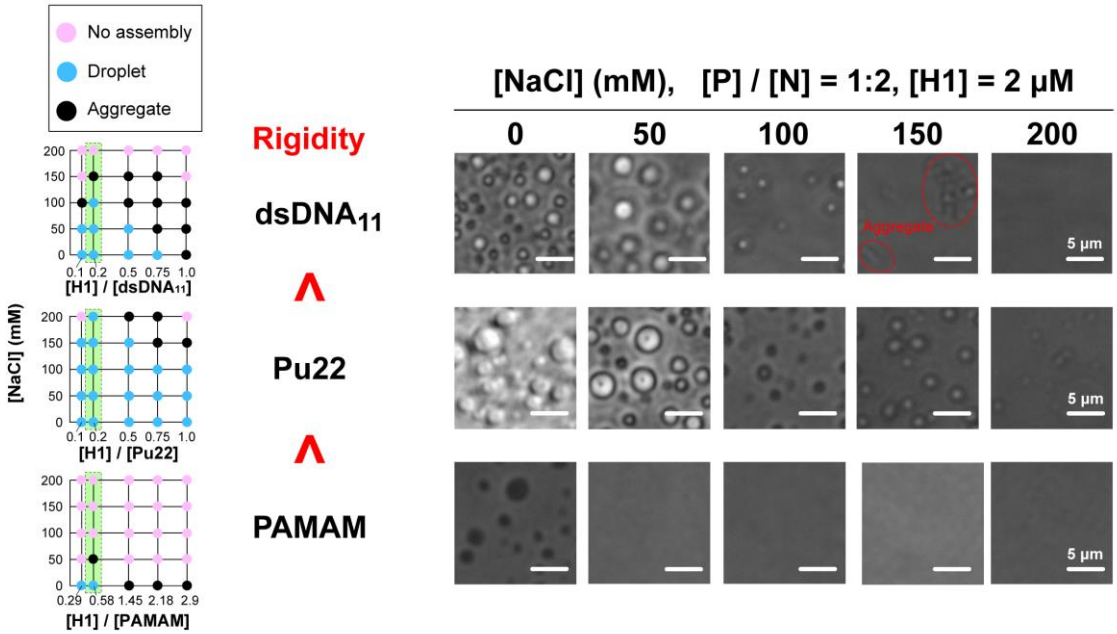

Figure 3.26. Effect of the rigidity of the anionic molecules on the salt tolerance of droplets formed with H1. Left: Phase diagrams of the aqueous mixtures of H1 and anionic molecules with different rigidity. The solution states were plotted as the NaCl concentration vs. the molar mixing ratio of H1 to DNAs (10 μM) or PAMAM (3.44 μM). Right: Phase contrast microscopic images of solutions containing DNA (10 μM) or PAMAM (3.44 μM) and H1 (2 μM), i.e., with a charge ratio ([Positive] / [Negative] = [P] / [N]) of 0.5, in the presence of 0–200 mM NaCl (green shaded region in the phase diagrams). The more-rigid PAMAM and less-rigid dsDNA lost their ability to form droplets in the presence of 150 mM or less of NaCl. On the other hand, G-quadruplex-forming Pu22 was able to form droplets even in the presence of 200 mM NaCl, indicating that the G-quadruplex has the highest phase separation ability among the anionic molecules used in this experiment; scale bar = 5 μm.

The correlation between the LLPS ability of DNAs with the same number of charges [Pu22, dsDNA11, and poly(dA)] and charge density (**Figure 3.27**) also suggests the importance of increasing the charge density via structuring. In addition to the planar interfaces preferred for π-π stacking on the top and bottom surfaces, the formation of high-charge-density interfaces on the side surfaces that allow strong electrostatic contacts[71] provides unique features favorable for droplet formation. I thus concluded that the densification of the electrostatic and stacking interactions via the formation of such structures is a key to the high LLPS ability of quadruplex folding structures.

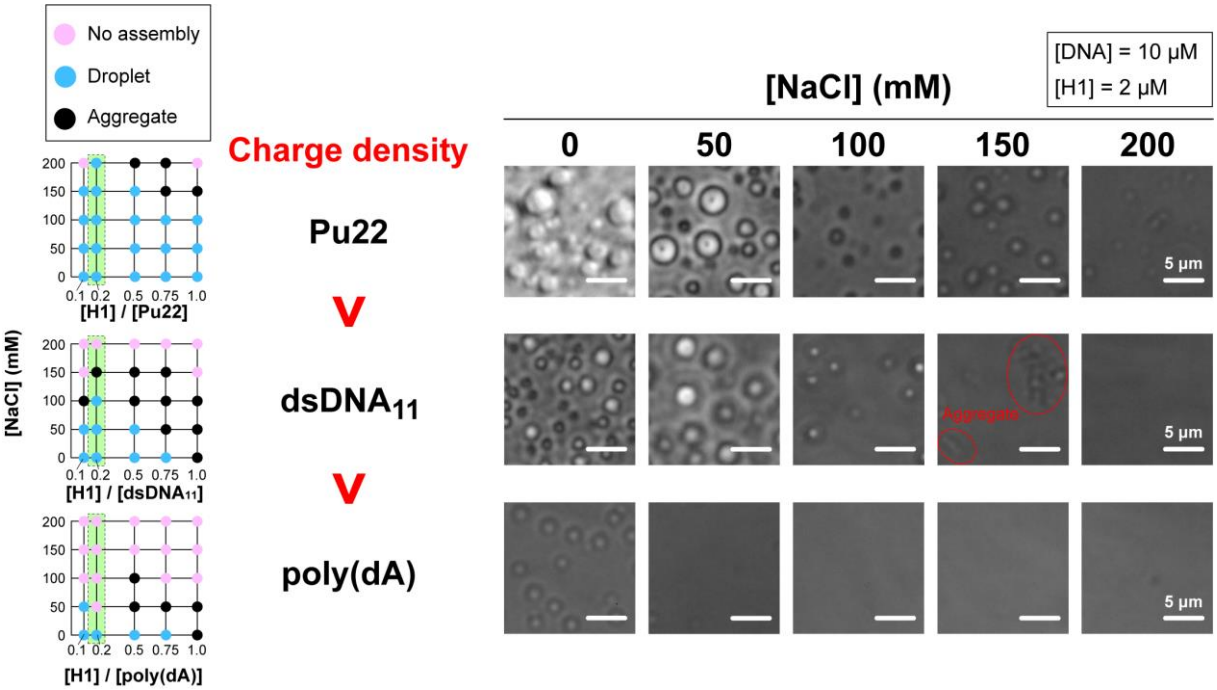

Figure 3.27. Effect of the linear charge density of the DNA sequences on the phase behavior of the DNA/H1 system. Left: Phase diagram of the DNA/H1 system as a function of the NaCl concentration and molar mixing ratio of DNA (10 μM) and H1 (1–10 μM) for the G-quadruplex Pu22, duplex $dsDNA_{11}$, and randomly structured poly(dA). Right: Phase contrast microscopic images of a solution containing DNA (10 μM) and H1 (2 μM) in the presence of 0–200 mM NaCl (green shaded region in the phase diagrams); scale bar = 5 μm.

The possible existence of G-quadruplex droplets in the cell nucleus is suggested by the fact that the droplets formed by G-quadruplexes became larger with increasing molecular concentration, even at physiological ionic strength, unlike random structured DNA (**Figure 3.28**). The quadruplexes in the nucleus are inhomogeneously distributed depending on the surrounding environment and protein binding. For example, G-quadruplex DNAs and RNAs are concentrated in the promoter and telomere regions of specific genes to form G-quadruplex clusters.[14,15] The concentrations of G-quadruplex DNAs and RNAs thus formed in the nucleus could potentially exceed the thresholds of LLPS locally and transiently, and could be involved, for example, in H1-mediated chromatin LLPS that changes over time.[52] Careful observations of quadruplex DNAs in cells from the perspective of LLPS will shed new light on the role of quadruplex DNAs.

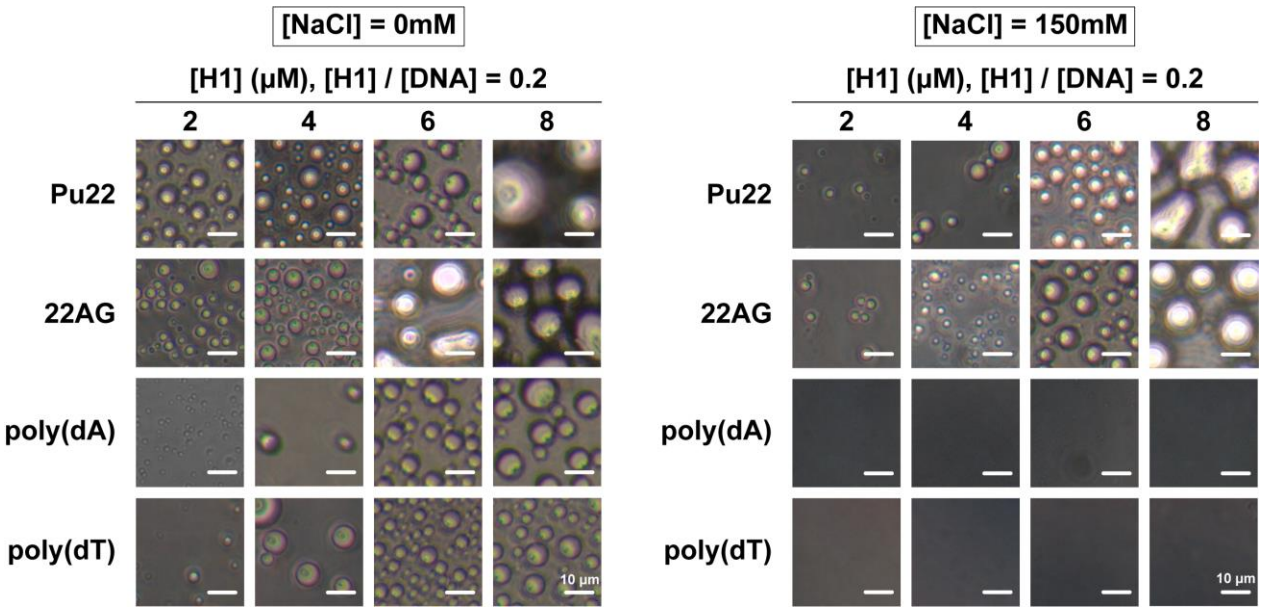

Figure 3.28. Effect of the ssDNA/H1 molecular concentration on salt tolerance. Phase contrast microscopic images of solutions containing a constant ratio of ssDNA (10–40 μM) and H1 (2–8 μM), i.e., [H1]/[ssDNA] = 0.2, in TE buffer (pH = 7.4) in the absence (left panel) or presence (right panel) of 150 mM NaCl; scale bar = 10 μm.

3.4. Conclusion

In summary, I have demonstrated that the formation of quadruplex structures in single-strand DNA (ssDNA), including guanine-based parallel and anti-parallel G-quadruplexes and cytosine-based i-motif structures, promotes the formation of liquid-like droplets with linker histone H1 via liquid-liquid phase separation (LLPS). The quadruplex folding is maintained or, in some cases, promoted due to the binding of H1 coupled to the droplet formation. Increasing the quadruplex content decreases both the motility and the density of the molecules that comprise the droplet. These droplets are likely formed via not only electrostatic interactions between the anionic ssDNA and the cationic C-terminus of H1, but also via π-π interactions between the quadruplex structures. Thus, DNA quadruplex structures may be capable of regulating LLPS-mediated dynamic chromatin condensation in the nucleus. DNA and RNA with G-quadruplex structures can selectively interact with nuclear proteins such as fused in sarcoma (FUS) and hnRNPA1, which cause amyotrophic lateral sclerosis (ALS) and tend to phase-separate.[72,73] Accordingly, I expect that the quadruplex structure can act as a hub that regulates biological processes such as chromatin condensation in the nucleus via LLPS.

3.5 References

(1) Kouzarides, T. Chromatin Modifications and Their Function. *Cell* **2007**, *128* (4), 693–705.

(2) Criscione, S. W.; Teo, Y. V.; Neretti, N. The Chromatin Landscape of Cellular Senescence. *Trends Genet*. **2016**, *32* (11), 751–761.

(3) Grunstein, M. Histone Acetylation in Chromatin Structure and Transcription. *Nature* **1997**, *389* (6649), 349–352.

(4) Erdel, F.; Rippe, K. Formation of Chromatin Subcompartments by Phase Separation. *Biophys. J*. **2018**, *114* (10), 2262–2270.

(5) Banani, S. F.; Lee, H. O.; Hyman, A. A.; Rosen, M. K. Biomolecular Condensates: Organizers of Cellular Biochemistry. *Nat. Rev. Mol. Cell Biol*. **2017**, *18* (5), 285–298.

(6) Boeynaems, S.; Alberti, S.; Fawzi, N. L.; Mittag, T.; Polymenidou, M.; Rousseau, F.; Schymkowitz, J.; Shorter, J.; Wolozin, B.; Van Den Bosch, L.; Tompa, P.; Fuxreiter, M. Protein Phase Separation: A New

Phase in Cell Biology. *Trends Cell Biol.* **2018**, *28* (6), 420–435.

(7) Iwashita, K.; Mimura, M.; Shiraki, K. Control of Aggregation, Coaggregation, and Liquid Droplet of Proteins Using Small Additives. *Curr. Pharm. Biotechnol.* **2018**, *19* (12), 946–955.

(8) Larson, A. G.; Elnatan, D.; Keenen, M. M.; Trnka, M. J.; Johnston, J. B.; Burlingame, A. L.; Agard, D. A.; Redding, S.; Narlikar, G. J. Liquid Droplet Formation by HP1α Suggests a Role for Phase Separation in Heterochromatin. *Nature* **2017**, *547* (7662), 236–240.

(9) Strom, A. R.; Emelyanov, A. V.; Mir, M.; Fyodorov, D. V.; Darzacq, X.; Karpen, G. H. Phase Separation Drives Heterochromatin Domain Formation. *Nature* **2017**, *547* (7662), 241–245.

(10) Gibson, B. A.; Doolittle, L. K.; Schneider, M. W. G.; Jensen, L. E.; Gamarra, N.; Henry, L.; Gerlich, D. W.; Redding, S.; Rosen, M. K. Organization of Chromatin by Intrinsic and Regulated Phase Separation. *Cell* **2019**, *179* (2), 470–484.e21.

(11) Shin, Y.; Chang, Y.-C.; Lee, D. S. W.; Berry, J.; Sanders, D. W.; Ronceray, P.; Wingreen, N. S.; Haataja, M.; Brangwynne, C. P. Liquid Nuclear Condensates Mechanically Sense and Restructure the Genome. *Cell* **2018**, *175* (6), 1481–1491.e13.

(12) Turner, A. L.; Watson, M.; Wilkins, O. G.; Cato, L.; Travers, A.; Thomas, J. O.; Stott, K. Highly Disordered Histone H1− DNA Model Complexes and Their Condensates. *Proc. Natl. Acad. Sci. U. S. A.* **2018**, *115* (47), 11964–11969.

(13) Burge, S.; Parkinson, G. N.; Hazel, P.; Todd, A. K.; Neidle, S. Quadruplex DNA: Sequence, Topology and Structure. *Nucleic Acids Res*. **2006**, *34* (19), 5402–5415.

(14) Yoshida, W.; Saikyo, H.; Nakabayashi, K.; Yoshioka, H.; Bay, D. H.; Iida, K.; Kawai, T.; Hata, K.; Ikebukuro, K.; Nagasawa, K.; Karube, I. Identification of G-Quadruplex Clusters by High-Throughput Sequencing of Whole-Genome Amplified Products with a G-Quadruplex Ligand. *Sci. Rep.* **2018**, *8* (1), 3116.

(15) Xu, Y.; Suzuki, Y.; Ito, K.; Komiyama, M. Telomeric Repeat-Containing RNA Structure in Living Cells. *Proc. Natl. Acad. Sci. U. S. A.* **2010**, *107* (33), 14579–14584.

(16) Murat, P.; Balasubramanian, S. Existence and Consequences of G-Quadruplex Structures in DNA. *Curr. Opin. Genet. Dev.* **2014**, *25* (1), 22–29.

(17) Paeschke, K.; Simonsson, T.; Postberg, J.; Rhodes, D.; Lipps, H. J. Telomere End-Binding Proteins

Control the Formation of G-Quadruplex DNA Structures in Vivo. *Nat. Struct. Mol. Biol*. **2005**, *12* (10), 847–854.

(18) Hoffmann, R. F.; Moshkin, Y. M.; Mouton, S.; Grzeschik, N. A.; Kalicharan, R. D.; Kuipers, J.; Wolters, A. H. G.; Nishida, K.; Romashchenko, A. V.; Postberg, J.; Lipps, H.; Berezikov, E.; Sibon, O. C. M.; Giepmans, B. N. G.; Lansdorp, P. M. Guanine Quadruplex Structures Localize to Heterochromatin. *Nucleic Acids Res.* **2016**, *44* (1), 152–163.

(19) Elbaum-Garfinkle, S.; Kim, Y.; Szczepaniak, K.; Chen, C. C.-H.; Eckmann, C. R.; Myong, S.; Brangwynne, C. P. The Disordered P Granule Protein LAF-1 Drives Phase Separation into Droplets with Tunable Viscosity and Dynamics. *Proc. Natl. Acad. Sci. U. S. A.* **2015**, *112* (23), 7189–7194.

(20) Bhamla, M. S.; Benson, B.; Chai, C.; Katsikis, G.; Johri, A.; Prakash, M. Hand-Powered Ultralow-Cost Paper Centrifuge. *Nat. Biomed. Eng.* 2017, *1* (1), 0009.

(21) Perišić, O.; Schlick, T. Dependence of the Linker Histone and Chromatin Condensation on the Nucleosome Environment. *J. Phys. Chem. B* **2017**, *121* (33), 7823–7832.

(22) Shakya, A.; King, J. T. Non-Fickian Molecular Transport in Protein–DNA Droplets. *ACS Macro Lett.* **2018**, *7* (10), 1220–1225.

(23) Ambrus, A.; Chen, D.; Dai, J.; Jones, R. A.; Yang, D. Solution Structure of the Biologically Relevant G-Quadruplex Element in the Human c-MYC Promoter. Implications for G-Quadruplex Stabilization. *Biochemistry* **2005**, *44* (6), 2048–2058.

(24) Carvalho, J.; Queiroz, J. A.; Cruz, C. Circular Dichroism of G-Quadruplex: A Laboratory Experiment for the Study of Topology and Ligand Binding. *J. Chem. Educ*. **2017**, *94* (10), 1547–1551.

(25) Masiero, S.; Trotta, R.; Pieraccini, S.; De Tito, S.; Perone, R.; Randazzo, A.; Spada, G. P. A Non-Empirical Chromophoric Interpretation of CD Spectra of DNA G-Quadruplex Structures. *Org. Biomol. Chem.* **2010**, *8* (12), 2683–2692.

(26) Gray, D. M.; Ratliff, R. L.; Vaughan, M. R. Circular Dichroism Spectroscopy of DNA. In *Methods Enzymol*.; Academic Press, **1992**, *211*, 389–406.

(27) Kurinomaru, T.; Maruyama, T.; Izaki, S.; Handa, K.; Kimoto, T.; Shiraki, K. Protein–Poly(Amino Acid) Complex Precipitation for High-Concentration Protein Formulation. *J. Pharm. Sci.* **2014**, *103* (8), 2248–2254.

(28) Matsuda, A.; Mimura, M.; Maruyama, T.; Kurinomaru, T.; Shiuhei, M.; Shiraki, K. Liquid Droplet of Protein-Polyelectrolyte Complex for High-Concentration Formulations. *J. Pharm. Sci.* **2018**, *107* (10), 2713–2719.

(29) Mimura, M.; Tsumura, K.; Matsuda, A.; Akatsuka, N.; Shiraki, K. Effect of Additives on Liquid Droplet of Protein–Polyelectrolyte Complex for High-Concentration Formulations. *J. Chem. Phys.* **2019**, *150* (6), 064903.

(30) Brangwynne, C. P.; Eckmann, C. R.; Courson, D. S.; Rybarska, A.; Hoege, C.; Gharakhani, J.; Jülicher, F.; Hyman, A. A. Germline P Granules Are Liquid Droplets That Localize by Controlled Dissolution/Condensation. *Science* **2009**, *324* (5935), 1729–1732.

(31) Taylor, N. O.; Wei, M.-T.; Stone, H. A.; Brangwynne, C. P. Quantifying Dynamics in Phase-Separated Condensates Using Fluorescence Recovery after Photobleaching. *Biophys. J.* **2019**, *117* (7), 1285–1300.

(32) Wei, M.-T.; Elbaum-Garfinkle, S.; Holehouse, A. S.; Chen, C. C.-H.; Feric, M.; Arnold, C. B.; Priestley, R. D.; Pappu, R. V.; Brangwynne, C. P. Phase Behaviour of Disordered Proteins Underlying Low Density and High Permeability of Liquid Organelles. *Nat. Chem*. **2017**, *9* (11), 1118–1125.

(33) Lin, Y.; Protter, D. S. W.; Rosen, M. K.; Parker, R. Formation and Maturation of Phase-Separated Liquid Droplets by RNA-Binding Proteins. *Mol. Cell* **2015**, *60* (2), 208–219.

(34) Gabelica, V.; Maeda, R.; Fujimoto, T.; Yaku, H.; Murashima, T.; Sugimoto, N.; Miyoshi, D. Multiple and Cooperative Binding of Fluorescence Light-up Probe Thioflavin T with Human Telomere DNA G-Quadruplex. *Biochemistry* **2013**, *52* (33), 5620–5628.

(35) Nicoludis, J. M.; Barrett, S. P.; Mergny, J.-L.; Yatsunyk, L. A. Interaction of Human Telomeric DNA with N-Methyl Mesoporphyrin IX. *Nucleic Acids Res.* **2012**, *40* (12), 5432–5447.

(36) Xue, Y.; Kan, Z.-Y.; Wang, Q.; Yao, Y.; Liu, J.; Hao, Y.-H.; Tan, Z. Human Telomeric DNA Forms Parallel-Stranded Intramolecular G-Quadruplex in K+ Solution under Molecular Crowding Condition. *J. Am. Chem. Soc.* **2007**, *129* (36), 11185–11191.

(37) Koga, S.; Williams, D. S.; Perriman, A. W.; Mann, S. Peptide-Nucleotide Microdroplets as a Step towards a Membrane-Free Protocell Model. *Nat. Chem.* **2011**, *3* (9), 720–724.

(38) Maskevich, A. A.; Stsiapura, V. I.; Kuzmitsky, V. A.; Kuznetsova, I. M.; Povarova, O. I.; Uversky, V. N.; Turoverov, K. K. Spectral Properties of Thioflavin T in Solvents with Different Dielectric Properties

and in a Fibril-Incorporated Form. *J. Proteome Res.* **2007**, *6* (4), 1392–1401.

(39) Sackett, D. L.; Wolff, J. Nile Red as a Polarity-Sensitive Fluorescent Probe of Hydrophobic Protein Surfaces. *Anal. Biochem*. **1987**, *167* (2), 228–234.

(40) Mohanty, J.; Barooah, N.; Dhamodharan, V.; Harikrishna, S.; Pradeepkumar, P. I.; Bhasikuttan, A. C. Thioflavin T as an Efficient Inducer and Selective Fluorescent Sensor for the Human Telomeric G-Quadruplex DNA. *J. Am. Chem. Soc.* **2013**, *135* (1), 367–376.

(41) González, V.; Hurley, L. H. The C-Terminus of Nucleolin Promotes the Formation of the c-MYC G-Quadruplex and Inhibits c-MYC Promoter Activity. *Biochemistry* **2010**, *49* (45), 9706–9714.

(42) Ambrus, A.; Chen, D.; Dai, J.; Bialis, T.; Jones, R. A.; Yang, D. Human Telomeric Sequence Forms a Hybrid-Type Intramolecular G-Quadruplex Structure with Mixed Parallel/Antiparallel Strands in Potassium Solution. *Nucleic Acids Res*. **2006**, *34* (9), 2723–2735.

(43) Simpson, A. J.; Kingery, W. L.; Shaw, D. R.; Spraul, M.; Humpfer, E.; Dvortsak, P. The Application of 1H HR-MAS NMR Spectroscopy for the Study of Structures and Associations of Organic Components at the Solid- Aqueous Interface of a Whole Soil. *Environ. Sci. Technol.* **2001**, *35* (16), 3321–3325.

(44) Li, H.-R.; Chen, T.-C.; Hsiao, C.-L.; Shi, L.; Chou, C.-Y.; Huang, J.-R. The Physical Forces Mediating Self-Association and Phase-Separation in the C-Terminal Domain of TDP-43. *Biochim. Biophys. Acta: Proteins Proteomics* **2018**, *1866* (2), 214–223.

(45) Smargiasso, N.; Rosu, F.; Hsia, W.; Colson, P.; Baker, E. S.; Bowers, M. T.; De Pauw, E.; Gabelica, V. G-Quadruplex DNA Assemblies: Loop Length, Cation Identity, and Multimer Formation. J. *Am. Chem. Soc.* **2008**, *130* (31), 10208–10216.

(46) Smirnov, I. V.; Shafer, R. H. Electrostatics Dominate Quadruplex Stability. *Biopolymers* **2007**, *85* (1), 91–101.

(47) Lannan, F. M.; Mamajanov, I.; Hud, N. V. Human Telomere Sequence DNA in Water-Free and High-Viscosity Solvents: G-Quadruplex Folding Governed by Kramers Rate Theory. *J. Am. Chem. Soc.* **2012**, *134* (37), 15324–15330.

(48) Rajendran, A.; Endo, M.; Hidaka, K.; Tran, P. L. T.; Mergny, J.-L.; Gorelick, R. J.; Sugiyama, H. HIV-1 Nucleocapsid Proteins as Molecular Chaperones for Tetramolecular Antiparallel G-Quadruplex Formation. *J. Am. Chem. Soc*. **2013**, *135* (49), 18575–18585.

(49) Phan, A. T.; Mergny, J. Human Telomeric DNA: G-quadruplex, I-motif and Watson–Crick Double Helix. *Nucleic Acids Res.* **2002**, *30* (21), 4618–4625.

(50) Choi, J.; Kim, S.; Tachikawa, T.; Fujitsuka, M.; Majima, T. PH-Induced Intramolecular Folding Dynamics of i-Motif DNA. *J. Am. Chem. Soc*. **2011**, *133* (40), 16146–16153.

(51) Lin, Y.; Mori, E.; Kato, M.; Xiang, S.; Wu, L.; Kwon, I.; McKnight, S. L. Toxic PR Poly-Dipeptides Encoded by the C9orf72 Repeat Expansion Target LC Domain Polymers. *Cell* **2016**, *167* (3), 789–802.e12.

(52) Shakya, A.; Park, S.; Rana, N.; King, J. T. Liquid-Liquid Phase Separation of Histone Proteins in Cells: Role in Chromatin Organization. *Biophys. J.* **2020**, *118* (3), 753–764.

(53) Park, S.; Barnes, R.; Lin, Y.; Jeon, B.-J.; Najafi, S.; Delaney, K. T.; Fredrickson, G. H.; Shea, J.-E.; Hwang, D. S.; Han, S. Dehydration Entropy Drives Liquid-Liquid Phase Separation by Molecular Crowding. *Commun. Chem.* **2020**, *3* (1), 83.

(54) Rutledge, L. R.; Campbell-Verduyn, L. S.; Wetmore, S. D. Characterization of the Stacking Interactions between DNA or RNA Nucleobases and the Aromatic Amino Acids. *Chem. Phys. Lett.* **2007**, *444* (1), 167–175.

(55) Hobza, P.; Šponer, J. Structure, Energetics, and Dynamics of the Nucleic Acid Base Pairs: Nonempirical Ab Initio Calculations. *Chem. Rev.* **1999**, *99* (11), 3247–3276.

(56) Vernon, R. M.; Chong, P. A.; Tsang, B.; Kim, T. H.; Bah, A.; Farber, P.; Lin, H.; Forman-Kay, J. D. Pi-Pi Contacts Are an Overlooked Protein Feature Relevant to Phase Separation. *eLife* **2018**, *7*, e31486.

(57) Czyżnikowska, Ż.; Lipkowski, P.; Góra, R. W.; Zaleśny, R.; Cheng, A. C. On the Nature of Intermolecular Interactions in Nucleic Acid Base-Amino Acid Side-Chain Complexes. *J. Phys. Chem. B* **2009**, *113* (33), 11511–11520.

(58) Alshareedah, I.; Kaur, T.; Ngo, J.; Seppala, H.; Kounatse, L.-A. D.; Wang, W.; Moosa, M. M.; Banerjee, P. R. Interplay between Short-Range Attraction and Long-Range Repulsion Controls Reentrant Liquid Condensation of Ribonucleoprotein–RNA Complexes. *J. Am. Chem. Soc.* **2019**, *141* (37), 14593–14602.

(59) Lin, Y.-H.; Forman-Kay, J. D.; Chan, H. S. Sequence-Specific Polyampholyte Phase Separation in Membraneless Organelles. *Phys. Rev. Lett.* **2016**, *117* (17), 178101.

(60) Uversky, V. N. Intrinsically Disordered Proteins in Overcrowded Milieu: Membrane-Less Organelles, Phase Separation, and Intrinsic Disorder. *Curr. Opin. Struct. Biol.* **2017**, *44*, 18–30.

(61) Shakya, A.; King, J. T. DNA Local-Flexibility-Dependent Assembly of Phase-Separated Liquid Droplets. *Biophys. J.* **2018**, *115* (10), 1840–1847.

(62) Vieregg, J. R.; Lueckheide, M.; Marciel, A. B.; Leon, L.; Bologna, A. J.; Rivera, J. R.; Tirrell, M. V. Oligonucleotide–Peptide Complexes: Phase Control by Hybridization. *J. Am. Chem. Soc.* **2018**, *140* (5), 1632–1638.

(63) Nott, T. J.; Craggs, T. D.; Baldwin, A. J. Membraneless Organelles Can Melt Nucleic Acid Duplexes and Act as Biomolecular Filters. *Nat. Chem.* **2016**, *8* (6), 569–575.

(64) Cohen, H.; Sapir, T.; Borovok, N.; Molotsky, T.; Di Felice, R.; Kotlyar, A. B.; Porath, D. Polarizability of G4-DNA Observed by Electrostatic Force Microscopy Measurements. *Nano Lett.* **2007**, *7* (4), 981–986.

(65) Chen, Z.; Chen, L.; Ma, H.; Zhou, T.; Li, X. Aptamer Biosensor for Label-Free Impedance Spectroscopy Detection of Potassium Ion Based on DNA G-Quadruplex Conformation. *Biosens. Bioelectron*. **2013**, *48*, 108–112.

(66) Borgia, A.; Borgia, M. B.; Bugge, K.; Kissling, V. M.; Heidarsson, P. O.; Fernandes, C. B.; Sottini, A.; Soranno, A.; Buholzer, K. J.; Nettels, D.; Kragelund, B. B.; Best, R. B.; Schuler, B. Extreme Disorder in an Ultrahigh-Affinity Protein Complex. *Nature* **2018**, *555* (7694), 61–66.

(67) Conicella, A. E.; Dignon, G. L.; Zerze, G. H.; Schmidt, H. B.; D'Ordine, A. M.; Kim, Y. C.; Rohatgi, R.; Ayala, Y. M.; Mittal, J.; Fawzi, N. L. TDP-43 α-Helical Structure Tunes Liquid–Liquid Phase Separation and Function. *Proc. Natl. Acad. Sci. U. S. A*. **2020**, *117* (11), 5883–5894.

(68) Fraccia, T. P.; Jia, T. Z. Liquid Crystal Coacervates Composed of Short Double-Stranded DNA and Cationic Peptides. *ACS Nano* **2020**, *14* (11), 15071–15082.

(69) Guittet, E.; Renciuk, D.; Leroy, J.-L. Junctions between I-Motif Tetramers in Supramolecular Structures. *Nucleic Acids Res.* **2012**, *40* (11), 5162–5170.

(70) Vorlíčková, M.; Kejnovská, I.; Sagi, J.; Renčiuk, D.; Bednářová, K.; Motlová, J.; Kypr, J. Circular Dichroism and Guanine Quadruplexes. *Methods* **2012**, *57* (1), 64–75.

(71) Alberti, P.; Mergny, J.-L. DNA Duplex–Quadruplex Exchange as the Basis for a Nanomolecular

Machine. *Proc. Natl. Acad. Sci. U. S. A.* **2003**, *100* (4), 1569–1573.

(72) Zhang, Q.-S.; Manche, L.; Xu, R.-M.; Krainer, A. R. HnRNP A1 Associates with Telomere Ends and Stimulates Telomerase Activity. *RNA* **2006**, *12* (6), 1116–1128.

(73) Takahama, K.; Takada, A.; Tada, S.; Shimizu, M.; Sayama, K.; Kurokawa, R.; Oyoshi, T. Regulation of Telomere Length by G-Quadruplex Telomere DNA- and TERRA-Binding Protein TLS/FUS. *Chem. Biol.* **2013**, *20* (3), 341–350.

Chapter 4.

Site-specific effects of acetylation within histone H3 tail peptide on liquid-liquid phase separation with DNA

4.1. Introduction

Membraneless compartments are ubiquitously observed in both eukaryotic and prokaryotic cells, which play a crucial role in the spatiotemporal organization of complex intracellular milieu,[1–3] such as stress granules,[1] P-granules,[4] Cajal body,[5] and chromatin subcompartments (heterochromatin and super-enhancer).[6] The formation of these compartments is now generally recognized to be induced via liquid-liquid phase separation (LLPS). The compartments formed via LLPS are droplet-like, which exhibit fluid properties as a liquid (e.g., fusion, wetting, dripping)[4,7] and can therefore be rapidly and reversibly formed in response to changes in the intracellular environment.[2,8] As such dynamic formation of droplets is expected to provide appropriate regulation of various biological processes,[1,2] the molecular mechanisms that govern droplet formation have recently been investigated intensively.[9]

Much of the formation of intracellular droplets is caused by attractive multivalent interactions involving intrinsically disordered regions (IDRs) of proteins and/or nucleic acids.[9] These interactions include charge-charge, cation-π, π-π stacking, and hydrogen bonding. Post-translational modifications (PTMs) of proteins have been proposed as key mechanism to control dynamic droplets formation because the attractive interactions can be regulated through reversible processes via enzyme reactions.[10] For instance, intracellular droplets, germline P granules, are assembled/dis-assembled coupled to phosphorylation/de-phosphorylation of serin-rich IDRs of MEG proteins.[11]

Acetylation is a representative PTM that is frequently introduced into various proteins and is closely related to LLPS as it neutralizes the positive charge of lysine residues.[12] One of the most biologically important IDRs that undergo acetylation is the histone tails (the terminal regions of histone proteins), which are involved in DNA repair, histone deposition, and transcriptional regulation.[13,14] In the eukaryotic cells, four histone proteins (H2A, H2B, H3, and H4) form nucleosomes with DNA, followed by assembly into chromatin. A recent report suggests that chromatin contains sites that is potentially organized into phase-

separated subcompartments.[15] The key insight into the mechanisms of LLPS-mediated chromatin organization is that the LLPS capability of intact nucleosome arrays is impaired when histone tails are deleted or hyperacetylated.[16] This suggests that acetylation, which regulates the electrostatic interactions between the cationic histone tails and the anionic DNA, can be important in LLPS of chromatin.

The biological function of acetylation varies markedly depending on where it is introduced into the histone tail. For instance, acetylation of histone H3 at lysine 9 (hereinafter referred to as H3K9) and that of H3K18 is involved in transcription initiation[17] and DNA replication,[18] respectively. H4K16 acetylation is critical for DNA repairs.[19] The biological functions inherent in the acetylation sites within histone tails have been extensively addressed,[13,14,17,20,21] but their site-dependences in the context of LLPS remain elusive. Here, I focused on the N-terminal tail peptide of histone H3, which is most frequently acetylated histone protein,[22,23] and examined the association between the acetylation site and LLPS. First, I newly developed a binary LLPS system in which a chemically synthesized H3 peptide (1-20 residues) is mixed with DNA to form droplets. Application of this system to H3 peptides in which different lysine residues were acetylated revealed that the LLPS behaviors differed depending on the acetylation site. More specifically, the acetylation site near the peptide end exhibited a more marked inhibitory effect on droplets formation compared to that near the center of the peptide. The findings obtained here will facilitate the fundamental understanding of LLPS-mediated chromatin organization. In addition, my extendable binary LLPS system (e.g., application to other histone tails, various post-translational modifications, and their combinations), can be expected to contribute to the universal understanding of LLPS mechanisms involving PTMs.

4.2. Materials and methods

4.2.1. Materials

Tris-EDTA (TE) buffer [10 mM Tris-HCl; 1 mM EDTA; pH = 7.4] was obtained from Takara Bio Inc. (Shiga, Japan). NovaSyn® TGR resin and *O*-(7-Azabenzotriazol-1-yl)-*N*,*N*,*N*′,*N*′-tetramethyluronium Hexafluorophosphate (HATU) were obtained from Merck KGaA (Darmstadt, Germany). 3*H*-[1,2,3]Triazolo[4,5-*b*]pyridin-3-ol (HOAt), *N*-ethyldiisopropylamine (DIPEA), piperidine, potassium cyanide (KCN), ninhydrin, diethyl ether, ethanol (EtOH), methanol (MeOH), dichloromethane (DCM), *N,N*-Dimethylformamide (DMF), acetic anhydride, acetic acid, acetonitrile phenol, and sodium chloride (NaCl)

were obtained from Fujifilm Wako Pure Chemical Corp. (Osaka, Japan). *N*-methylpyrrolidone (NMP), trifluoroacetic acid (TFA), Fmoc-Ala-OH, Fmoc-Arg(Pbf)-OH, Fmoc-Thr(*t*Bu)-OH, Fmoc-Lys(Boc)-OH, Fmoc-Lys(Ac)-OH, Fmoc-Glu(O*t*Bu)-OH, Fmoc-Ser(*t*Bu)-OH, Fmoc-Gly-OH, Fmoc-Pro-OH, and Fmoc-Leu-OH were obtained from Watanabe Chemical Industries, Ltd. (Hiroshima, Japan). Acetaldehyde (ca. 2% in DMF) and 1,6-hexanediol were obtained from Tokyo Chemical Industry Co., Ltd. (Tokyo, Japan). Histone H3 tail peptide with N-terminal modification with carboxytetramethylrhodamine (TAMRA) was obtained from Biologica Co. (Aichi, Japan). Poly(ethylene glycol) (PEG; Mw. 10,000 Da) was obtained in Sigma Chemical Co. (St. Louis, MO, USA).

The 35 base-pairs DNA sequence [5'-GCATG TGGAT CCGAA ACTAG ACTAT ACGCG GCCGC-3'] was synthesized and purified by Eurofins Genomics (Ebersberg, Germany). The complementary DNA sequences were dissolved in TE buffer (pH = 7.4) and annealed as follows; 50 μM of complementary DNA sequences in TE buffer (pH = 7.4) was heated to 95°C for 5 minutes and the cooled to 25°C at a rate of 1°C/min using a PCR thermal cycler (TP-600; Takara Bio Inc., Shiga, Japan).

4.2.2. Peptide synthesis

Histone H3 peptides with and without acetylated lysine residues were synthesized by standard Fmoc solid-phase synthesis method as described below. Prior to the synthesis, the resin was swollen by incubating it in NMP solution for 15 minutes at room temperature (RT), and then washed five times with NMP. Four molar amounts of Fmoc-amino acid, HOAt, HATU and DIPEA dissolved in dehydrated NMP were used for each coupling. The reaction mixture was shaken and incubated for 15 minutes at RT for each coupling step. The completion of coupling reactions was monitored with Kaiser test as follows; a small amount of the resin after the coupling reaction was added to a solution of equal volume of 50 mg/ml ninhydrin in EtOH, 4 g/mL phenol in EtOH, and 0.2 mM KCN in pyridine, and heated at 100°C for 3 minutes. For proline coupling, an additional chloranil test was performed as follows; a small amount of the resin after the coupling reaction was added to a solution of equal volume of 2% acetaldehyde in DMF and 20 mg/mL chloranil in DMF, and heated at 100°C for 3 minutes. In both tests, the completion of the coupling reaction was confirmed by the color change of the solution after heating.

For Fmoc deprotection steps, 20% piperidine in NMP was used and reaction mixture was shaken and incubated for 15 minutes at RT. The resin was then washed five times with NMP and the next coupling reaction

proceeded. After completion of the peptide elongation, the N-terminus of peptide was acetylated by using four molar amounts of acetic anhydride and eight molar amounts of DIPEA in NMP. Then, the resin was washed three times with MeOH and DCM, respectively.

After completion of peptide synthesis, peptide cleavage from the resin and deprotection of side-chain protecting groups were performed by shaking with cleavage cocktail [32.1 mg phenol in TFA (2.85 mL), TIPS (90 μL), and ultra-pure water (60 μL)] for three hours, and then the resin was removed with a filter, and the solvent was evaporated using rotary evaporator (EYELA N-1110; Tokyo Rikakikai Co., Ltd., Tokyo, Japan) equipped with diaphragm type vacuum pump (EYELA NVP-1000V; Tokyo Rikakikai Co., Ltd.). The crude peptide precipitate obtained by adding diethyl ether cooled at 4°C to the reaction mixture was collected by centrifugation and decantation.

The crude peptide was purified by semipreparative, reverse-phase high performance liquid chromatography (RP-HPLC) using COSMOSIL 5C18-AR-II (10 mm I.D. x 250 mm) on a Shimadzu instrument with a linear gradient system of 5:95–35:65 (0.08% TFA in acetonitrile : 0.1% TFA in H_2O) over 30 minutes (for H3, H3K4ac, H3K9ac, H3K14ac, and H3K18ac peptide) or 10:90–40:60 (0.08% TFA in acetonitrile : 0.1% TFA in H_2O) over 30 minutes (for H3ac peptide) at the flow rate of 3.0 mL/min at 40°C. The purity of the obtained H3 peptides was evaluated based on the peak areas in analytical HPLC traces at 220 nm and matrix-assisted laser desorption ionization-time of flight mass (MALDI-TOF-MS) spectra. MALDI-TOF MS (m/z): 2225.31 $[M + H]^+$ for H3, 2267.30 $[M + H]^+$ for H3K4ac, H3K9ac, H3K14ac and H3K18ac, 2394.30 $[M + H]^+$ for H3ac. The concentration of each peptide was determined by amino acid analysis.

4.2.3. Phase-contrast microscopy imaging

In the well of 384-well black clear-bottom microplate (Greiner Bio-One, Kremsmüster, Australia), solutions (10 μL) of 100 μM H3 peptide in TE buffer (pH = 7.4) were mixed with solutions (10 μL) of 10 μM DNA in TE buffer (pH = 7.4). After incubation for 2 h at 25°C, images of the solution were obtained using a phase-contrast microscope (Eclipse Ts2R, Nikon, Tokyo, Japan) equipped with a DS-Fi3 digital camera (Nikon, Tokyo, Japan). The collision process of the droplets was observed via time-lapse photography (increments:1.0 s) using a phase-contrast microscope after allowing solutions containing 50 μM H3 peptide and 5.0 μM DNA to incubate for 1 h at room temperature.

To obtain the phase diagrams of the concentration of PEG vs. that of NaCl, solutions (30 μL) containing 50

μM H3 peptide, 5 μM DNA, 0-20% PEG and 0-300 mM NaCl in TE buffer (pH = 7.4) were prepared in the wells of 384-well microplates using an Andrew+ liquid handling robot (Andrew Alliance SA, Geneva, Switzerland). After overnight incubation at 25°C with a lid to avoid evaporation, images of the solution were obtained using a phase-contrast microscope as described above. The same procedure was used to obtain the phase diagram of the concentration of peptide vs. that of DNA, in which the solutions were prepared as follows: solutions (10 μL) containing 2-200 μM H3 peptide were mixed with solutions (10 μL) of 0.05-40 μM DNA in TE buffer (pH = 7.4).

4.2.4. Confocal fluorescence microscopy imaging

Solutions (100 μL) containing 50 μM TAMRA-modified H3 peptide and 5 μM FAM-modified DNA in TE buffer (pH = 7.4) was prepared in a PCR tube. An aliquot (90 μL) of mixture was placed on a cell-culture dish, and the samples were imaged using an FV1000 confocal microscope (Olympus Co., Tokyo, Japan) at 60x with an excitation wavelength of 488 nm for FAM, and 543 nm for TAMRA.

For fluorescence recovery after photobleaching (FRAP) measurements, a solution (100 μL) containing 50 μM H3 peptide and 5 μM DNA was prepared, where either the DNA or the H3 peptide was fluorescently modified. Aliquot (90 μL) of the mixtures were placed on a cell-culture dish and incubated for 30 min, then, the samples were imaged using confocal microscope and the 488 nm or 543 nm laser was applied to the region of interest at full power for 1.0 s, and the fluorescence recovery was then recorded for 1 min.

4.2.5. Effect of histone acetyltransferase (HAT) activity on H3peptide/DNA droplets formation

The activity of HAT protein p300 was measured using commercially available fluorescence detection-based HAT assay kit (Active motif, Inc., Tokyo, Japan) according to the instructions in its detailed procedure, with minor modifications. Briefly, in the well of 96-well microplate, solutions (20 μL) containing 125 μM of originally synthesized histone H3 peptide with or without 12.5 μM DNA were mixed to the solutions (30 μL) containing 1.67 μg/mL p300 catalytic domain, 83.3 μM Acetyl-CoA with or without 25 μM anacardic acid in the HAT Assay Buffer. The mixed solution was incubated at room temperature for 0-60 min, and the reaction was stopped by adding the Stop Solution (50 μL). Then, the final Developing Solution (100 μL) was added to each sample, incubated for 15 min, and the fluorescence intensity was measured using a microplate reader (Cytation 5; BioTek Instruments, Inc., Winooski, VT, USA) with excitation at 400 nm and emission at 420-650 nm. Accordingly, HAT activity was expressed as fluorescence intensity (arbitrary unit).

To investigate the effect of HAT activity on droplets formation, turbidity measurements were performed as follows. Solutions (10 μL) containing 125 μM of H3 peptide and 12.5 μM DNA were mixed to the solutions (15 μL) containing 1.67 μg/mL p300 catalytic domain, 83.3 μM Acetyl-CoA with or without 25 μM anacardic acid in TE buffer, in the well of 384-well microplate. After well mixing the solution by pipetting, the absorbance at 600 nm was measured for 1 hour at 10-second intervals using a microplate reader.

The solutions were prepared using the same procedure, and phase contrast microscopy images of the solution were taken at specific times after the addition of the HAT solution to the H3 peptide/DNA mixtures.

4.2.6. Turbidity measurements

In the well of 384-well microplate, solutions (10 μL) of 100 μM H3 peptide with or without acetylation were mixed with solutions (10 μL) of 0-16 μM DNA in TE buffer (pH = 7.4). After incubation (10 min, 25°C), their absorbance at 600 nm were recorded using microplate reader.

In a test of the effects of 1,6-hexanediol on droplets stability, solutions (20 μL) of 100 μM H3 peptide and 10 μM DNA were mixed with solutions (20 μL) of 0-40% 1,6-hexanediol in TE buffer (pH = 7.4), and after incubation (10 min, 25°C), turbidity measurements were conducted as described above.

4.2.7. Thermal stability of DNA in the presence of H3 peptide under salt-depleted conditions

The thermal melting curves of DNA were obtained by using a spectrophotometer equipped with the TMSPC-8 melting temperature analysis system (UV-1800; Shumadzu Co., Tokyo, Japan). Solutions (120 μL) containing 1 μM DNA and 0-12.5 μM H3 peptide in TE buffer (pH = 7.4) were incubated at 10°C for 20 min in a 1 cm quartz cell, then, heated to 95°C at a rate of 1.0°C/min and the absorbance change of the solutions were monitored at 260 nm. The melting temperature (*Tm*) of DNA was determined as previously reported.[24] Briefly, in the obtained thermal melting curve, the upper and lower baselines were obtained from the linear regions before and after the DNA dissociation, and 'melted fraction' was calculated as: Melted fraction = $(A - A_L) / (A_U - A_L)$, where A, A_L, and A_U are the absorbance of the sample, upper baseline, and lower baseline, respectively. Then, the temperature at which the melting fraction was 0.5 was defined as *Tm*.

4.2.8. Circular dichroism (CD) measurements

Solutions (300 μL) containing 50 μM of H3 peptide in TE buffer (pH = 7.4) were placed in a 1 mm quartz cuvette, and the CD measurements were performed at 25°C using a spectropolarimeter (J-1100; Japan

Spectroscopic Co., Ltd., Tokyo, Japan). The CD spectra of the samples were corrected by subtracting the corresponding spectra of the buffer solution in the absence of peptide.

4.3. Results and discussion

4.3.1. LLPS of histone H3 peptide and nucleosomal linker DNA

A peptide consisting of 20 amino acids, corresponding to the sequence of the N-terminal tail of histone H3, was obtained by solid phase peptide synthesis (**Figures 4.1** and **4.2**). Circular dichroism (CD) spectra showed that the synthesized H3 peptide exhibited a completely random structure, consistent with the property of intrinsically disordered histone H3 tail (**Figure 4.3**).[25] The cationic H3 tail has been suggested to be involved in the chromatin organization through electrostatic interactions with the linker DNA moieties that connect nucleosomes.[25] Considering the association between chromatin organization and LLPS,[15] a 35-base-pair DNA sequence designed based on the sequence and length of the known nucleosomal linker DNA[26] was selected as a partner molecule to generate LLPS by mixing with the H3 peptide (**Figure 4.4A**, for DNA sequence, see in Materials and Methods Section).

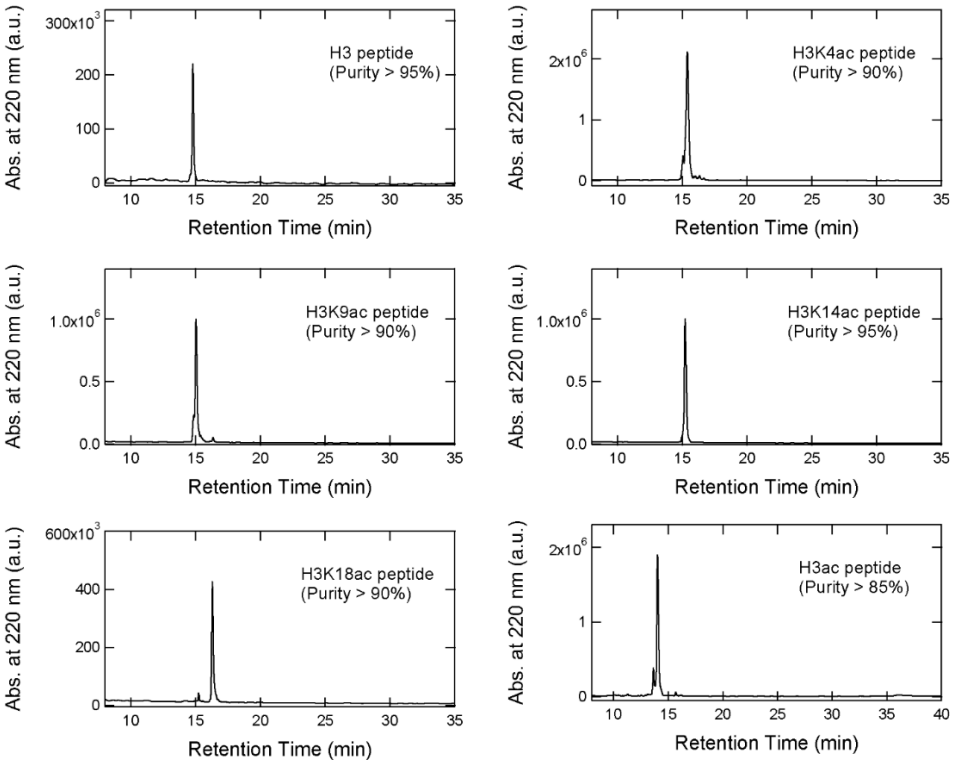

Figure 4.1. RP-HPLC traces of the purified peptides.

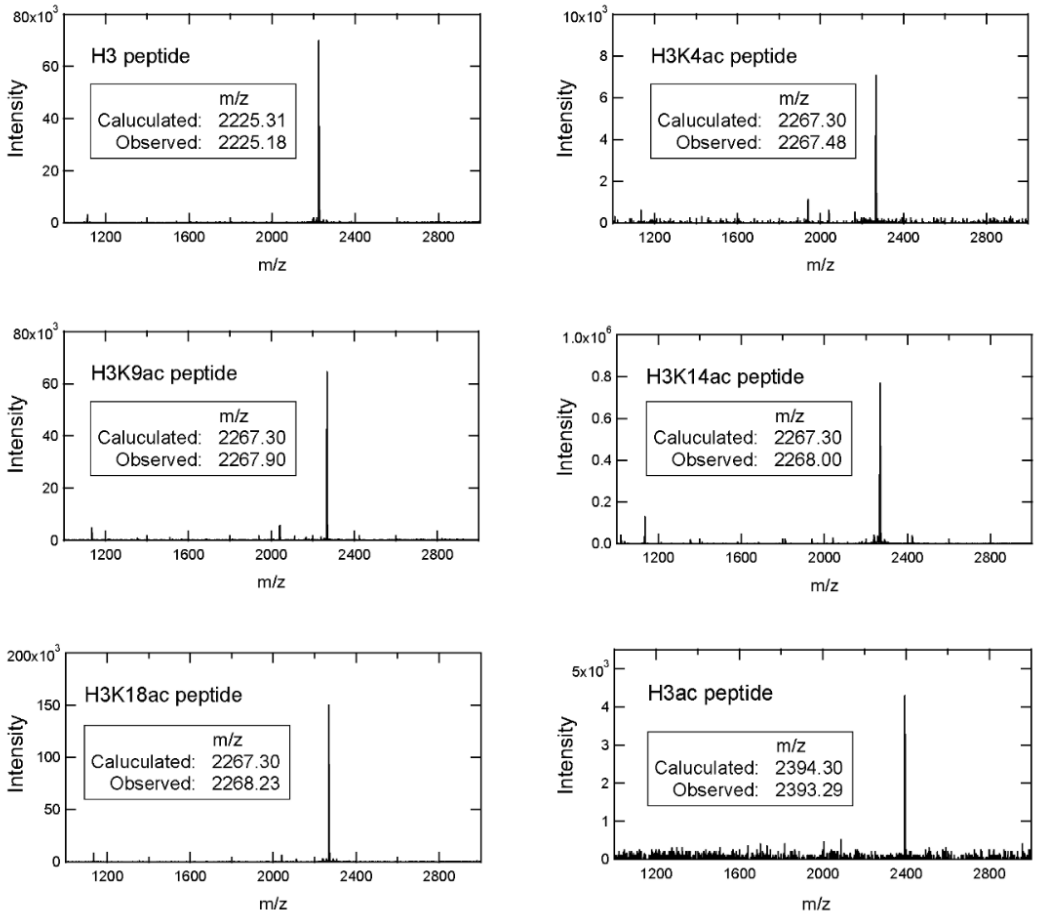

Figure 4.2. MALDI-TOF MS spectrum of purified peptides. Calculated and obtained m/z values are shown.

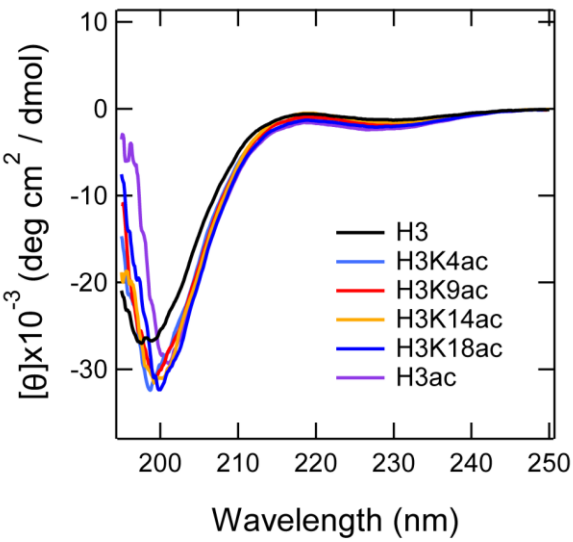

Figure 4.3. CD spectra of solutions containing 100 µM peptide in TE buffer (pH = 7.4)

LLPS can be induced when oppositely charged cationic peptides and DNA are mixed at charge ratios close to 1, as in our previous reports.[27,28] Based on this knowledge, 50 μM of H3 peptide and 5 μM of DNA (approximately equal in charge) were mixed in Tris-EDTA (TE) buffer at physiological pH (pH = 7.4). Phase-contrast microscopy image showed the formation of spherical droplets in the solution (**Figure 4.4B**). The droplets fused quickly in a few seconds upon collision (**Figure 4.4B**), indicating that the droplets exhibited fluidic properties, unlike solid-like aggregates.[29] To examine the localization of molecules, a mixture of a carboxytetramethylrhodamine (TAMRA)-modified H3 peptide and a carboxyfluorescein (FAM)-modified DNA was observed with confocal fluorescence microscopy. As expected, both molecules were highly concentrated within the droplets (**Figure 4.4C**). Fluorescence recovery after photobleaching (FRAP) measurement, which is used to determine macroscopic molecular motility,[30] has again shown that both H3 peptide and DNA are dynamically diffused within the droplets (**Figure 4.4D**). Given that full-length histone H3 protein has been reported to form solid-like aggregates with DNA,[31] my results suggest that the interaction of the tail region, which is exposed to the solvent due to protrusion from the nucleosome, rather than the globular domain buried inside the nucleosome, is important for histone H3 to bind to DNA while maintaining fluidity.

Whether droplets are formed even under solution conditions similar to the intracellular environment is important from a biological point of view. Cells contain high concentrations of biopolymers that reach up to 400 mg/ml.[32,33] Such a crowded environment is often mimicked by the addition of inert polymers (e.g., polyethylene glycol (PEG) or dextran) or proteins in in vitro LLPS systems.[34] Accordingly, we examined the phase behavior of H3 peptide/DNA mixtures in the presence of various concentrations of NaCl and PEG (Mw = 10,000). The droplets dissolved under physiological ionic strength in the absence of PEG, suggesting that electrostatic interaction is the dominant driving force for droplet formation (**Figure 4.4E**). With increasing PEG concentration, the stability of the droplets against increasing ionic strength improved. For instance, the droplets were maintained even under 300 mM NaCl in the presence of 20% PEG. LLPS was promoted by PEG perhaps due to exclusion volume effects and dehydration effects, as reported in other polyelectrolytes systems.[35,36]

As described above, I have shown for the first time that the N-terminal tail peptide of histone H3 is a nucleosome component potentially responsible for forming droplets with DNA. My simple binary LLPS

system associated with LLPS-mediated chromatin organization showed that these droplets were maintained even under solution conditions close to the intracellular environment.

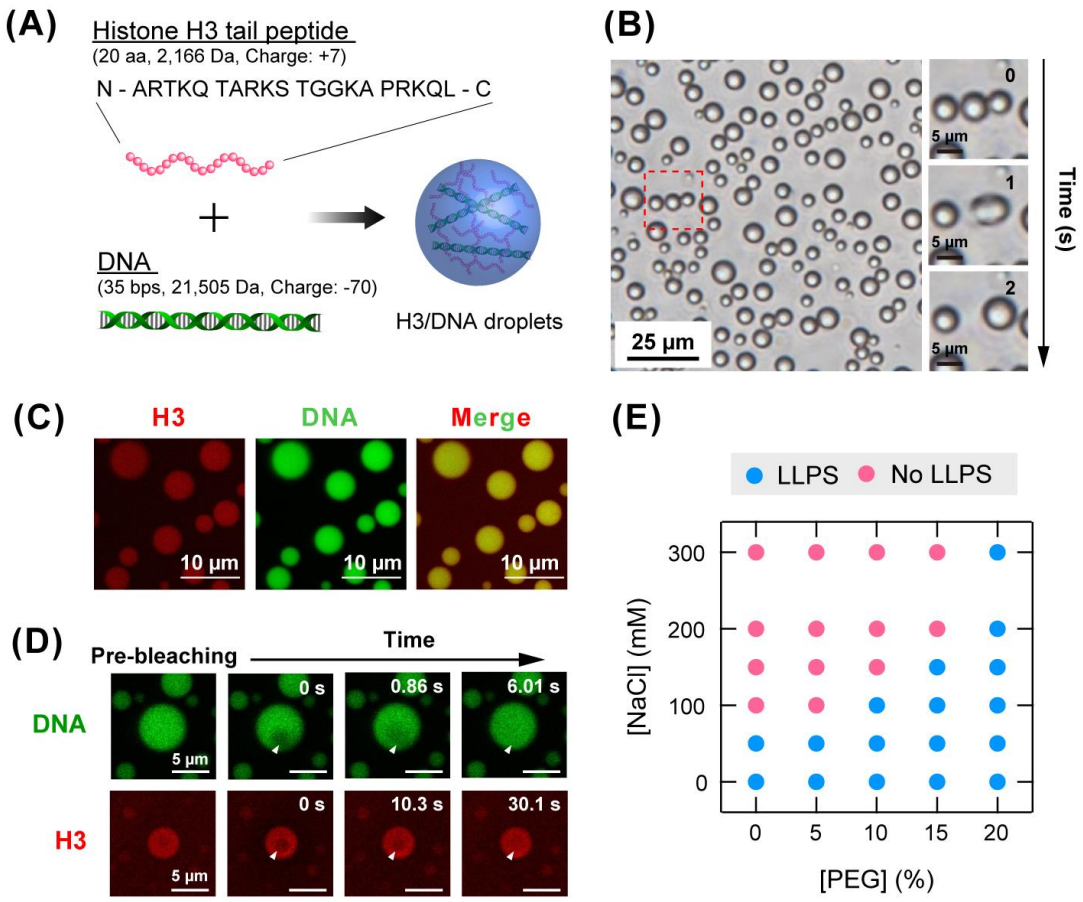

Figure 4.4. N-terminal tail of histone H3 peptide forms droplets through LLPS with DNA. (A) Characteristics of the molecules used in this study and schematic illustration of droplet formation by mixing H3 peptide and DNA. (B) A phase-contrast microscopy image of the solution containing H3 peptide (50 μM) and DNA (5 μM); Scale bar = 25 μm (left). A fusion process of the H3/DNA droplets; scale bar = 5 μm (right). (C) Confocal fluorescence microscopy images of the solution containing TAMRA-modified H3 peptide (50 μM) and FAM-modified DNA (5 μM); scale bar = 10 μm. (D) Confocal fluorescence microscopy images during FRAP experiments. White arrowheads indicate the bleached area; scale bar = 5 μm. (E) Phase diagram of aqueous mixtures of H3 peptide (50 μM) and DNA (5 μM) in the presence of various concentration of PEG and NaCl. All experiments in this study were carried out in 10 mM Tris-EDTA buffer (pH = 7.4), except for the HAT assay (see below).

4.3.2. Nonspecific acetylation of H3 peptide by HAT proteins dissolves droplets

Subsequently, I examined the effect of acetylation in the LLPS of the H3 peptide/DNA system. The N-terminal tail of histone H3 is acetylated in the nucleus by histone acetyltransferases (HATs), such as p300 and GCN5.[37] These enzymes transfer the acetyl group of acetyl-CoA to an ε-NH_2 group of the lysine residues within H3 tail (**Figure 4.5A**). To confirm that the synthesized H3 peptide could be enzymatically acetylated, the time course of acetylation of the H3 peptide (50 μM) by the recombinant p300 catalytic domain (a HAT that non-specifically acetylates H3 tail peptide)[38] was measured in the presence of Acetyl-CoA (50 μM). I found that the acetylation of H3 peptide proceeded regardless of the presence of LLPS-inducing DNA, and in both cases the reaction was completed in about 30 min (**Figure 4.5B**).

The effect of enzymatic acetylation of H3 peptide on LLPS was then evaluated from the turbidity change of the solutions. Mixing the H3 peptide and DNA to form droplets muddied the solution, and the turbidity remained almost constant over 20 minutes (**Figure 4.5C**). Addition of p300 and acetyl-CoA rapidly decreased the turbidity and was became completely transparent in 10 minutes (**Figures 4.5C, D**). This decrease was due to enzymatic acetylation as the presence of HAT inhibitor, anacardic acid,[39] did not reduce the turbidity (**Figure 4.5C**). Phase-contrast microscopy images during the HAT assay also showed that the formed droplets were gradually dissolved by the addition of p300 and acetyl-CoA (**Figure 4.5E**), consistent with the previous report using nucleosome arrays.[16] Under the current conditions, an average of at most one lysine residue per molecule was acetylated since an equal amount of acetyl-CoA was added to the peptide. Given that the time required to dissolve the droplets (~10 min) was shorter than the completion of the p300 reaction (~30 min), it is likely that the droplet formation was almost suppressed despite the nonspecific acetylation of only a small portion of the H3 tail peptide. Thus, even partial acetylation of the H3 peptide dramatically inhibit LLPS with DNA.

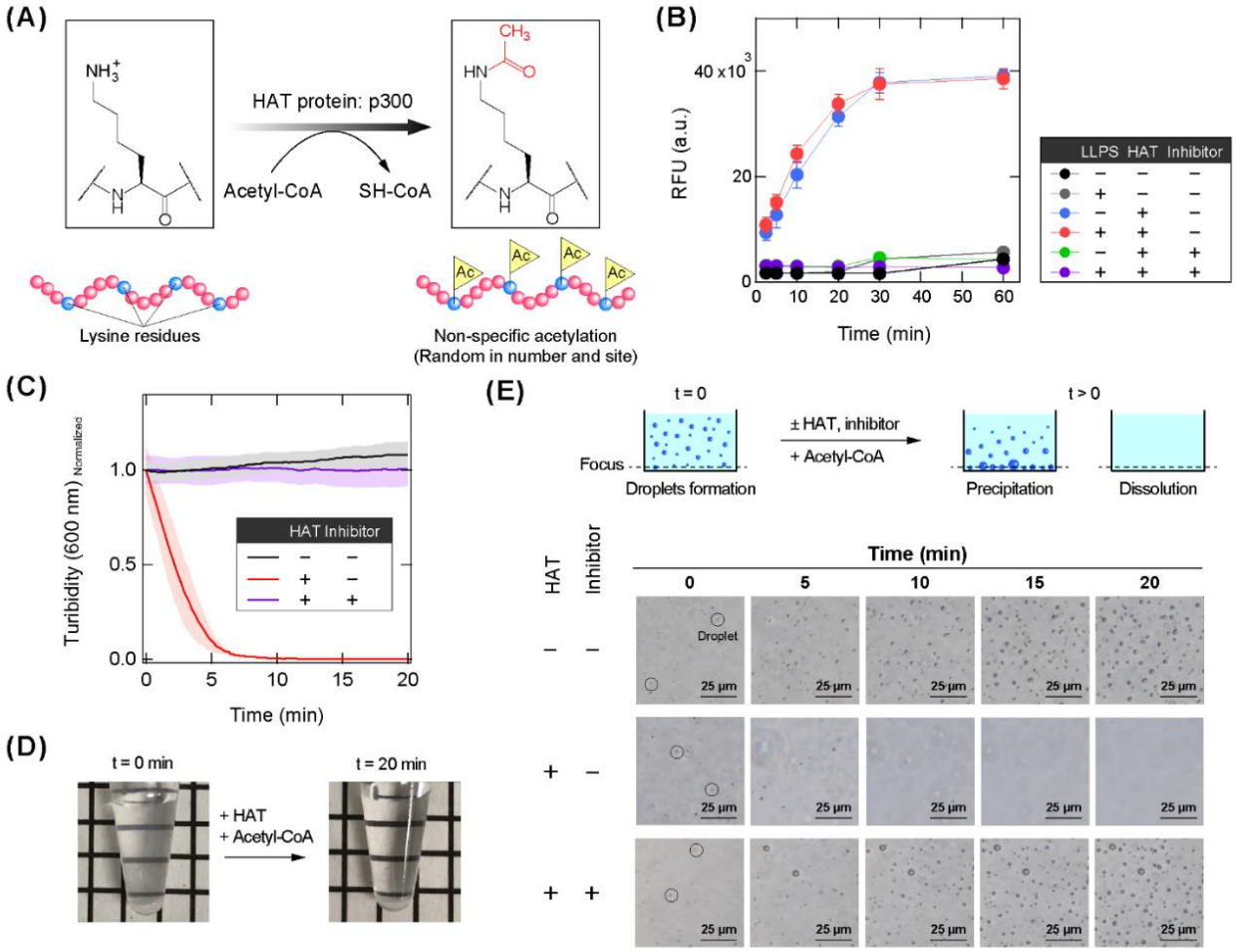

Figure 4.5. Acetylation of H3 tail peptide by HAT protein dissolves droplets. (A) Schematic representation of non-specific acetylation of H3 peptide by HAT protein p300 in the presence of acetyl-CoA. (B) Monitoring HAT reactions based on the fluorescence of the H3 peptide in the presence or absence of DNA. HAT activity was evaluated from the fluorescence intensity of the reaction product, SH-CoA, which was fluorescently labeled after the reaction. Anacardic acid (15 μM) was used as a HAT inhibitor. (C) Time courses of solution turbidity after addition of HAT, acetyl-CoA and/or its inhibitor to a solution containing H3 peptide (50 μM) and DNA (5 μM) in TE buffer (pH = 7.4). (D) An image of the turbid solution containing H3 peptide/DNA droplets and that of the solution 20 minutes after the addition of HAT and acetyl-CoA. (E) Phase-contrast microscopy images of the solution during HAT assay as shown in (C). The circles indicate some of the small droplets that are settling under gravity; scale bar = 25 μm.

4.3.3. Acetylation site-dependent inhibition of LLPS in H3peptide and DNA mixtures

Acetylation at different sites in the H3 tail results in unique biological functions.[13,14,17,20,21] To clarify the relationship between this difference and LLPS, I synthesized H3 peptides in which different (H3K4ac, H3K9ac, H3K14ac, and H3K18ac) and all lysine residues were acetylated (H3ac) (**Figure 4.6A**), and

compared them with unmodified H3 peptide.

Phase-contrast microscopy images showed that for the peptides other than H3ac, droplets formed in mixtures of 50 μM peptides and 5 μM DNA (**Figure 4.6B**). Interestingly, even though the monoacetylated peptides had the same charge, the droplet size distributions two hours after mixing were reduced relative to the unmodified H3 peptide in a site-depending manner; peptides acetylated near the end (H3K4ac and H3K18ac) formed droplets of smaller size than near the center (H3K9ac and H3K14ac), i.e., in the following order: H3 > H3K9ac ≈ H3K14ac > H3K4ac ≈ H3K18ac (**Figure 4.6C**). Although the overall decrease in droplet size can be explained by the loss of the positive charge of H3 peptide due to acetylation, the acetylation-site-dependence suggests that factors not understood in terms of the number of charges alone contribute to the interactions between H3 peptide and DNA, which modulates the LLPS behavior. These results indicate that LLPS of H3 peptide/DNA mixtures is inhibited not only by the number of acetylation but also by its site.

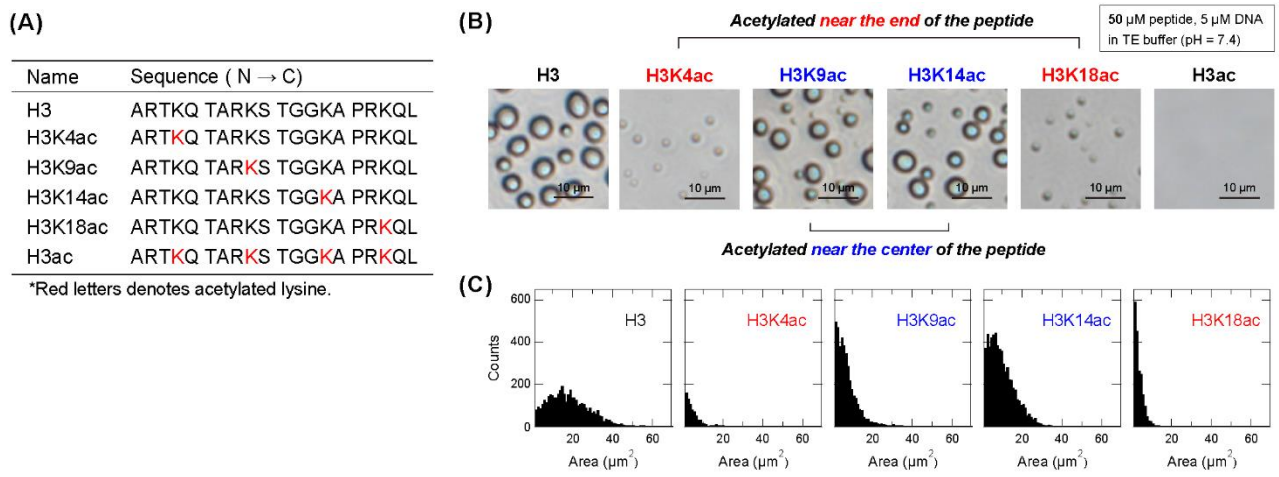

Figure 4.6. Site and number dependence of acetylation of H3 peptide on LLPS of H3 peptide/DNA mixture. (A) List of names and sequences of synthesized H3 peptides, acetylation sites are indicated in red letters. (B) Phase-contrast microscopy images after 2 hours of preparation of the solutions containing the peptides (50 μM) and DNA (5 μM) in TE buffer (pH = 7.4); scale bar = 10 μm. (C) Size distribution of the droplets formed in the solution under the same condition as panel A. The values were obtained by analyzing the fluorescence-microscopy images using image-processing software image J.

To gain more insight into the effects of acetylation sites and numbers on LLPS behavior, phase diagrams of the concentration of the peptide vs. that of the DNA were obtained based on phase-contrast microscopic observations. The phase diagrams of the peptides other than H3ac displayed typical reentrant phase behavior,[40,41] that is, at a constant peptide concentration, when the DNA concentration is increased, a phase transition from non-LLPS to LLPS occurs above a certain DNA concentration (condensation point; C_{con}), and the transitions to non-LLPS occurs when exceeding the de-condensation point (C_{decon}) due to the destabilization of the association by excess anionic charge supply (**Figures 4.7A, B**).[42] The H3ac did not undergo LLPS under all conditions examined. Consistent with the results of droplet sizes (**Figure 4.6**), the area corresponding to LLPS of the unmodified H3 peptide was apparently the largest among all peptides, followed by those near the center (H3K9ac and H3K14ac) and those near the end (H3K4ac and H3K18ac) (**Figure 4.7B**). Similarly, C_{con} values in a 50 μM peptide solution was lower for H3K9ac and H3K14ac than those for H3K4ac and H3K18ac, and C_{decon} values were the opposite (**Figures 4.7C** and **4.8**).

Taken together, investigation of the phase behaviors of acetylated H3 peptides and DNA mixtures showed that (i) acetylation of the H3 peptide inhibits LLPS, (ii) the degree of inhibition is acetylation site-dependent, i.e., acetylation near the ends of the H3 peptide inhibited LLPS more than that near the center, and (iii) acetylation of all lysine residues within the H3 peptide almost completely impair the LLPS capability. These results suggest the existence of a regulatory mechanism for LLPS of H3 peptide/DNA mixtures depending on the acetylation site within the H3 peptide.

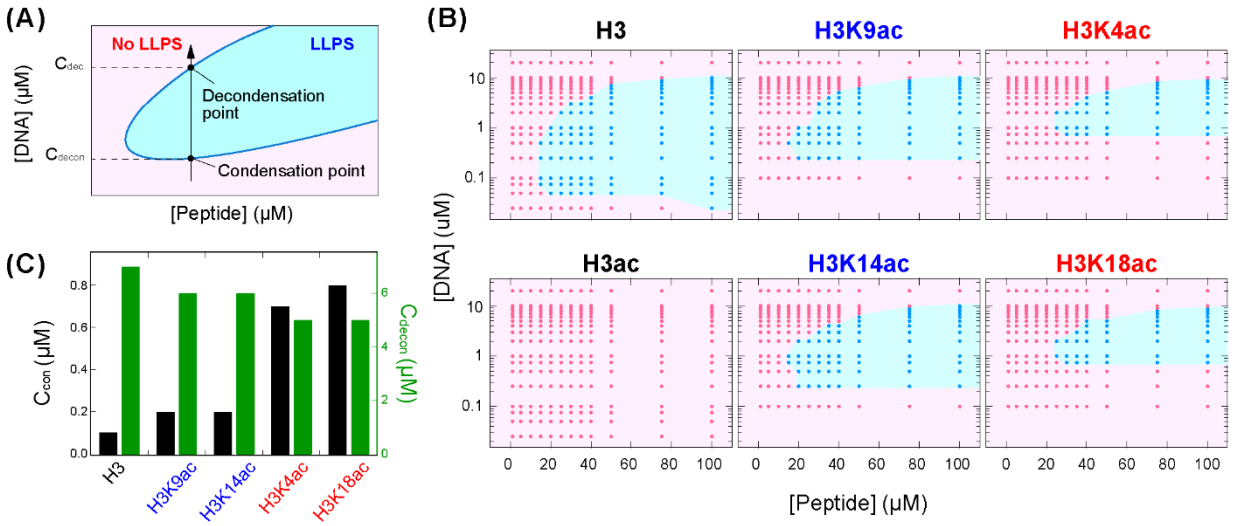

Figure 4.7. Phase diagrams of acetylated / non-acetylated H3 peptides and DNA mixtures. (A) Schematic representation of a typical phase diagram of a peptide/DNA mixture. The arrows indicate that the peptide/DNA mixture shows reentrant phase behavior when the DNA concentration increases at a constant peptide concentration. (B) Phase diagrams of acetylated / non-acetylated H3 peptide and DNA mixtures. The blue region shows the solution conditions where LLPS was identified, and the pink region where it was not. (C) Condensation points (C_{con}) and de-condensation points (C_{decon}) of the DNA for each peptide (50 μM).

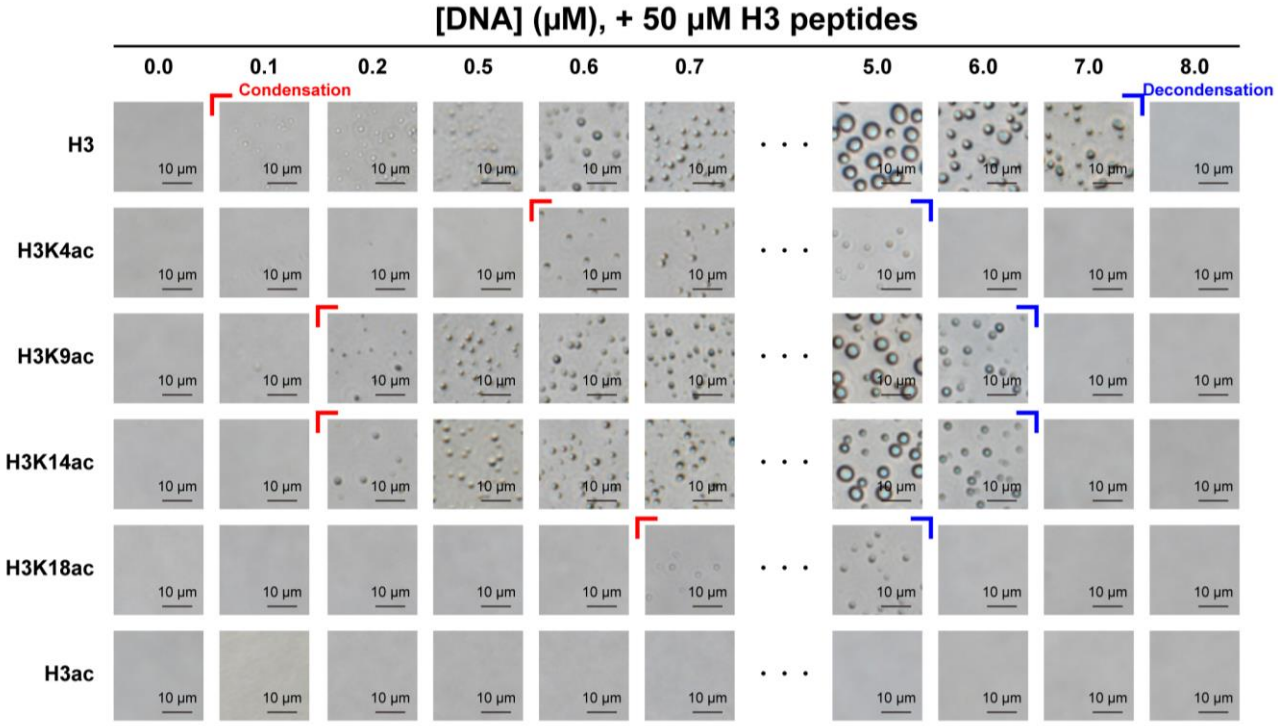

Figure 4.8. Phase-contrast microscopy images of the solutions containing H3 peptide (50 μM) and DNA (0-8.0 μM) in TE buffer (pH = 7.4); scale bar = 10 μm.

4.3.4. Molecular interactions for acetylation-site-dependent LLPS inhibition of H3 peptide and DNA mixtures

To explore the molecular mechanism of acetylation-site-dependent LLPS inhibition in H3 peptide and DNA mixtures, I subsequently determined the most favorable peptide-DNA binding stoichiometry to produce maximum turbidity.[41,43] The addition of the DNA to the solutions containing each peptide (50 μM), except for H3ac, increased the turbidity of the solutions due to droplet formation (**Figure 4.9A**). Decreases in solution turbidity were observed when the DNA concentration was further increased, as is generally seen in reentrant phase separation.[42] The charge ratio ([positive charges of H3 peptide] / [negative charges of DNA]) with the highest turbidity was around 1.0 for the unmodified H3 peptide, which is similar to the electrostatic binary LLPS systems,[44,45] suggesting that LLPS was caused almost entirely by electrostatic interactions between cationic residues (i.e., 4 lysine and 3 arginine) of H3 peptides and the phosphate groups of DNA, consistent with the dissolution of the droplets by NaCl (**Figure 4.3E**). Interestingly, monoacetylation shifted this charge ratio; 1.1 and 1.4 for the H3 peptides acetylated near the center (H3K9ac and H3K14ac) and near the end (H3K4ac and H3K18ac), respectively. This suggests that acetylation and its site within the H3 peptide may affect the binding stoichiometry to the DNA and may imply the possible contribution of non-electrostatic interactions to LLPS.

I then attempted to clarify the contributing factors by examining the driving forces of droplets formation. To this end, we examined the effects of NaCl and 1,6-hexaneiol, known to inhibit electrostatic and hydrophobic interactions, respectively.[46,47] The H3 peptide can form droplets with DNA in the presence of NaCl up to 90 mM, while the monoacetylated H3 peptides were completely dissolved at ionic strengths of only 10 mM, independent of the acetylation site (**Figure 4.9B**). This suggests that the loss of only one cationic lysine residue within the H3 peptide markedly attenuated the stabilizing effect of the electrostatic interaction.

Addition of 1,6-hexanediol to a solution containing the unmodified H3 peptide/DNA droplets slightly decreased the turbidity (**Figure 4.9C**), while apparently rather increased the droplet size in phase-contrast microscopy images (**Figure 4.10**). This seemingly inconsistent behavior may be due not only to the inhibition of hydrophobic interactions, but also to the decrease in dielectric constant and the change in the surface tension of the droplets. However, it should be clear that at least the suppression of hydrophobic

interaction alone did not inhibit droplet formation.

For the H3 peptides acetylated near the end (H3K9ac and H3K14ac), the turbidity in the solutions containing the droplets decreased gradually as the concentration of 1,6-hexanediol increased and was almost lost above 15% (**Figure 4.9C**), leaving only small droplets (**Figure 4.10**). In contrast, those near the center (H3K4ac and H3K18ac) became completely transparent with the addition of only 2.5% 1,6-hexanediol (**Figure 4.9C**). These results suggest that (i) hydrophobic interactions play an essential role in the LLPS of H3K4ac and H3K18ac, while not in the case of H3K9ac and H3K14ac, or (ii) the contribution of electrostatic interactions in the case of H3K9ac and H3K14ac is sufficient to undergo LLPS, assuming that the hydrophobic interactions were completely inhibited by 1,6-hexanediol. In either case, the balance between the driving forces essential for the formation of LLPS (electrostatic and hydrophobic interactions between the H3 peptides and DNA) may have altered depending on the acetylation site within the H3 peptide.

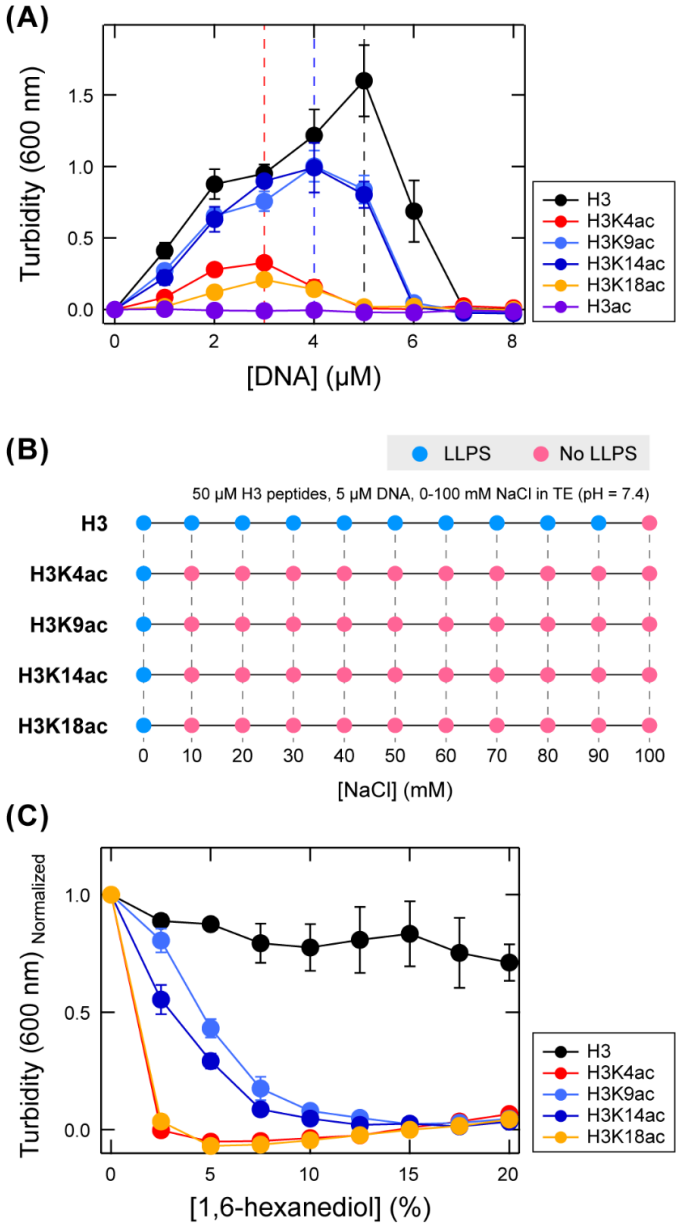

Figure 4.9. Molecular interactions for H3 peptide/DNA droplets formation. (A) Turbidity of solutions that contain various H3 peptides (50 μM) and DNA (0-8 μM) in TE buffer (pH = 7.4). (B) Phase diagram of solutions containing H3 peptides (50 μM) and DNA (5 μM) against NaCl concentration (0-100 mM). (C) Turbidity of solutions containing H3 peptides (50 μM) and DNA (5 μM) in the presence of 0-20% 1,6-hexanediol.

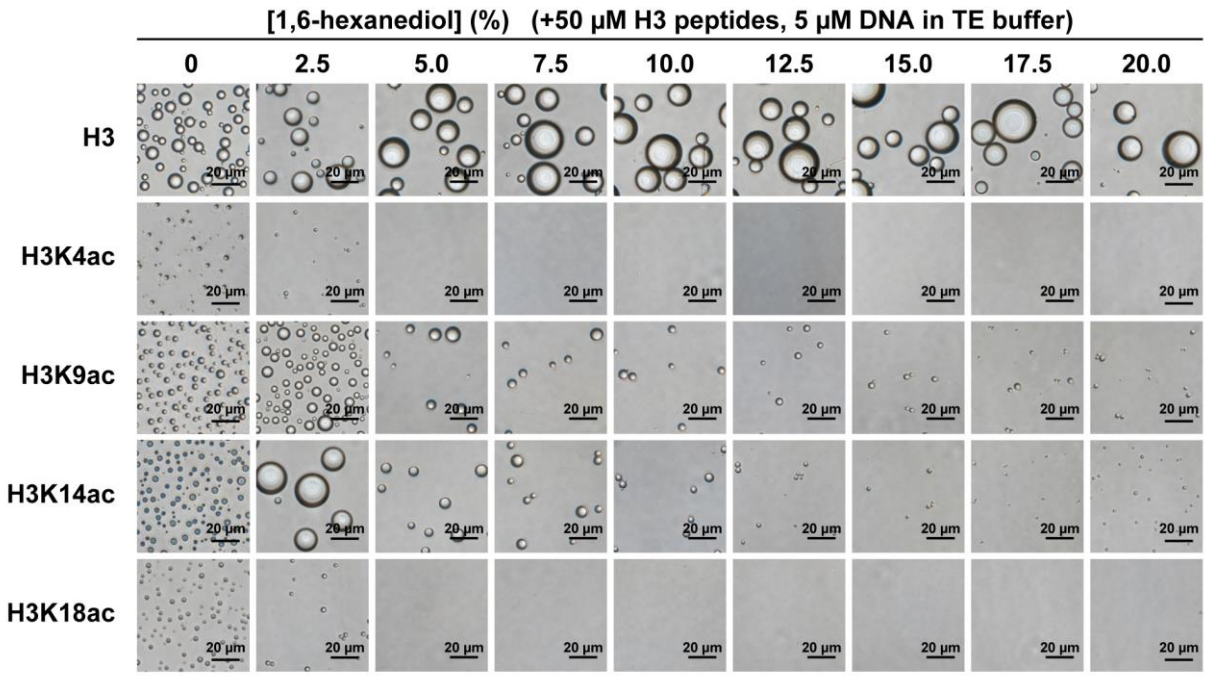

Figure 4.10. Phase-contrast microscopy images of solutions that contain peptide (50 μM) and DNA (5 μM) in the presence of 0-20.0% 1,6-hexanediol; scale bar = 20 μm.

Effect of H3 peptides binding on DNA thermal stabilization; correlation with its LLPS ability.

Changes in the balance of interactions between the peptides and DNA depending on the acetylation site may affect the strength of these bindings. I performed thermal melting experiments of DNA in the presence of the peptides to evaluate binding affinity of the peptides to DNA. A previous report on histone H4 showed that complete acetylation of the tail peptide lowers the binding constant to DNA by 4-5 orders of magnitude, reducing the ability to increase the melting temperature (*Tm*) of the DNA associated with binding of the tail peptide (20°C to 5°C).[48] Based on this correlation, we hypothesized that the H3 peptides with higher thermal stabilization effects on DNA would have higher binding affinities.

The melting curves of the solutions containing 1 μM DNA and 0-12.5 μM peptides showed that the unmodified H3 peptide markedly improved the thermal stability of DNA in a concentration-dependent manner; The *Tm* value of DNA increased from 50°C to 72°C by the addition of 12.5 μM of H3 peptide (**Figure 4.11A**). Interestingly, the thermal stabilizing effects of the monoacetylated H3 peptides was

correlated with the LLPS capability; the acetylation with higher LLPS capability showed higher thermal stabilization effect (**Figures 4.11B** and **4.12**).

It should be noted that our thermal melting experiments were performed under non-LLPS conditions. The process of LLPS can be divided into two steps: the first step is the formation of soluble complexes of peptides and DNA, and the second step is the formation of droplets with further association of the complexes.[49,50] Therefore, the results obtained from the experiments here can be expected to evaluate the molecular interactions involved in the formation of soluble complexes, and thus the acetylation site may contribute to the binding affinity of H3 peptide to DNA for this step. However, the second step is the rate-limiting in the generation of LLPS, so another possibility is that the acetylation sites may lead to a change in the binding pattern (e.g., binding sites and number) of the peptide to the DNA surface, contributing to a further association step by altering the physicochemical properties of the soluble complex. This consideration is supported by the results obtained from the turbidity measurements indicating that the binding stoichiometry of peptide to DNA depends on the acetylation site (**Figure 4.9A**). However, due to the technical limitations of evaluating the physicochemical properties of soluble complexes and the interactions between complexes, further studies will be needed to determine the detailed molecular mechanisms.

The findings of this study propose a regulatory mechanism for LLPS of H3 peptide and DNA mixtures in an acetylation site-dependent manner, which is expected to be relevant to biology. Acetylation/de-acetylation of histone tails modulates chromatin organization via LLPS, which is expected to play a crucial role in transcriptional regulation by determining the recruitment to chromatin of nuclear proteins, such as transcription factors that bind to DNA, and so called 'reader' proteins that recognize the specific acetylation sites on histone tails.[51] For instance, it has been reported that acetylation of histone tails promotes the binding of the transcription factor TFIIA to nucleosomal DNA,[52] and that acetylated histone H3K14 is involved in the chromatin remodeling by recruiting the Sth1 protein.[53] Acetylated H3K9 has also been reported to regulate transcription initiation by super elongation complex recruitment.[54] The mechanism by which these proteins are recruited into chromatin is still unclear, it might possibly involve changes in LLPS behavior depending on the acetylation site.

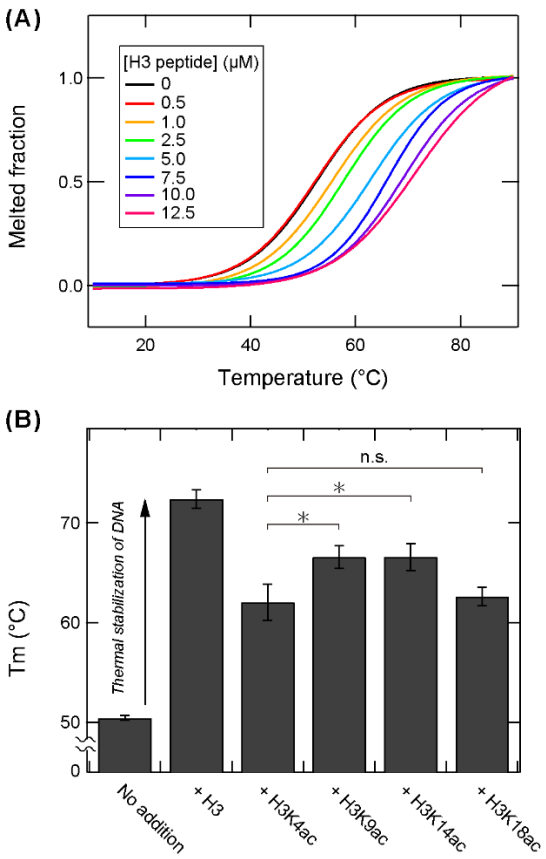

Figure 4.11. Thermal stabilization of DNA by binding of H3 peptides. (A) UV melting curves of DNA (1 μM) in the presence of 0-12.5 μM H3 peptide. Melted fraction indicates the populations in which double strands dissociate into single strands, and the temperature at which this value is 0.5 was defined as Tm. The detailed analysis of the melting curve is described in the Experimental section of the Supporting Information. (B) Tm values of DNA in the presence of 12.5 μM acetylated/non-acetylated H3 peptide. The values are shown as mean values ± SD (n=3). *P < 0.05, and not significance (n.s.) means P > 0.98.

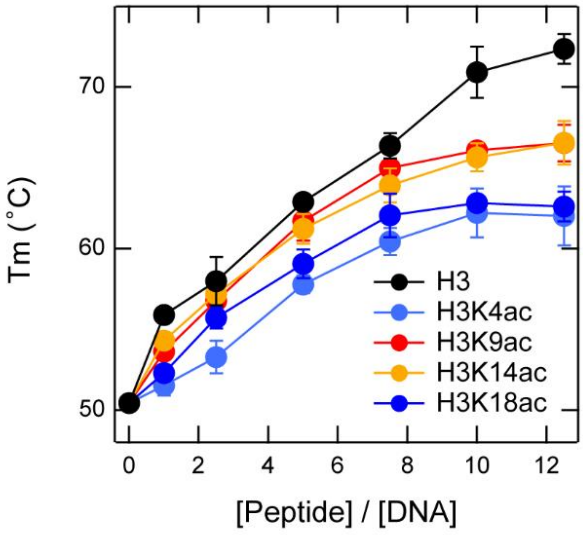

Figure 4.12. Melting temperature of DNA (1 μM) in the presence of each peptide (0-12.5 μM) .

4.4. Conclusion

In summary, I first demonstrated that histone H3 tail peptide forms droplets with nucleosomal linker DNA via liquid-liquid phase separation (LLPS). Subsequently, I showed that the formation of these droplets is inhibited by enzymatic acetylation of the H3 peptide. By employing peptide with different acetylation sites, I found that the LLPS inhibitory effect was dependent on the acetylation site within the H3 peptide, i.e., the acetylation site was near the end of the peptide, its LLPS inhibitory effect was more significant than that near the center. The acetylation site affected the balance between electrostatic and hydrophobic interactions between H3 peptide and DNA. As a result, the binding affinity of H3 peptide to DNA was changed, which likely modulates the LLPS behavior. Extending the picture of the results obtained in this simple binary system to more complex systems, such as nucleosomes and chromatin, my findings may indicate that acetylation near the end of the histone tails has a more significant LLPS inhibitory effect.

The extensibility of my simple H3 peptide/DNA model LLPS system (e.g., application to other histone tails, various post-translational modifications and their combinations, DNA of different sequences and lengths, and additional histone-binding proteins, etc.) makes it an effective strategy to gain fundamental insight of the effects of post-translational modifications on not only LLPS-mediated chromatin organization mechanism, but also on general biomolecular LLPS mechanisms. Furthermore, it is interesting to note that the regulatory mechanism of histone acetylation/de-acetylation, which has been closely associated with diseases such as cancer,[51] plays a crucial role in chromatin phase separation, considering that aberrant phase separation in cells is also associated with diseases such as cancer and neurodegenerative diseases.[55,56]

References

(1) Alberti, S. Phase Separation in Biology. *Curr. Biol*. **2017**, *27* (20), R1097–R1102.

(2) Banani, S. F.; Lee, H. O.; Hyman, A. A.; Rosen, M. K. Biomolecular Condensates: Organizers of Cellular Biochemistry. *Nat. Rev. Mol. Cell Biol.* **2017**, *18* (5), 285–298.

(3) Hondele, M.; Sachdev, R.; Heinrich, S.; Wang, J.; Vallotton, P.; Fontoura, B. M. A.; Weis, K. DEAD-Box ATPases Are Global Regulators of Phase-Separated Organelles. *Nature* **2019**, *573* (7772), 144–148.

(4) Brangwynne, C. P.; Eckmann, C. R.; Courson, D. S.; Rybarska, A.; Hoege, C.; Gharakhani, J.; Jülicher, F.; Hyman, A. A. Germline P Granules Are Liquid Droplets That Localize by Controlled Dissolution/Condensation. *Science* **2009**, *324* (5935), 1729–1732.

(5) Neugebauer, K. M. Special Focus on the Cajal Body. *RNA Biol.* **2017**, *14* (6), 669–670.

(6) Sabari, B. R.; Dall'Agnese, A.; Boija, A.; Klein, I. A.; Coffey, E. L.; Shrinivas, K.; Abraham, B. J.; Hannett, N. M.; Zamudio, A. V.; Manteiga, J. C.; Li, C. H.; Guo, Y. E.; Day, D. S.; Schuijers, J.; Vasile, E.; Malik, S.; Hnisz, D.; Lee, T. I.; Cisse, I. I.; Roeder, R. G.; Sharp, P. A.; Chakraborty, A. K.; Young, R. A. Coactivator Condensation at Super-Enhancers Links Phase Separation and Gene Control. *Science* **2018**, *361* (6400).

(7) Dogra, P.; Joshi, A.; Majumdar, A.; Mukhopadhyay, S. Intermolecular Charge-Transfer Modulates Liquid–Liquid Phase Separation and Liquid-to-Solid Maturation of an Intrinsically Disordered PH-Responsive Domain. *J. Am. Chem. Soc.* **2019**, *141* (51), 20380–20389.

(8) Boeynaems, S.; Alberti, S.; Fawzi, N. L.; Mittag, T.; Polymenidou, M.; Rousseau, F.; Schymkowitz, J.; Shorter, J.; Wolozin, B.; Van Den Bosch, L.; Tompa, P.; Fuxreiter, M. Protein Phase Separation: A New Phase in Cell Biology. *Trends Cell Biol.* **2018**, *28* (6), 420–435.

(9) Dignon, G. L.; Best, R. B.; Mittal, J. Biomolecular Phase Separation: From Molecular Driving Forces to Macroscopic Properties. *Annu. Rev. Phys. Chem.* **2020**, *71*, 53–75.

(10) Luo, Y.-Y.; Wu, J.-J.; Li, Y.-M. Regulation of Liquid-Liquid Phase Separation with Focus on Post-Translational Modifications. *Chem. Commun.* **2021**, *57* (98), 13275–13287.

(11) Wang, J. T.; Smith, J.; Chen, B.-C.; Schmidt, H.; Rasoloson, D.; Paix, A.; Lambrus, B. G.; Calidas, D.; Betzig, E.; Seydoux, G. Regulation of RNA Granule Dynamics by Phosphorylation of Serine-Rich, Intrinsically Disordered Proteins in C. elegans. *Elife* **2014**, *3*, e04591.

(12) Picaud, S.; Filippakopoulos, P. SPOTing Acetyl-Lysine Dependent Interactions. *Microarrays (Basel)* **2015**, *4* (3), 370–388.

(13) Ramazi, S.; Allahverdi, A.; Zahiri, J. Evaluation of Post-Translational Modifications in Histone Proteins: A Review on Histone Modification Defects in Developmental and Neurological Disorders. *J. Biosci.* **2020**, *45*, 135.

(14) Darling, A. L.; Uversky, V. N. Intrinsic Disorder and Posttranslational Modifications: The Darker Side

of the Biological Dark Matter. *Front. Genet.* **2018**, *9*, 158.

(15) Erdel, F.; Rippe, K. Formation of Chromatin Subcompartments by Phase Separation. *Biophys. J.* **2018**, *114* (10), 2262–2270.

(16) Gibson, B. A.; Doolittle, L. K.; Schneider, M. W. G.; Jensen, L. E.; Gamarra, N.; Henry, L.; Gerlich, D. W.; Redding, S.; Rosen, M. K. Organization of Chromatin by Intrinsic and Regulated Phase Separation. *Cell* **2019**, *179* (2), 470-484.e21.

(17) Khan, S. A.; Reddy, D.; Gupta, S. Global Histone Post-Translational Modifications and Cancer: Biomarkers for Diagnosis, Prognosis and Treatment? *World J. Biol. Chem.* **2015**, *6* (4), 333–345.

(18) Li, B.; Su, T.; Ferrari, R.; Li, J.-Y.; Kurdistani, S. K. A Unique Epigenetic Signature Is Associated with Active DNA Replication Loci in Human Embryonic Stem Cells. *Epigenetics* **2014**, *9* (2), 257–267.

(19) Sharma, G. G.; So, S.; Gupta, A.; Kumar, R.; Cayrou, C.; Avvakumov, N.; Bhadra, U.; Pandita, R. K.; Porteus, M. H.; Chen, D. J.; Cote, J.; Pandita, T. K. MOF and Histone H4 Acetylation at Lysine 16 Are Critical for DNA Damage Response and Double-Strand Break Repair. *Mol. Cell. Biol.* **2010**, *30* (14), 3582–3595.

(20) Tan, M.; Luo, H.; Lee, S.; Jin, F.; Yang, J. S.; Montellier, E.; Buchou, T.; Cheng, Z.; Rousseaux, S.; Rajagopal, N.; Lu, Z.; Ye, Z.; Zhu, Q.; Wysocka, J.; Ye, Y.; Khochbin, S.; Ren, B.; Zhao, Y. Identification of 67 Histone Marks and Histone Lysine Crotonylation as a New Type of Histone Modification. *Cell* **2011**, *146* (6), 1016–1028.

(21) Clayton, A. L.; Hazzalin, C. A.; Mahadevan, L. C. Enhanced Histone Acetylation and Transcription: A Dynamic Perspective. *Mol. Cell* **2006**, *23* (3), 289–296.

(22) Xu, Y.-M.; Du, J.-Y.; Lau, A. T. Y. Posttranslational Modifications of Human Histone H3: An Update. *Proteomics* **2014**, *14* (17–18), 2047–2060.

(23) Li, C.; Choi, H.-P.; Wang, X.; Wu, F.; Chen, X.; Lü, X.; Jing, R.; Ryu, H.; Wang, X.; Azadzoi, K. M.; Yang, J.-H. Post-Translational Modification of Human Histone by Wide Tolerance of Acetylation. *Cells* **2017**, *6* (4), 34.

(24) Owczarzy, R. Melting Temperatures of Nucleic Acids: Discrepancies in Analysis. *Biophys. Chem.* **2005**, *117* (3), 207–215.

(25) Zandian, M.; Gonzalez Salguero, N.; Shannon, M. D.; Purusottam, R. N.; Theint, T.; Poirier, M. G.;

Jaroniec, C. P. Conformational Dynamics of Histone H3 Tails in Chromatin. *J. Phys. Chem. Lett.* **2021**, *12* (26), 6174–6181.

(26) Bass, M. V.; Nikitina, T.; Norouzi, D.; Zhurkin, V. B.; Grigoryev, S. A. Nucleosome Spacing Periodically Modulates Nucleosome Chain Folding and DNA Topology in Circular Nucleosome Arrays. *J. Biol. Chem.* **2019**, *294* (11), 4233–4246.

(27) Mimura, M.; Tomita, S.; Shinkai, Y.; Hosokai, T.; Kumeta, H.; Saio, T.; Shiraki, K.; Kurita, R. Quadruplex Folding Promotes the Condensation of Linker Histones and DNAs via Liquid-Liquid Phase Separation. *J. Am. Chem. Soc.* **2021**, *143* (26), 9849–9857.

(28) Matsuda, A.; Mimura, M.; Maruyama, T.; Kurinomaru, T.; Shiuhei, M.; Shiraki, K. Liquid Droplet of Protein-Polyelectrolyte Complex for High-Concentration Formulations. *J. Pharm. Sci.* **2018**, *107* (10), 2713–2719.

(29) Patel, A.; Lee, H. O.; Jawerth, L.; Maharana, S.; Jahnel, M.; Hein, M. Y.; Stoynov, S.; Mahamid, J.; Saha, S.; Franzmann, T. M.; Pozniakovski, A.; Poser, I.; Maghelli, N.; Royer, L. A.; Weigert, M.; Myers, E. W.; Grill, S.; Drechsel, D.; Hyman, A. A.; Alberti, S. A Liquid-to-Solid Phase Transition of the ALS Protein FUS Accelerated by Disease Mutation. *Cell* **2015**, *162* (5), 1066–1077.

(30) Taylor, N. O.; Wei, M.-T.; Stone, H. A.; Brangwynne, C. P. Quantifying Dynamics in Phase-Separated Condensates Using Fluorescence Recovery after Photobleaching. *Biophys. J.* **2019**, *117* (7), 1285–1300.

(31) Shakya, A.; Park, S.; Rana, N.; King, J. T. Liquid-Liquid Phase Separation of Histone Proteins in Cells: Role in Chromatin Organization. *Biophys. J.* **2020**, *118* (3), 753–764.

(32) Zimmerman, S. B.; Trach, S. O. Estimation of Macromolecule Concentrations and Excluded Volume Effects for the Cytoplasm of Escherichia Coli. *J. Mol. Biol.* **1991**, *222* (3), 599–620.

(33) McGuffee, S. R.; Elcock, A. H. Diffusion, Crowding & Protein Stability in a Dynamic Molecular Model of the Bacterial Cytoplasm. *PLoS Comput. Biol.* **2010**, *6* (3), e1000694.

(34) André, A. A. M.; Spruijt, E. Liquid–Liquid Phase Separation in Crowded Environments. *Int. J. Mol. Sci.* **2020**, *21* (16), 5908.

(35) Bai, Q.; Zhang, Q.; Jing, H.; Chen, J.; Liang, D. Liquid–Liquid Phase Separation of Peptide/Oligonucleotide Complexes in Crowded Macromolecular Media. *J. Phys. Chem. B* **2021**, *125* (1), 49–57.

(36) Park, S.; Barnes, R.; Lin, Y.; Jeon, B.-J.; Najafi, S.; Delaney, K. T.; Fredrickson, G. H.; Shea, J.-E.; Hwang, D. S.; Han, S. Dehydration Entropy Drives Liquid-Liquid Phase Separation by Molecular Crowding. *Commun. Chem.* **2020**, *3*, 83.

(37) Peserico, A.; Simone, C. Physical and Functional HAT/HDAC Interplay Regulates Protein Acetylation Balance. *J. Biomed. Biotechnol.* **2011**, *2011*, 371832.

(38) Zhang, Y.; Xue, Y.; Shi, J.; Ahn, J.; Mi, W.; Ali, M.; Wang, X.; Klein, B. J.; Wen, H.; Li, W.; Shi, X.; Kutateladze, T. G. The ZZ Domain of P300 Mediates Specificity of the Adjacent HAT Domain for Histone H3. *Nat. Struct. Mol. Biol.* **2018**, *25* (9), 841–849.

(39) Balasubramanyam, K.; Swaminathan, V.; Ranganathan, A.; Kundu, T. K. Small Molecule Modulators of Histone Acetyltransferase P300. *J. Biol. Chem.* **2003**, *278* (21), 19134–19140.

(40) Banerjee, P. R.; Milin, A. N.; Moosa, M. M.; Onuchic, P. L.; Deniz, A. A. Reentrant Phase Transition Drives Dynamic Substructure Formation in Ribonucleoprotein Droplets. *Angew. Chem. Int. Ed. Engl.* **2017**, *56* (38), 11354–11359.

(41) Alshareedah, I.; Kaur, T.; Ngo, J.; Seppala, H.; Kounatse, L.-A. D.; Wang, W.; Moosa, M. M.; Banerjee, P. R. Interplay between Short-Range Attraction and Long-Range Repulsion Controls Reentrant Liquid Condensation of Ribonucleoprotein–RNA Complexes. *J. Am. Chem. Soc.* **2019**, *141* (37), 14593–14602.

(42) Nakashima, K. K.; Vibhute, M. A.; Spruijt, E. Biomolecular Chemistry in Liquid Phase Separated Compartments. *Front. Mol. Biosci.* **2019**, *6*, 21.

(43) Chollakup, R.; Smitthipong, W.; Eisenbach, C. D.; Tirrell, M. Phase Behavior and Coacervation of Aqueous Poly(acrylic acid)−Poly(allylamine) Solutions. *Macromolecules* **2010**, *43* (5), 2518–2528.

(44) Mousseau, F.; Vitorazi, L.; Herrmann, L.; Mornet, S.; Berret, J.-F. Polyelectrolyte Assisted Charge Titration Spectrometry: Applications to Latex and Oxide Nanoparticles. *J. Colloid Interface Sci.* **2016**, *475*, 36–45.

(45) Karoui, H.; Seck, M. J.; Martin, N. Self-Programmed Enzyme Phase Separation and Multiphase Coacervate Droplet Organization. *Chem. Sci.* **2021**, *12* (8), 2794–2802.

(46) Lin, Y.; Mori, E.; Kato, M.; Xiang, S.; Wu, L.; Kwon, I.; McKnight, S. L. Toxic PR Poly-Dipeptides Encoded by the C9orf72 Repeat Expansion Target LC Domain Polymers. *Cell* **2016**, *167* (3), 789–

802.e12.

(47) Mimura, M.; Tsumura, K.; Matsuda, A.; Akatsuka, N.; Shiraki, K. Effect of Additives on Liquid Droplet of Protein–Polyelectrolyte Complex for High-Concentration Formulations. *J. Chem. Phys.* **2019**, *150* (6), 064903.

(48) Hong, L.; Schroth, G. P.; Matthews, H. R.; Yau, P.; Bradbury, E. M. Studies of the DNA Binding Properties of Histone H4 Amino Terminus. Thermal Denaturation Studies Reveal That Acetylation Markedly Reduces the Binding Constant of the H4 "Tail" to DNA. *J. Biol. Chem.* **1993**, *268* (1), 305–314.

(49) Turner, A. L.; Watson, M.; Wilkins, O. G.; Cato, L.; Travers, A.; Thomas, J. O.; Stott, K. Highly Disordered Histone H1−DNA Model Complexes and Their Condensates. *Proc. Natl. Acad. Sci. U. S. A.* **2018**, *115* (47), 11964–11969.

(50) Priftis, D.; Laugel, N.; Tirrell, M. Thermodynamic Characterization of Polypeptide Complex Coacervation. *Langmuir* **2012**, *28* (45), 15947–15957.

(51) Gong, F.; Chiu, L.-Y.; Miller, K. M. Acetylation Reader Proteins: Linking Acetylation Signaling to Genome Maintenance and Cancer. *PLoS Genet.* **2016**, *12* (9), e1006272.

(52) Lee, D. Y.; Hayes, J. J.; Pruss, D.; Wolffe, A. P. A Positive Role for Histone Acetylation in Transcription Factor Access to Nucleosomal DNA. *Cell* **1993**, *72* (1), 73–84.

(53) Chen, G.; Li, W.; Yan, F.; Wang, D.; Chen, Y. The Structural Basis for Specific Recognition of H3K14 Acetylation by Sth1 in the RSC Chromatin Remodeling Complex. *Structure* **2020**, *28* (1), 111–118.e3.

(54) Gates, L. A.; Shi, J.; Rohira, A. D.; Feng, Q.; Zhu, B.; Bedford, M. T.; Sagum, C. A.; Jung, S. Y.; Qin, J.; Tsai, M.-J.; Tsai, S. Y.; Li, W.; Foulds, C. E.; O'Malley, B. W. Acetylation on Histone H3 Lysine 9 Mediates a Switch from Transcription Initiation to Elongation. *J. Biol. Chem.* **2017**, *292* (35), 14456–14472.

(55) Spannl, S.; Tereshchenko, M.; Mastromarco, G. J.; Ihn, S. J.; Lee, H. O. Biomolecular Condensates in Neurodegeneration and Cancer. *Traffic* **2019**, *20* (12), 890–911.

(56) Timmermann, S.; Lehrmann, H.; Polesskaya, A.; Harel-Bellan, A. Histone Acetylation and Disease. *Cell. Mol. Life Sci.* **2001**, *58* (5–6), 728–736.

Chapter 5.

General Discussion

Liquid-liquid phase separation (LLPS), driven by protein-DNA interactions, allows for the formation of dynamic molecular compartments in the nucleus, which are believed to play an essential role in the regulation of biological processes. The basic knowledge of the LLPS mechanism is expected to be contribute not only to the understanding of ambiguous intracellular LLPS, but also to the development of biotechnologies such as intracellular LLPS control system. In this study, I used binary systems consisting of DNA and cationic polypeptides including proteins and synthesized peptides to clarify the effects of their chemical nature, higher-order structures, and modifications on the LLPS process. This chapter describes the general discussion of the insights obtained from this study, as well as the challenges and future research directions.

Generally, anionic DNA and cationic polypeptides generate LLPS through electrostatic interactions as the main driving force. Interestingly, as shown in Chapter 2, phase diagrams of single-stranded DNA-based oligomers and linker histone H1 (H1) suggested that in addition to the expected electrostatic interactions involving the phosphate groups of DNAs, intermolecular interactions involving deoxyribose and nucleobases promote LLPS. These nonionic moieties of DNA probably promote LLPS through cation-π and van der Waals interactions with exposed cationic and polar amino acid residues of H1. Even the individual interactions, which are weaker and more unstable than charge-charge interactions, may have made a significant contribution to LLPS through their multipoint interactions. Another possible mechanism is that deoxyribose and nucleobases may have affected the flexibility of the DNA strand and that contributed to the phase behavior with H1. Unfortunately, the understanding of the detailed mechanism of this remains limited. To solve this problem, new techniques will be needed to evaluate weak and multipoint intermolecular interactions, which are crucial in LLPS generation. Regardless of the challenges, the findings of this study, obtained through a unique approach that utilizes nucleic acid-based oligomers, will be useful in understanding the role of the chemical nature of nucleic acids in intracellular LLPS, such as the differential contribution of DNA and RNA, and the effects of epigenetic modifications and damage of nucleic acids.

Proteins and nucleic acids are often fold into a variety of higher-order structures depending on their sequence, solution environment, and inter- and intra-molecular interactions. It is known that proteins that act as scaffolds

in the formation of intracellular droplets tend to have regions without defined structure known as intrinsically disordered regions (IDRs). This structural feature is thought to favor flexible and multi-point interactions to drive LLPS. However, the effect of the higher-order structures of nucleic acids on LLPS with cationic polypeptides is still poorly understood. Chapter 3 presents that among the various DNA structures, the formation of 'quadruplex' structures in single-stranded DNA (ssDNA) including G-quadruplexes and i-motif structure, promote droplets formation with H1 and decrease molecular motility within droplets. Phase diagrams of H1 with DNA and stability tests of the droplets to additives indicated that in addition to electrostatic interactions between the DNA and the IDRs of H1, π-π stacking between quadruplex DNAs could potentially drive droplets formation, unlike in the electrostatically driven LLPS of duplex DNA and H1. This difference in driving force may be attributed to the characteristics of the quadruplex structure: (i) sides with high charge density and (ii) wide hydrophobic top and bottom planes exposed to the solvent.

The folding of DNA into quadruplexes is affected by interactions with metal ions, proteins, and molecular crowding agents. Structural analysis of DNA based on circular dichroism and binding assays using G-quadruplex-selective probes showed that quadruplex folding is maintained, or in some cases, it is promoted by binding to H1 coupled to droplets formation. Promotion of quadruplex folding was also observed with cationic poly-l-lysine and its derivatives, regardless of droplets formation, suggesting that this folding promotion effect is due to non-specific electrostatic interactions with cationic polymers. Note that the high-resolution magic angle spinning nuclear magnetic resonance (HR-MAS-NMR) spectra indicate that the G-quadruplex inside the droplets shows a structural polymorphism. The folding state of DNA and the detailed interactions between quadruplex DNA and H1 as well as between DNAs within the droplets which is a unique environment of high molecular concentration, low dielectric constant, and high viscosity, require further study.

Numerous previous studies have shown that folding of DNA into quadruplex structures plays a crucial role in the chromatin organization and gene transcription. Therefore, the findings of this study suggest that the quadruplex structure may have some contribution to these biological processes 'through LLPS'. In addition, it is also expected to contribute to the development of biotechnologies, such as the control system of intracellular LLPS by promoting/inhibiting the quadruplex folding with additives or light irradiation. The development of such technologies will help us to further understand the biological significance of quadruplex structures and intracellular LLPS.

In Chapter 4, I focused on the effect of physicochemical properties of the cationic polypeptide, especially the effect of acetylation, one of the major post-translational modifications (PTMs) known to play a key role in the control of LLPS. Acetylation is frequently observed in histone tails, and it is involved in gene transcriptional regulation and DNA repair. In the context of biological LLPS, it has been reported that droplet formation in chromatin-associated nucleosome arrays is inhibited by acetylation of histone tails. Consistent with this, the developed novel binary LLPS system composed of histone H3 tail peptide and DNA showed that electrostatically formed H3 peptide/DNA droplets were dissolved by acetylation of the H3 peptide by histone acetyltransferase. This is due to the neutralization of the positive charge of the lysine residues within the H3 peptide by acetylation, which attenuates the electrostatic interactions between the peptide the DNA.

To investigate the effect of acetylation site within the H3 tail on LLPS with DNA, H3 peptides with different sites acetylated were prepared. Even though the total charge of all peptides with one lysine residue acetylated are the same, interestingly, the obtained phase diagrams showed that the LLPS ability of H3 peptides differed depending on the acetylation site, i.e., H3K4ac and H3K18ac peptides acetylated near the end of the peptide were less likely to generate LLPS than H3K9ac and H3K14ac peptides acetylated near the center. The stability of the droplets in the presence of the additives (NaCl and 1,6-hexanediol) indicated that the balance of electrostatic and hydrophobic interactions between H3 peptide and DNA is dependent on the acetylation site. As another experimental evidence for this difference in interactions, the thermal stabilizing effect of DNA shown by the acetylated H3 peptides was correlated with the LLPS ability.

In the context of biology, acetylation sites of the H3 tail are known to play different roles, for instance, acetylation of H3K4 and H3K9 is involved in activation and initiation of transcription, respectively. Since these acetylation site-specific roles are thought to be associated with the recruitment of proteins such as RNA polymerase and transcription factors to chromatin, it is possible that acetylation site-dependent changes in LLPS behavior contribute to this recruitment. The biological significance of the findings is limited because the H3 peptide and DNA are partial elements of chromatin, and therefore the proposed concept may require further validation by applying more complex systems, such as the nucleosome array and real chromatin in nucleus. It is important to further accumulate basic knowledge about the site-dependence of methylation and phosphorylation within the histone tails and the effect of combinations of PTMs on LLPS with DNA.

Chapter 6.

General Conclusion

This thesis describes the mechanism of liquid-liquid phase separation (LLPS) of DNA and cationic polypeptide, including linker histone H1(H1) and histone H3 tail peptide, involved in chromatin organization by using binary systems. Chapter 2 presents the role of components of single-stranded DNA (ssDNA) on LLPS with H1, showing that not only the expected electrostatic interactions involving the phosphate groups of ssDNA, but also the interactions involving the nonionic deoxyribose and nucleobases have a role in promoting LLPS. Chapter 3 focused on the role of higher-order structures of DNA, and it was first reported that folding of DNA into quadruplex structures including G-quadruplex and i-motif promotes LLPS with H1. The quadruplex structure has high charge density sides and a wide hydrophobic plane exposed to the solvent, and experimental results suggest that the droplet formation is driven by π-π stacking between DNAs in addition to electrostatic interactions with H1. In Chapter 4, a novel binary system consisting of histone H3 tail peptide and DNA was developed, which demonstrated the control mechanism of LLPS depending on the acetylation sites of the histone H3 tail, i.e., the acetylation near the ends of the histone H3 tails showed a significant LLPS inhibitory effect.

Flexible and multipoint interactions between biomolecules play a crucial role in the regulation of intracellular LLPS. However, such complicated molecular interaction networks are still difficult to evaluate, and little understood, unlike specific interactions such as enzyme-substrate or antibody-antigen interactions, which have been studied intensively. To solve this problem, it is necessary to develop novel techniques that allow us to (1) analyze unstable and complicated interactions between biomolecules, and (2) directly measure various physicochemical properties of small volume droplets in solution. The fundamental insight obtained in this thesis on the LLPS mechanism of mixed solutions of DNA and cationic polypeptides is expected to contribute to the development of the emerging field of 'biological phase separation'. Additionally, the systematic approach described here, which combines experiments utilizing binary model systems with chemical molecular design, will present better understanding the LLPS mechanism of biomolecules. In the near future, interdisciplinary research that sheds light on the complicated interaction networks including two or more biomolecules will lead to the development of various fields including biology and biotechnology.

List of Publications

Related publications

(1) **Masahiro Mimura**, Shunsuke Tomita, Hiroka Sugai, Yoichi Shinkai, Sayaka Ishihara, Ryoji Kurita, Uncharged moieties of DNA modulate liquid-liquid phase separation with cationic linker histone H1, *Frontiers in Cell and Developmental biology*, **2021**, 9, 710729.

(2) **Masahiro Mimura**, Shunsuke Tomita, Yoichi Shinkai, Yakuya Hosokai, Hiroyuki Kumeta, Tomohide Saio, Kentaro Shiraki, Ryoji Kurita, Quadruplex folding promotes the condensation of linker histones and DNAs via liquid-liquid phase separation, *Journal of American Chemical Society*, **2021**, 143, 9849–9857.

(3) **Masahiro Mimura**, Shunsuke Tomita, Hiroka Sugai, Tomoshi Kameda, Ryo Kitahara, Soichiro Kitazawa, Ryoji Kurita, *in preparation*.

Other publications

(1) Ayumi Matsuda[1], **Masahiro Mimura[1]**, Takuya Maruyama, Takaaki Kurinomaru, Mieda Shiuhei, Kentaro Shiraki, Liquid droplet of protein–polyelectrolyte complex for high-concentration formulations, *Journal of Pharmaceutical Sciences,* **2018**, *107*, 2713–2719. [1]These authors contributed equally to this paper.

(2) Kazuki Iwashita, **Masahiro Mimura**, Kentaro Shiraki, Control of aggregation, coaggregation, and liquid droplet of proteins using small additives, *Current Pharmaceutical Biotechnology,* **2018**, *19*, 946–955.

(3) **Masahiro Mimura**, Keisuke Tsumura, Ayumi Matsuda, Naoki Akatsuka, Kentaro Shiraki, Effect of additives on liquid droplet of protein–polyelectrolyte complex for high-concentration formulations, *The Journal of Chemical Physics*, **2019**, *150*, 064903.

(4) **Masahiro Mimura**, Shunsuke Tomita, Ryoji Kurita, Kentaro Shiraki, Array-based generation of response patterns with common fluorescent dyes for identification of proteins and cells, *Analytical Sciences*, **2019**, *35*, 99–102.

(5) Shunsuke Tomita, Hiroka Sugai, **Masahiro Mimura**, Sayaka Ishihara, Kentaro Shiraki, Ryoji Kurita, Optical fingerprints of proteases and their inhibited complexes provided by differential cross-reactivity of fluorophore-labeled single-stranded DNA, *ACS Applied Materials & Interfaces*, **2019**, *11*, 47428–47436.

(6) Kentaro Shiraki, **Masahiro Mimura**, Suguru Nishinami, Tomoto Ura, Effect of additives on liquid droplets and aggregates of proteins, *Biophysical Reviews*, **2020**, 12, 587–592.

(7) Hiroki Okada, **Masahiro Mimura**, Shunsuke Tomita, Ryoji Kurita, Affinity diversification of a polymer probe for pattern-recognition-based biosensing using chemical additives, *Analytical Sciences*, **2021**, *37*, 713–719.

(8) Keisuke Tsumura, Wei Lin Hsu, **Masahiro Mimura**, Aiko Horiuchi, Kentaro Shiraki, Lowering the viscosity of a high-concentration antibody solution by protein–polyelectrolyte complex, *Journal of Bioscience and Bioengineering*, **2022**, *133,* 17–24.

(9) Yuto Akahoshi, Hiroka Sugai, **Masahiro Mimura**, Yoichi Shinkai, Ryoji Kurita, Shunsuke Tomita, Kentaro Shiraki, *in preparation*.

Acknowledgements

I would like to express my sincere gratitude to all of you, including my research team and collaborators, for your dedication and cooperation. This study performed during the doctoral course at the University of Tsukuba could not have been accomplished without their invaluable supports.

First, I would like to express my deepest gratitude to Associate Professor Ryoji Kurita (University of Tsukuba). He has been continually supportive and understanding of my work. He has given me a great opportunity and environment to conduct my research and valuable supervision including fruitful discussions.

I am also indebted to Professor Kentaro Shiraki (University of Tsukuba), Professor Yohei Yamamoto (University of Tsukuba), and Associate Professor Seiya Tsujimura (University of Tsukuba) for useful insights from a range of diverse perspectives.

I also have benefited from the work of my collaborators: Dr. Yoichi Shinkai, Dr. Takuya Hosokai, Dr. Tomoshi Kameda (National Institute of Advanced Industrial Science and Technology (AIST)); Professor Tomohide Saio (Tokushima University); Dr. Hiroyuki Kumeda (Hokkaido University); Professor Ryo Kitahara, Assistant Professor Soichiro Kitazawa, Senior lecturer Takuya Yoshizawa (Ritsumeikan University); Mr. Shiuhei Mieda, Mr. Naoki Akatsuka, Dr. Ruriko Iibuchi (Terumo Corporation) provided expert assistance with equipment, experiments and invaluable discussions, and were always helpful.

I would also like to express special thanks to Dr. Shunsuke Tomita (AIST). He has been continually supportive and understanding of my work, and I am especially grateful for the countless hours of consultation and the freedom to explore many of my own interests during this work.

I would also like to express my sincere gratitude to the members of the Nano-Biodevice Research Group in AIST—Dr. Kyoko Yoshioka, Dr. Naoshi Kojima, Dr. Tsukuru Minamiki, Dr. Ryo Nishihara, Dr. Hiroka Sugai, Ms. Sayaka Ishihara.

My sincere thanks to the members and alumni of the Kurita laboratory—Mr. Hiroki Okada, Ms. Mari Okada, Mr. Ryosuke Esaka, Ms. Yuki Ichikawa, Mr. Yuma Tanaka, and Mr. Kosuke Morimoto. I also thank the members and alumni of the Shiraki Laboratory—Dr. Takaaki Kurinomaru, Dr. Shunsuke Yoshizawa, Dr. Kazuki Iwashita, Dr. Takahiro Nonaka, Mr. Ayumi Matsuda, Mr. Takumi Miyatake, Dr. Taehun Hong, Mr.

Akihiro Endo, Mr. Shogo Oki, Ms. Chika Shibata, Mr. Keisuke Tsumura, Mr. Suguru Nishinami, Mr. Tomoto Ura, Mr. Yoshiki Kihara, Mr. Yoshitaka Nakauchi, Mr. Akira Nomoto, Mr. Yuto Akahoshi, Mr. Hiroyuki Kawamura, Ms. Nanako Sakakibara, Mr. Kazuki Hyakudai, Mr. Shogo Kano, and Mr. Atuya Okubo. I would not have been able to accomplish the goal without our friendly rivalry.

I am grateful of my grandparents, parents, sister, Kuuta, and Ms. Ayana Suno without whom none of the achievements in this course of study would have been possible. In particular, my parents strongly encouraged me to follow my dreams and did everything they could to ensure that these dreams come true.

Finally, I would like to extend my deepest gratitude to all my friends for their continued support and encouragement. I am grateful for everyone's time and effort in making this thesis possible.

Masahiro Mimura

February 2022